

3 The MINER ν A Detector

Chapters 3 and 4 describe, respectively, the detector components and the assembly and installation of these components into the MINER ν A detector. This chapter will begin with an overview of the MINER ν A detector, and will then describe the active detector elements which are constructed from scintillator-fiber assemblies (Section 3.2, read-out by multi-anode photomultiplier tubes (Section 3.3 and digitized by custom electronics and a data acquisition system (Section 3.4). Also described here are the absorbers used as calorimetric absorbers and nuclear targets in MINER ν A (Section 3.3). Finally, we conclude with a discussion of results from the prototype vertical slice test (VST) in Section 3.5.

As a note to the reader, reference to the MINER ν A project structure is made frequently in Chapters 3 and 4 since it is the construction of these components that the MINER ν A project seeks to complete. For the reader's reference, we note that a listing of the gross work-breakdown structure (WBS) of the MINER ν A project can be found at the start of Chapter 8.

3.1 Detector Overview

For MINER ν A to meet its physics goals (Section 2.1), the detector must break new ground in the design of high-rate neutrino experiments. With final states as varied as high-multiplicity deep-inelastic reactions, coherent single- π^0 production and quasi-elastic neutrino scattering, the detector is a hybrid of a fully active fine-grained detector and a traditional calorimeter.

At the core of the MINER ν A design is a solid scintillator-strip detector, similar in principle to the recently commissioned K2K SciBar [5]. The plastic inner detector serves as the primary fiducial volume, where precise tracking, low density of material and fine sampling ensures that some of the most difficult measurements can be performed. These include multiplicity counting in deep-inelastic scattering, tracking of photons, detection of recoil protons in low- Q^2 quasi-elastic events, and particle identification by dE/dx . A side view of the detector is shown in Figure 1.

The scintillator detector cannot contain events due to its low density and low Z , and therefore, the MINER ν A design surrounds the scintillator fiducial volume with sampling detectors. At the low energies needed to study cross-sections of interest to neutrino-oscillation searches, many of the events contain energetic sideways-going particles, so these sampling detectors extend to the sides of the detector. Finally, energetic forward muons will enter the MINOS near detector, where their momentum can be measured magnetically and/or by range.

Except for the upstream veto, the entire MINER ν A detector is segmented transversely into an inner detector with planes of solid strips and an outer picture frame (OD)¹. For construction and handling convenience, a single plane of MINER ν A incorporates both the inner detector and OD, which serves as the support structure. Two planes of scintillator are mounted in one frame, called a "module", as illustrated in Figure 3. There are three distinct orientations of strips in the inner detector, offset by 60°, and labeled X, U, and V. The different strip orientations enable a three-dimensional reconstruction of tracks, and the 60° offset makes the hexagon a natural transverse cross-section for

¹The OD detector steel and portions of the support geometry were so that the OD steel may be magnetized as a future upgrade to MINER ν A. This would improve focusing of sideways muons into MINOS or help them to range out in the OD; however, this option is not part of the baseline design.

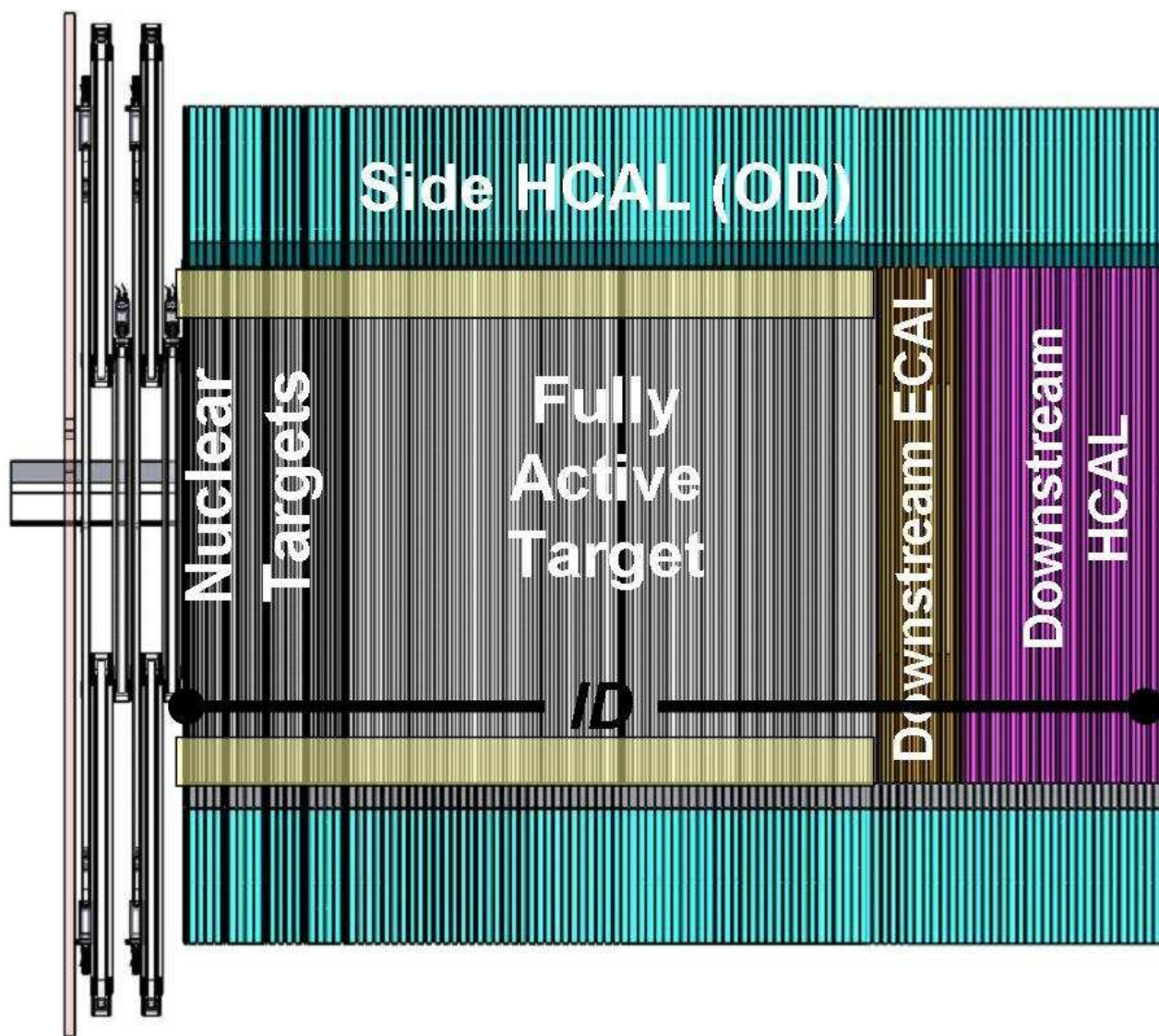


Figure 1: A side view schematic of the MINERνA detector

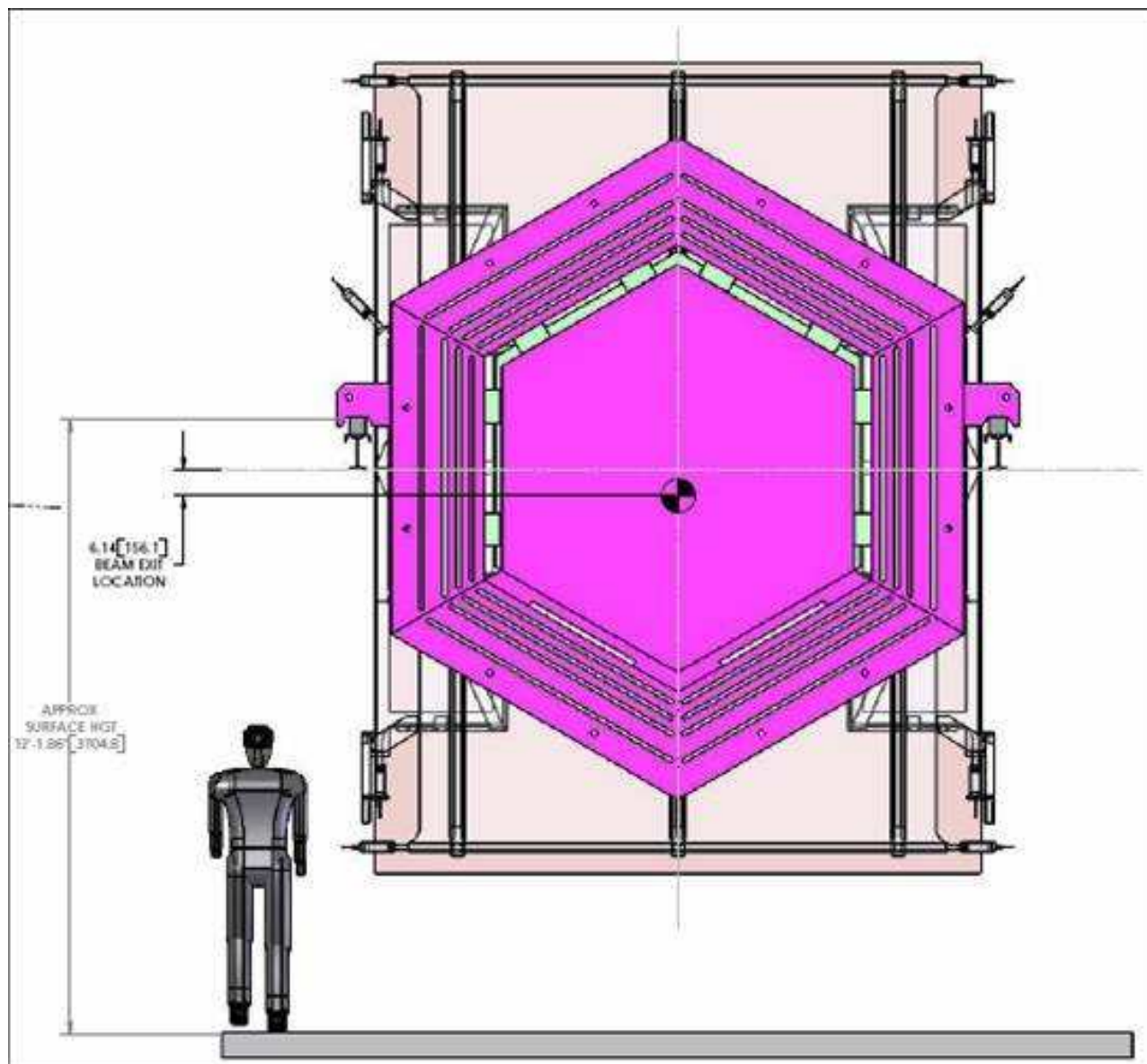


Figure 2: View from the back of the MINERνA detector to illustrate shape and scale. The tall structure at the far end of the view is the veto wall; the detector stand is not shown for ease of viewing.

the detector. As shown, the scintillator strips extend the full length of the hexagon and range between 205 and 400 cm in length.

The center of the detector is the fully active inner detector (ID), whose plastic core represents the fiducial volume for most analyses in MINER ν A. Calorimetric detectors in the central region of the detector are constructed by inserting absorber between adjacent planes as shown in Figure 3. Lead alloy absorbers, 30 cm from the edge of the ID and 0.2 cm thick, are inserted between layers of scintillator and at the front of each module to serve as a side electromagnetic calorimeter. This part represents the largest part of the detector in length, and the outer calorimeter surrounding the fully active planes are the largest part of the detector in mass.

The inner detector is surrounded by the picture frames of absorber and scintillator strips that make up the outer detector (OD). The OD consists of six “towers” (one sixth of a hexagon). Note that the strips in the OD run only in one direction, in the bend plane of the magnetic field. Three-dimensional tracks must therefore be matched from the inner detector and extrapolated outwards for an energy measurement or muon momentum measurement. A complication of the design is illustrated by the fact that the inner detector strips, which range in length from 120 to 240 cm, end inside the OD, and therefore bundled WLS fibers must travel through the gap between the OD planes of each module to the detector edge. The scintillator strips in the towers are rectangular in cross-section, $\sim 1.9 \times 1.5$ cm², and are arranged in rectangular layers of two strips per OD slot.

In the inner detector, MINER ν A’s sensitive elements are extruded triangular scintillator strips, 1.7 cm height with a 3.3 cm base, with embedded wavelength-shifting fibers. To improve coordinate resolution while maintaining reasonably large strips, these elements are triangular and assembled into planes (see for example Figure 45); this allows charge-sharing between neighboring strips in a single plane to interpolate the coordinate position.

The most downstream detectors are the hadronic calorimeters (HCALs) with a 1 inch absorbers per scintillator plane. as shown in Figure 4. Next are the electromagnetic calorimeters, shown in Figure 5, The electromagnetic calorimeters (ECALs) have one 0.2 cm Pb alloy absorber per scintillator plane. The absorbers only overlap the inner detector and not the outer detector where it would represent a negligible fraction of the absorber material. The fine granularity of the ECAL ensures excellent photon and electron energy resolution as well as a direction measurement for each. Finally, in the region labeled “nuclear targets” in Figure 1, there are sparsely placed absorbers in between active target modules to allow study of events on different nuclear targets. These targets are described in Section 3.3.

3.2 Scintillator Detectors

This section describes the MINER ν A scintillator components for the Inner (ID) and Outer (OD) Detectors, and related systems such as the Vertical Slice Test (VST). Section 3.2.1 addresses the requirements and performance criteria for the scintillator system. Section 3.2.2 provides an overview on the extruded scintillator preparation (MINER ν A project WBS 1). Section 3.2.3 describes the wavelength shifting (WLS) fibers (WBS 2) that will be used in the detectors. Section 3.2.4 discusses in detail the clear fiber cables (WBS 4).

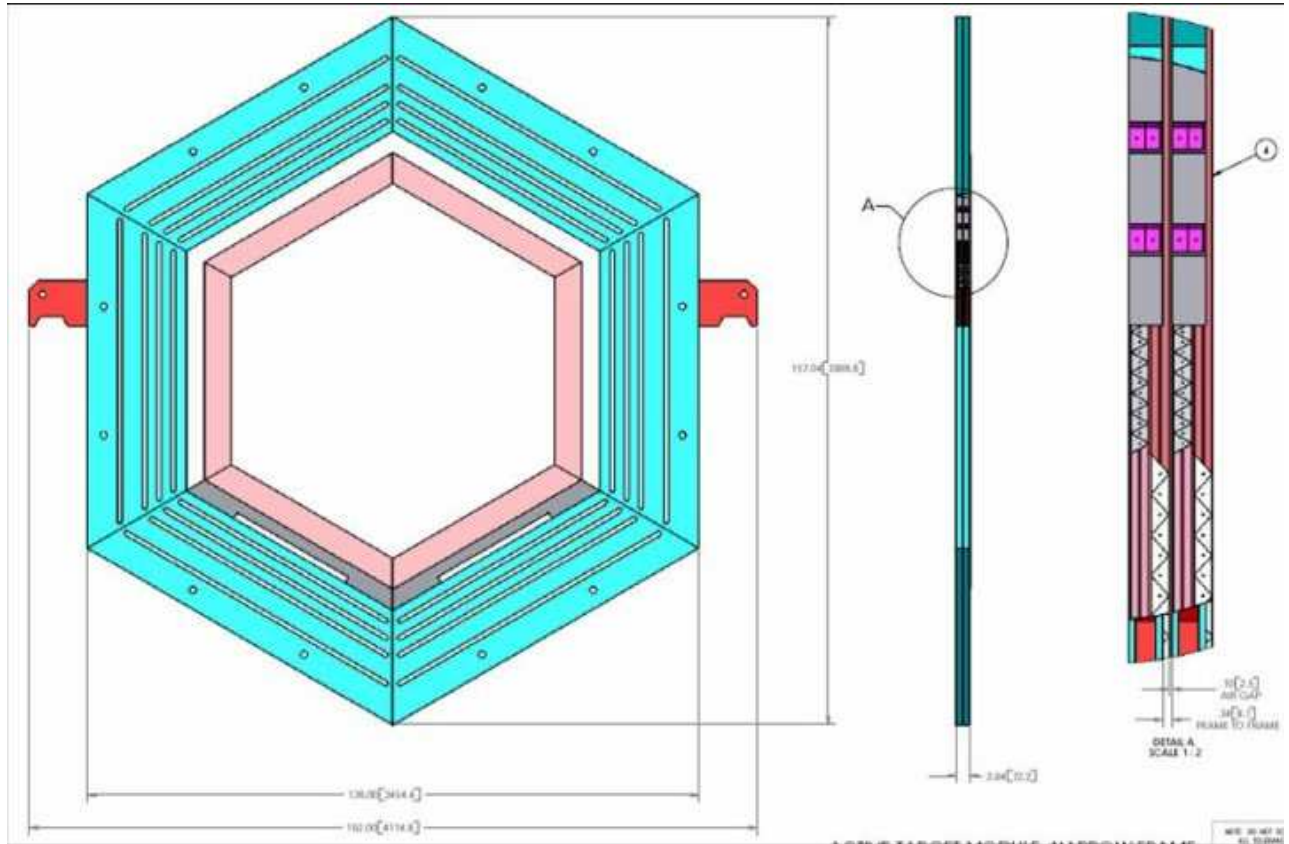


Figure 3: View of an active detector module. The figure at right shows a cut-away view from the side.

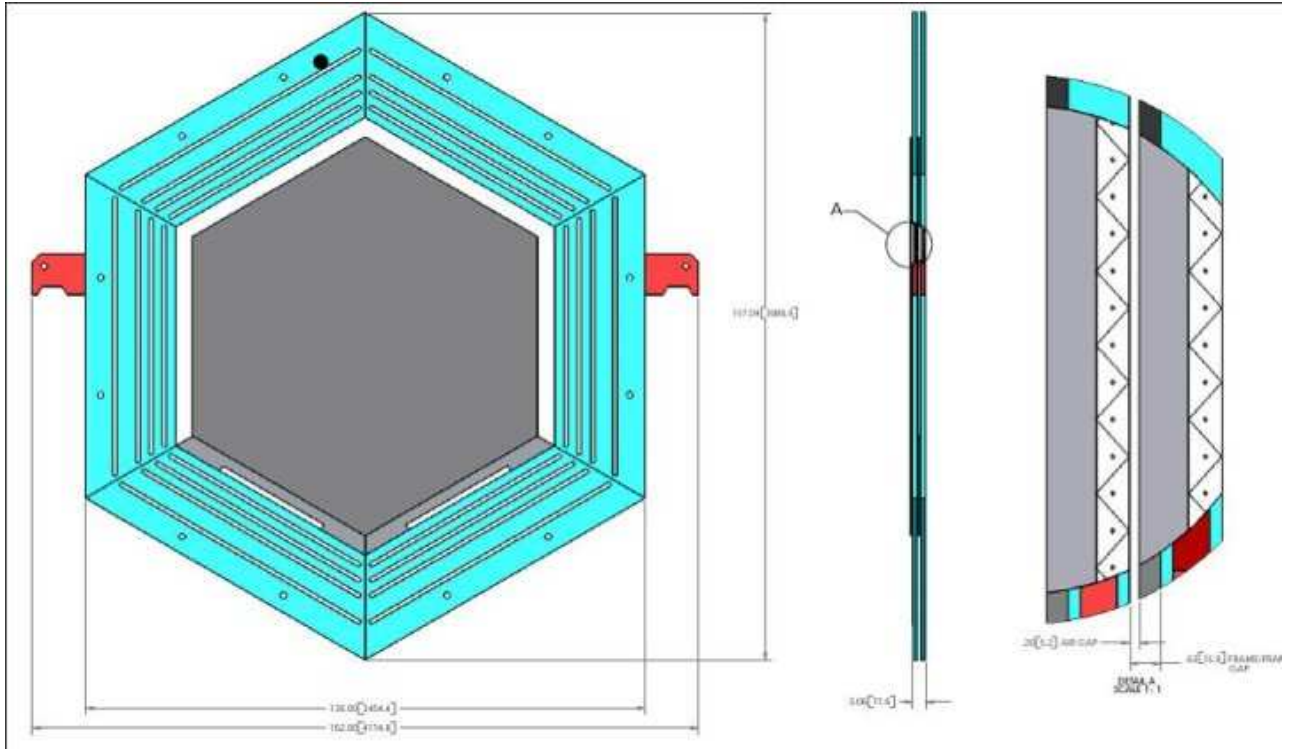


Figure 4: View of an HCAL detector module. The figure at right shows a cut-away view from the side.

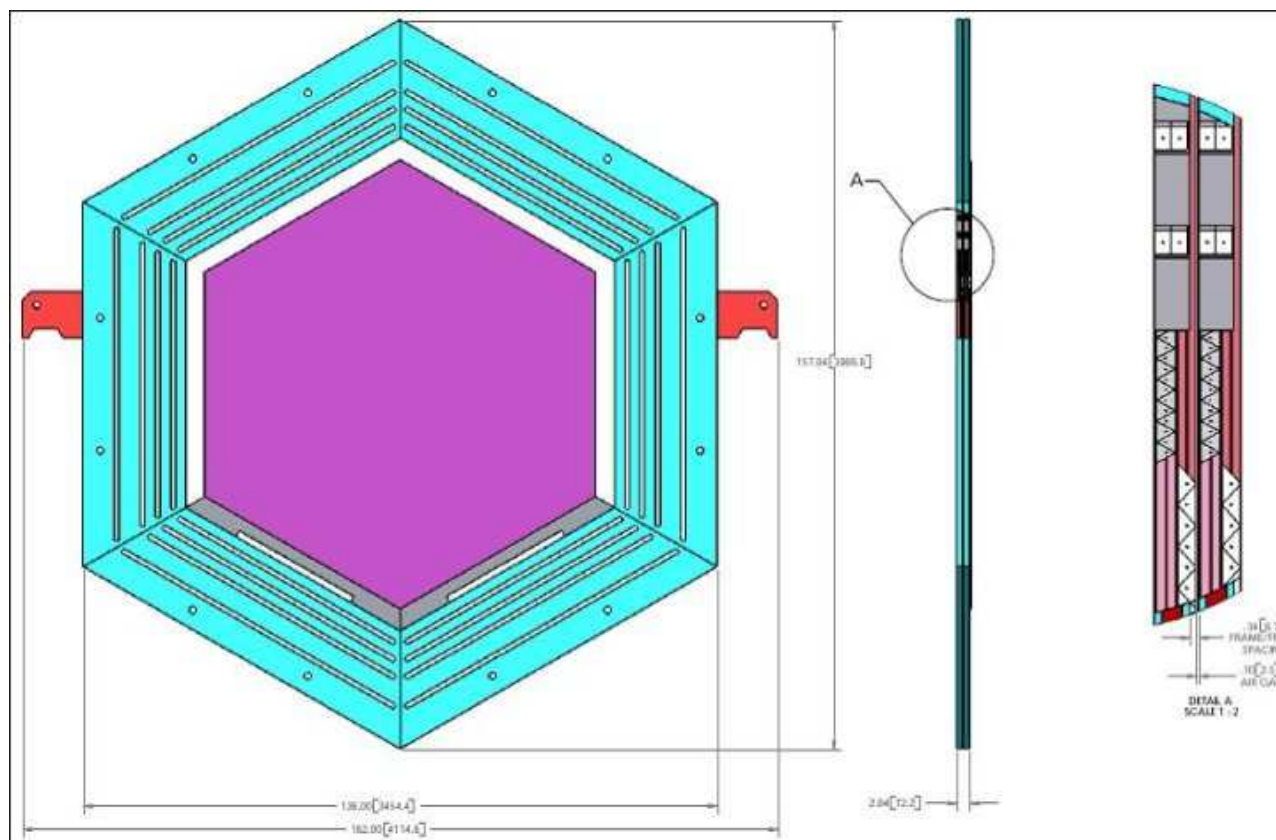


Figure 5: View of an ECAL detector module. The figure at right shows a cut-away view from the side.

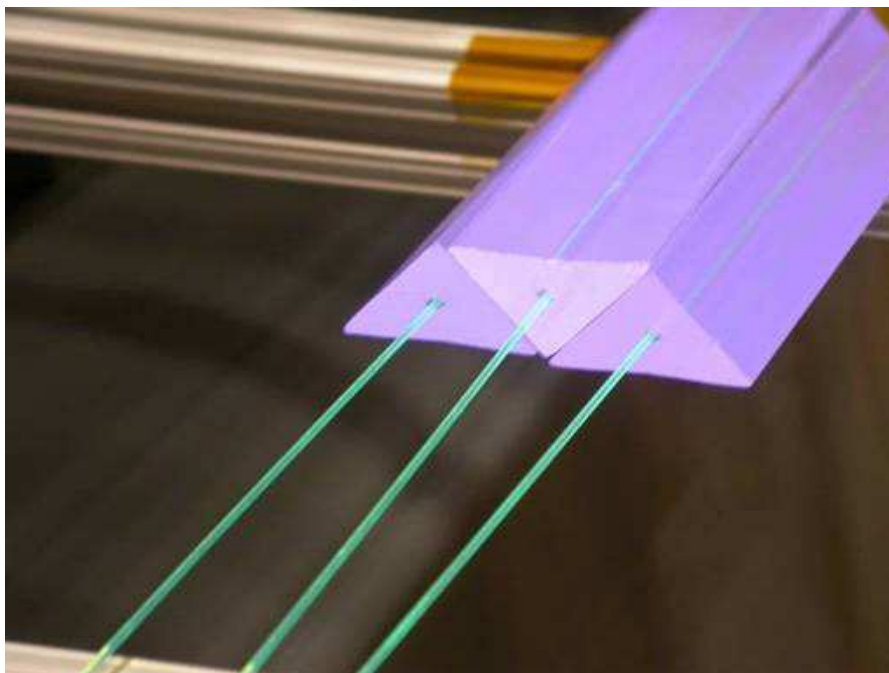


Figure 6: Prototype MINERνA scintillator bars, with wavelength-shifting fibers inserted.

3.2.1 Requirements and Performance Criteria

The MINERνA detectors utilize extruded plastic scintillator which is read out by wavelength shifting (WLS) fibers coupled to multi-pixel photodetectors. Figure 6 shows early prototypes of the scintillator and WLS fiber system. This technique provides excellent energy and spatial resolutions. The baseline design relies on existing technology for which performance measurements have been made. This same system is being used in the MINOS experiment. The major components that will be discussed in this Chapter are:

- The scintillator strips which consist of an extruded polystyrene core doped with blue-emitting fluorescent compounds, a co-extruded TiO_2 outer layer for reflectivity, and a hole in the middle for a WLS fiber. These strips are prepared with a triangular cross-section (3.3 cm base and 1.7 cm height) for the Inner Detector (ID) and with a rectangular profile (1.9 cm base by 1.5 cm height) for the Outer Detector (OD). Figure 6 shows an early prototype ID scintillator strip without the white reflective coating and with WLS fibers inserted in the holes.

- The WLS fibers which consist of Y11 fibers 175 ppm of dopant, multi-cladded with a 1.2 mm diameter. These fibers are glued into the hole of the scintillator strips manufactured by Kuraray with using an optical epoxy (Epon resin with TETA hardener). The fibers are read from one single end. The other end is mirrored.

- The clear fiber cables which consist of ribbons of 8 clear fibers (1.2 mm diameter, 109 cm maximum length) to carry the light from the detector modules to the photodetectors. Optical connectors are used for all fiber optics connections.

The technical requirements on the scintillator system have been established from a combination

of physical studies and practical considerations. The technical requirements for the Inner Detector scintillator are more stringent than those for the Outer Detector scintillator. However, in order to save time and money the same scintillator will be produced for both applications. The same co-extrusion procedure with the same raw materials will be utilized. Therefore only the specifications of the Inner Detector Scintillator-WLS-Clear Fiber system are listed here:

Scintillator Bar Specifications:

Cross-sectional uniformity: ± 0.5 mm base and height both, measured with a caliper to within 0.1 mm.

Length uniformity: 5%, must be cut at 1% precision later.

Minimum TiO₂ thickness: .13 mm for efficient light reflection (based on MINOS tests).

Scintillator Light Output Uniformity: 5%, measured to within 1%.

Attenuation Length: 5-6 cm or longer (with capstocking) or 25-30 cm or longer (without capstocking).

Light Output: The light output must be sufficient for measuring event vertices and multiplicities. We have determined that the required number of photoelectrons (pe) per layer, per minimum ionizing particle is 13.2 pe at normal incidence for the full fiber readout chain.

Fiducial Mass: The total mass in the fiducial volume of the Inner Detector varies for different physics analyses, but there should be a minimum of 3 tons fiducial mass for each analysis. A minimum transverse (longitudinal) distance of 35 cm (50 cm) is required for containment. For the MINERvA detector, the minimum transverse distance cut translates to a cut of 75 cm maximum distance from the center of the detector.

Uniformity: The light output at the end of the clear fiber should vary by no more than 30% with respect to the nominal location. This ensures that over 99% of the bars will meet the 13.2 photoelectron requirement.

WLS Fiber Attenuation and Mirroring: The light output at the far end of the scintillator bar must be above the minimum 13.2 photoelectrons per layer.

Clear Fiber Cable Transmission: The clear fiber transmission should be high enough that the minimum number of photoelectrons at the far end of the scintillator bar is 13.2 photoelectrons per layer.

Stability: The detector is expected to be able to operate for approximately 10 years, over that time the scintillator-fiber assembly light output is expected to decrease roughly $3 \pm 1\%$ per year (ref: B. Choudhary, NUMI-note 414). Due to this degradation, a safety factor of > 1.3 should be included in the light output requirement in order to allow operations over 10 years. Short-term variations must be measurable, at the few per cent level over a month.

Calibration: The detector energy levels must be absolutely calibrated at the 2% level.

Transverse Position Resolution: In order to do exclusive channel reconstruction and make precise vertex measurements the transverse coordinate resolution must be 3 mm.

Linearity: The non-linearity of the Inner Detector scintillator bar system should be less than 15%, and should be known to better than 5% (of 33% of itself).

Cross-talk: The cross-talk between adjacent bars should contribute no more than 10% of the intrinsic position resolution of 3 mm. Given the transverse dimensions of the scintillator triangle base, this translates to a requirement that the cross-talk between adjacent bars be less than 2%.

Longitudinal Vertex Resolution: In order to measure nuclear effects we require less than 10% contamination for any given nuclear target region. This requires that the longitudinal vertex resolution is no worse than 1 cm.

Cost: The cost should be as low as possible given the above requirements.

3.2.2 Scintillator Extrusion

Particle detection using extruded scintillator and optical fibers is a mature technology. MINOS has shown that co-extruded solid scintillator with embedded wavelength shifting (WLS) fibers and PMT readout produces adequate light for MIP tracking and that it can be manufactured with excellent quality control and uniformity in an industrial setting. MINER ν A intends to use this same technology for the active elements of its detectors. While in terms of size MINER ν A pales in comparison to MINOS, its system is similar in scale to other successful applications such as the K2K SCIBAR detector. Extrusion will also enable the use of different cross-sections throughout the detector to better address the experiment needs.

The extruded scintillator elements will be produced at Fermilab using the extrusion line jointly operated by Fermilab and the Northern Illinois Center for Accelerator and Detector Development (NICADD) at Northern Illinois University (NIU). NIU physicists and mechanical engineers have formed a collaboration to support development of the next generation of detectors at Fermilab's Scintillator Detector Development Technical Center. The extrusion line was purchased by NICADD in 2003. The co-extruder line was purchased by Fermilab in 2005. Fermilab and NICADD support and operate the extruder to ensure that the High Energy Physics community has access to high-quality extruded scintillator. Fermilab and NICADD personnel have been responsible for commissioning the extruder; simulations, production and prototyping of dies associated with specific detectors; and productions of extrusions for prototypes and detector construction.

MINER ν A has chosen a scintillator bar with a triangular profile and a hole in the middle for the Inner Detector (ID). The triangle has a 3.3-cm base and a 1.7-cm height, and a 2.6 mm hole for the WLS fiber. A drawing with the specifications and tolerances for this part is available (FNAL Drawing Number: 9291.000-MB-241845). A rectangular cross-section with a hole in the middle was selected for the Outer Detector (OD). The rectangle has a 1.9-cm base and a 1.5-cm height, and a 2.6 mm hole for a WLS fiber. A drawing with the specifications and tolerances for this part is available (FNAL Drawing Number: 9219.000-MB-241843).

Figure 7 shows the die for the ID scintillator strips mounted on the extruder. Figure 8 shows the die sections to produce the OD scintillator strips. Only the last sections of the die and the sizing tooling need to be changed to produce either strip type. All scintillator strips have the same composition: a polystyrene core (Dow Styron 663 W) doped with PPO (1% by weight) and POPOP (0.03% by weight). Both strips have a white, co-extruded, 0.25 mm thick TiO₂ reflective coating. This layer is introduced in a single step as part of a co-extrusion process. The composition of this capstocking is 15% TiO₂ (rutile) in polystyrene. In addition to its reflectivity properties, the layer facilitates the assembly of the scintillator strips into modules. The ruggedness of this coating enables the direct gluing of the strips to each other and to the module skins which results in labor and time savings for the experiment.

The scintillator bars production process is characterized by an "in-line", continuous extrusion

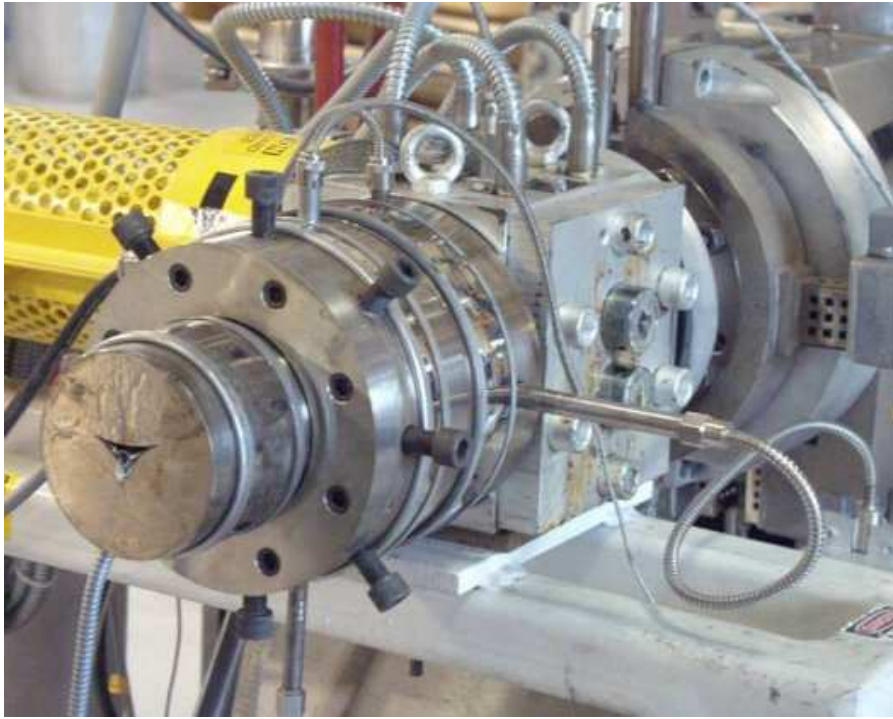


Figure 7: Die to produce MINERνA's triangular strips for ID scintillator.

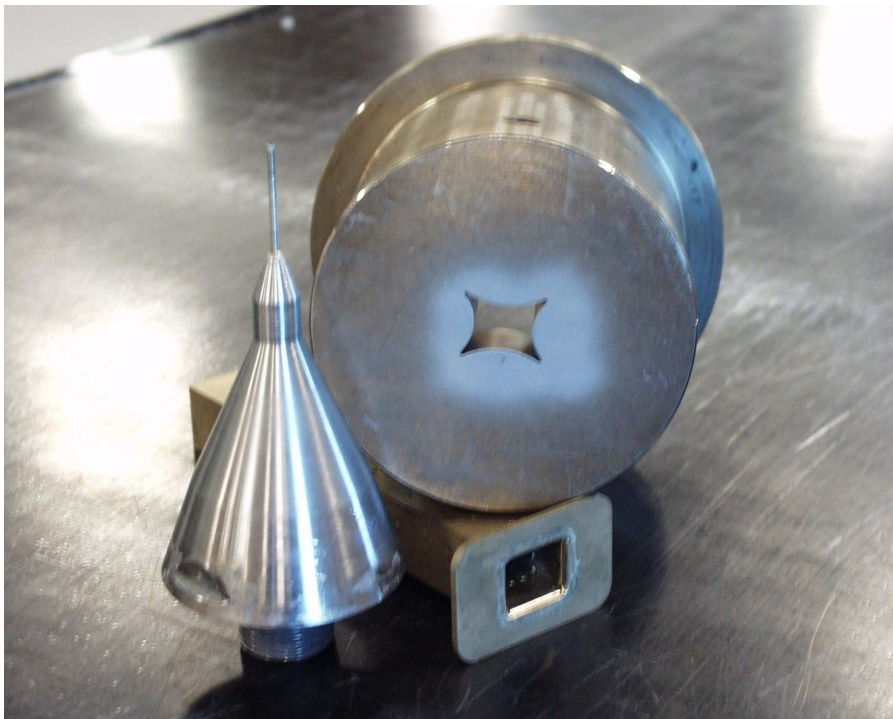


Figure 8: Die to produce MINERνA's rectangular strips for OD scintillator.

process as opposed to a batch process. The polystyrene pellets are dried in a nitrogen atmosphere and automatically conveyed to a gravimetric feeder. The dopant mixture is added periodically to a different gravimetric feeder that works surrogated to the pellet feeder. These feeders have the necessary precision and reliability to ensure a constant ratio delivered. The pellet feeder is controlled by computer to the output of the twin-screw extruder to ensure the correct composition and processing. The extruder is responsible for melting and mixing the polystyrene pellets and the dopants. A twin-screw extruder will provide the highest degree of mixing to achieve a very homogeneous concentration. The outer reflective coating is added through material injected from a second extrusion machine (co-extruder) which mixes the polystyrene and TiO₂ pellets. Currently the co-extruder is manually operated to start-up and to vary the thickness of the reflective coating. As the plastic emerges from the die, it goes directly into the cooling tank. There it is formed into the final shape using the sizing tooling and vacuum. It continues to be cooled with water and air until it can be handled.

A total of 13,312 triangular strips and 2,736 rectangular strips will be produced for the ID and OD, respectively. The ID bars will be cut at 3.8 m long and the OD bars at 3.5 m long. Each strip will contain two strips for the final detector module. By cutting a single strip into two sections, it is possible to minimize the amount of waste material and still have each strip of exactly the right length for its hexagon location.

The extrusion rate for both scintillator strips is of 75 Kg/h. The dies have also been tested at 50 and 100 Kg/h. There is little difference in the quality of the extruded bars at any of these three rates. However, it becomes harder to cool down the extruded part as the extrusion rate increases. The best compromise is reached with the 75-Kg/h extrusion rate. The schedule was develop with the possibility of using the lower rate (50 Kg/h) in case that either the overall process (extrusion and quality control activities) or the quality of the material would require it. The higher rate (100 Kg/h) could be used if the production is delayed or if there are personnel shortcomings as a means to keep within the projected schedule. The 23 metric tons of extruded scintillator for the full MINERνA design will require a production run of approximately 18 weeks.

Quality Assurance and Quality Control (QA/QC) procedures to ensure the light yield of the finished product will be established and maintained by Fermilab and NIU personnel throughout production. Figure 9 shows the quality control (QC) measurements for seven of the R&D extrusion runs to prepare co-extruded scintillator bars. Two main parameters will be checked during production at the Extrusion Facility: dimensions and light yield. Dimensions will be checked every 60 minutes using a caliper. The data will be entered in a computer and the file submitted daily to MINERνA-docDB. Light yield will be tested using a radioactive source. A reference sample will also be measured to monitor the stability of the equipment as well as to provide a minimum acceptable value. The results will also be uploaded into MINERνA-docDB. These measurements will be carried out on a QC sample (15 cm long). This short QC sample will be cut once every five full length scintillator strips. These two tests will be the basis of the Quality Control program. Additional testing will be performed if a problem is noticed. Measurements to determine the attenuation length of the material may be conducted at weekly intervals as a secondary proof of material quality and equipment stability.

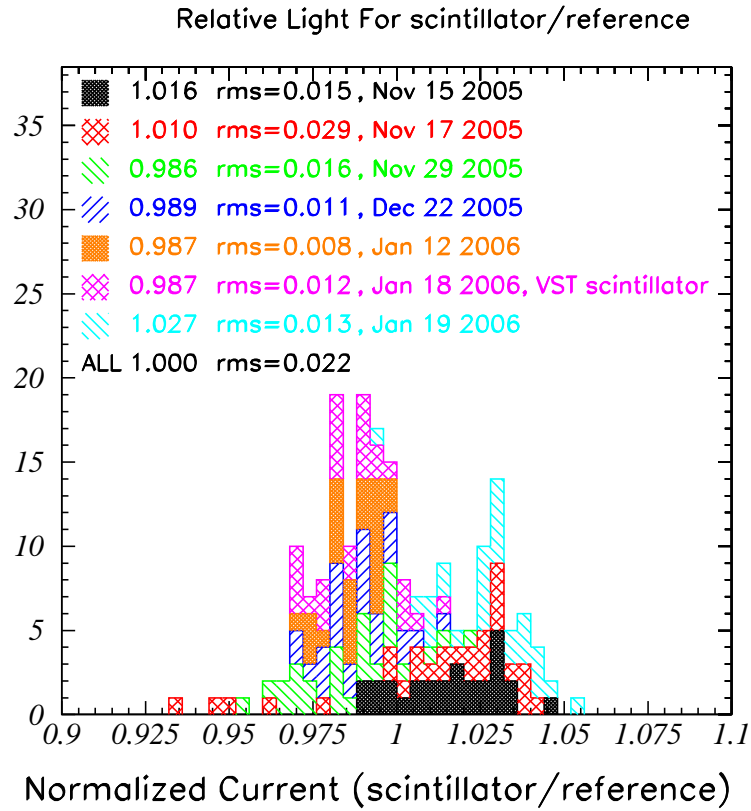


Figure 9: Light yield quality control measurements of the MINER ν A scintillator bars. The plot shows the sample measurement divided by the control measurement. The normalization is set to 1. The VST scintillator is labeled. The bottom number shows the RMS of all the bars.

3.2.3 Wavelength-shifting fibers

MINER ν A optical system uses 1.2 mm diameter, 175 ppm Y-11 doped, S-35 multicladd fiber from Kuraray. Kuraray fibers have a proven track record in many HEP experiments including CDF Plug Upgrade, CMS HCAL, MINOS ... The S-35 denotes a more flexible fiber than non-S fiber which MINOS and the CDF Plug Upgrade used in their scintillator planes.

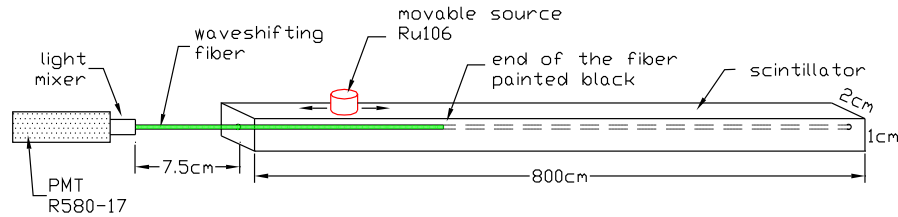


Figure 10: A schematic of the MINOS Scanner used to measure the WLS fibers.

The fibers will be manufactured in batches. (A batch is technically called a preform.) Five 3.2 m fibers from each batch will be tested using a fiber scanner called the MINOS Scanner, see Figure 10, to determine if the attenuation length is acceptable. The fiber is inserted into a long scintillator, a source moves over the scintillator, and the fiber is read out using a R580-17 Hamamatsu PMT. The PMT is readout by a picoammeter. The data are fit to a double exponential. Figure 11 shows the same fibers measured with mirrored and blackened ends. The quality control will be based on the amount of light at 320 cm from the readout end and the attenuation length. (Note, the longest WLS fibers in MINER ν A is about 320 cm.) A light pulser consisting of americium in sodium iodide will be used to maintain the calibration of the PMT. Each of these is determined by extrapolating a fit to 320 cm. Figure 12a shows the relative lights among the fibers at 320 cm. The three batches we have received are shown. Figure 12b shows the light loss after 320 cm of fiber. Figure 12 shows that the 3 batches appear to be equivalent.

MINER ν A will read-out only one end of its wavelength-shifting (WLS) fibers. To maximize light collection, we will mirror the unread end of each fiber using techniques developed at Fermilab. “Mirroring” consists of 3 steps: polishing the end to be mirrored, depositing the reflective surface on the fibers (a process called sputtering), and protecting the mirrors.

A technique called ice-polishing is used to prepare the fibers prior to applying the reflective coating. Ice-polishing can give a very good finish to many fibers at once. This technique is described in detail in [156].

The reflective coating is applied in a vacuum system dedicated to optical fiber mirroring at Fermilab. The number of fibers that can be sputtered per load depends on the diameter, but typically 1000–2000 fibers per pumpdown per unit can be coated. A 99.999% chemically pure aluminum coating is applied for good reflectivity. The coating is approximately 2500 Angstroms thick and is monitored using an oscillating quartz crystal sensor device. The aluminized ends are protected with a coat of epoxy.

After this process, MINER ν A will do a destructive measurement of the mirror reflectivity with 5 fibers from each sputtering session. Light output is measured through the unmirrored end of a fiber

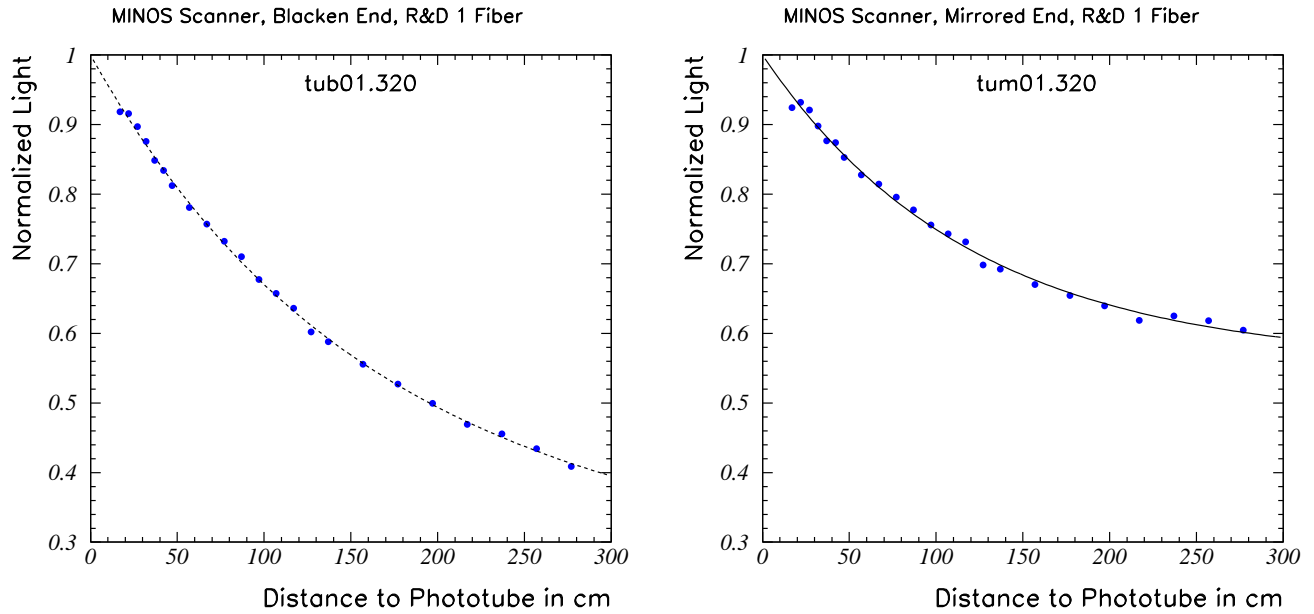


Figure 11: The measurement of the same fiber using the MINOS Scanner. The fiber is first measured with the mirror on. Next, the mirror is cut off and the end painted black. The fiber is remeasured. The fit is a double exponential, $p(1)e^{-x/p(2)} + p(3)e^{-x/p(4)}$, where x is the distance to the phototube and $p(i)$ are the parameters. The mirror reflectivity is determined by using these 2 fits extrapolated to the fiber end.

with ultra-violet light incident on the fiber near the mirrored end. Then, the mirrored end is cut off at 45° , painted black, and the light yield is remeasured with the UV light at the same place. Figure 13 shows the mirror reflectivity by scanning with the MINOS Scanner the same fiber with and without the mirror. The mirror reflectivity is measured to be about 80%. RMS of the mirroring is 5.5%, while the RMS of the mirroring for the CDF Plug Upgrade was 5.4%.

3.2.4 Fiber connectors and optical cables

We are using optical connectors from Fujikura/DDK (generically referred to as DDK connectors). These connectors were originally developed for the CDF Plug Upgrade by DDK, in consultation with Tsukuba University. Since then, they have been used by several other experiments such as FOCUS, STAR, and D0.

The DDK connectors consist of a ferrule, clip, and box (Figure 14). They snap together without screws or pins. These connectors were chosen for their ease of use. DDK has made a new ferrule die for our 1.2 mm diameter fibers, keeping the outside dimensions of the ferrule identical to the current model; thus, other parts of the connector do not need to be redesigned.

The hole position, diameter, and outer dimensions of the new ferrule have been precisely mea-

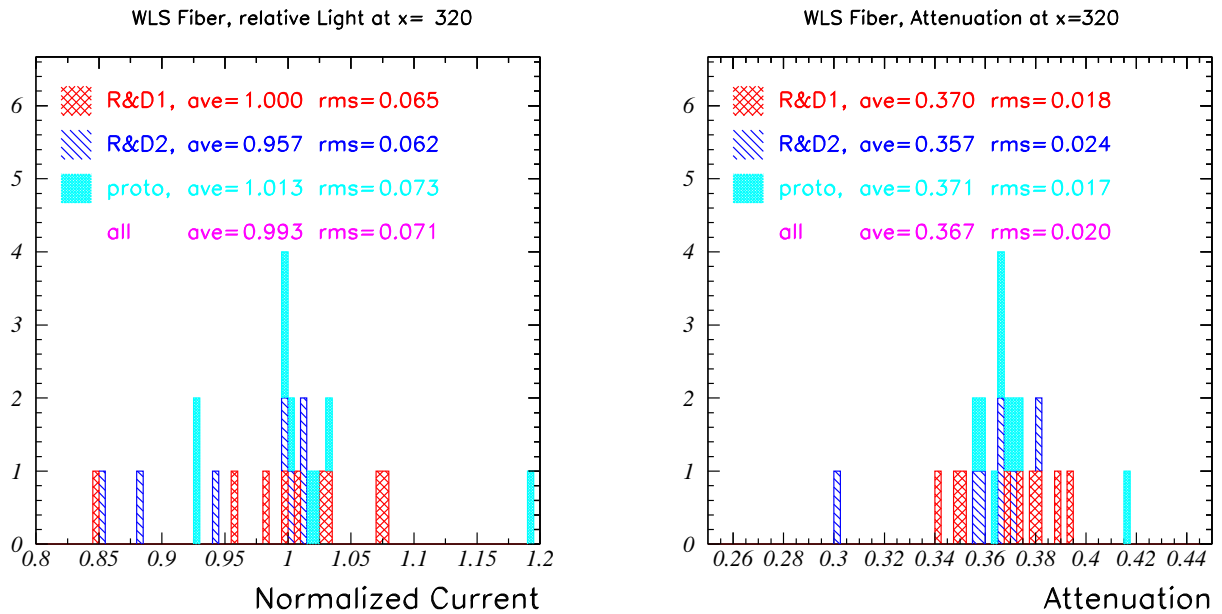


Figure 12: The left figure shows the relative light for the WLS fibers measured with the MINOS Scanner. Three batches were measured; R&D-1 Fibers (purchased May 2005), R&D-2 Fibers (purchased Aug 2006), and Prototype Fibers (purchased Dec 2006). The relative light was normalized to the R&D 1 Fibers, the fibers used for the VST. The right figure shows the light loss at 3.2m

sured. These measurements were done at SCIDET using the Coordinate Measuring Machine (CCM) and the Optical Gaging Products (OGP). The CCM measure objects mechanically, while the OGP measures objects optically. When the connectors are mated, the fiber holes line up to < 25 microns. The hole diameters are very similar, with the differences < 12 microns. The ferrules fit very tight in the box.

The transmission was measured using the new connectors. Figure 15 is a schematic which shows how the connector transmission is measured. We injected light into a pigtail using 1 m WLS fiber inserted into 0.5 m long coextruded scintillator. (By "pigtail", we mean a set of fibers put in one DDK optical connector with no DDK optical connector on the other end.) A source in a lead cone excited the scintillator. The light was readout using a PMT and a picoammeter. We measured the light before and after inserting a connector into a 2 m cable. Figure 16 shows transmission for 3 cables.

We have measured the light loss from a 1 m clear cable to be about 30% without optical grease between the connections. We injected light into a WLS pigtail using the same procedure as used to test the cable transmission, see Figure 17. We connected the DDK connector on a WLS pigtail to DDK connector on a clear pigtail with the other end going to a PMT. We then inserted a 1 m cable between the 2 DDK connectors and remeasured the system. Figure 18 shows the light loss for 3 cables by taking the ratio of light after the inserted cable to light without cable. We are planning on

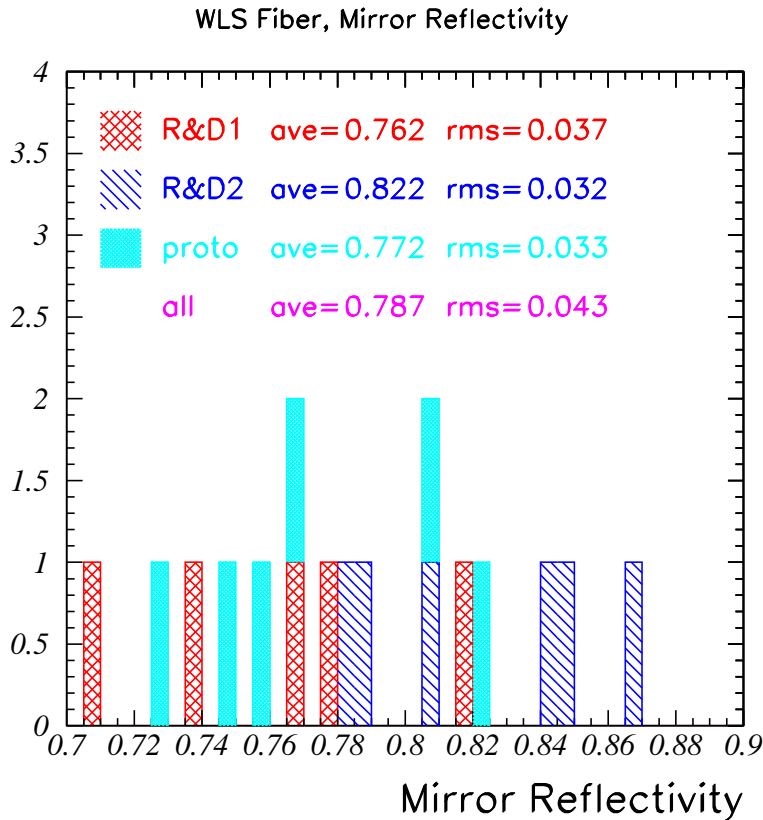


Figure 13: Plot shows of the mirror reflectivity for the 3 batches of fiber. Each batch was mirrored at a different time. Each entry is the ratio between the mirrored-end fiber fit and the blackened-end fiber fit extrapolated to the fiber end.

using optical grease between the connectors to increase the transmission. We have measured the light increase from optical grease to be about 16%. In order to determine the lifetime of optical grease, we have measured the transmission of 2 greased connections after 6 weeks. We have seen no change in the light transmission.

For the cables, we are using 1.2 mm, S-35 multicladd fiber from Kuraray to match the Kuraray WLS fiber. The S-35 denotes a more flexible fiber than non-S fiber. Five fibers from each batch will have their attenuation length checked using a cut-back test developed by CMS. The test uses a source, scintillator, and WLS fiber to inject light into the clear fiber. A 6.8 m attenuation length was measured for the R&D fibers using this procedure.

We will be manufacturing 2 kinds of optical cables; referred to as ODUs (optical decoder units) and cables. The ODUs are meant for the PMT boxes. ODUs are built the same way as cables, but they are not made light tight. Hence, they undergo the same cable QC procedure as cables do. At the PMT box factories the ODUs are cut in 2 and weaved into the cookie for the PMT box.

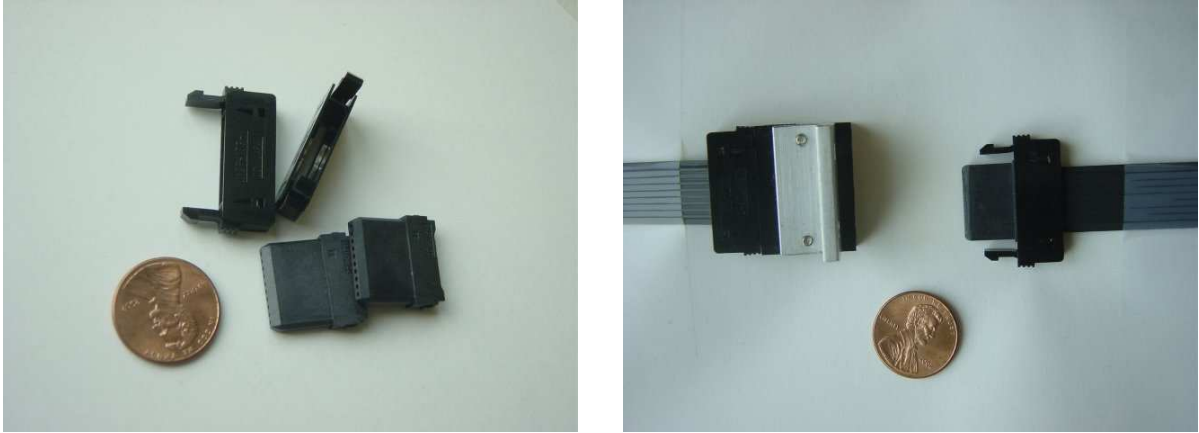


Figure 14: DDK connector parts. At the left, examples of the ferrules (bottom) and the clip (top). At the right, two completed CDF cables with the box to which they connect. The aluminum angle bolted onto the box is used to hold the box on an aluminum cover.

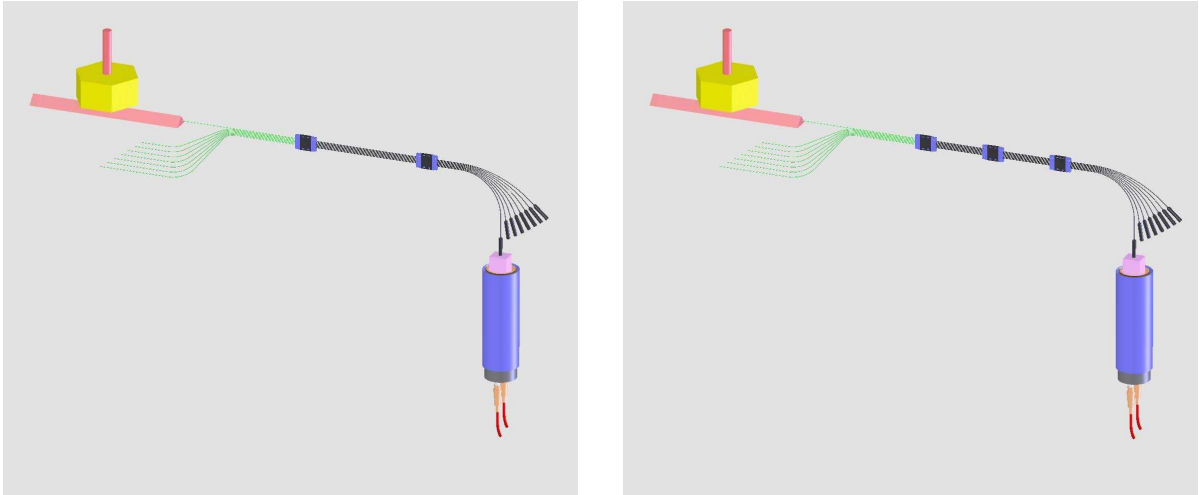


Figure 15: Schematic of apparatus used to measure the connector transmission. The left picture shows the light being measured with an optical cable inserted between 2 pigtails. The right picture has the connector inserted into the cable.

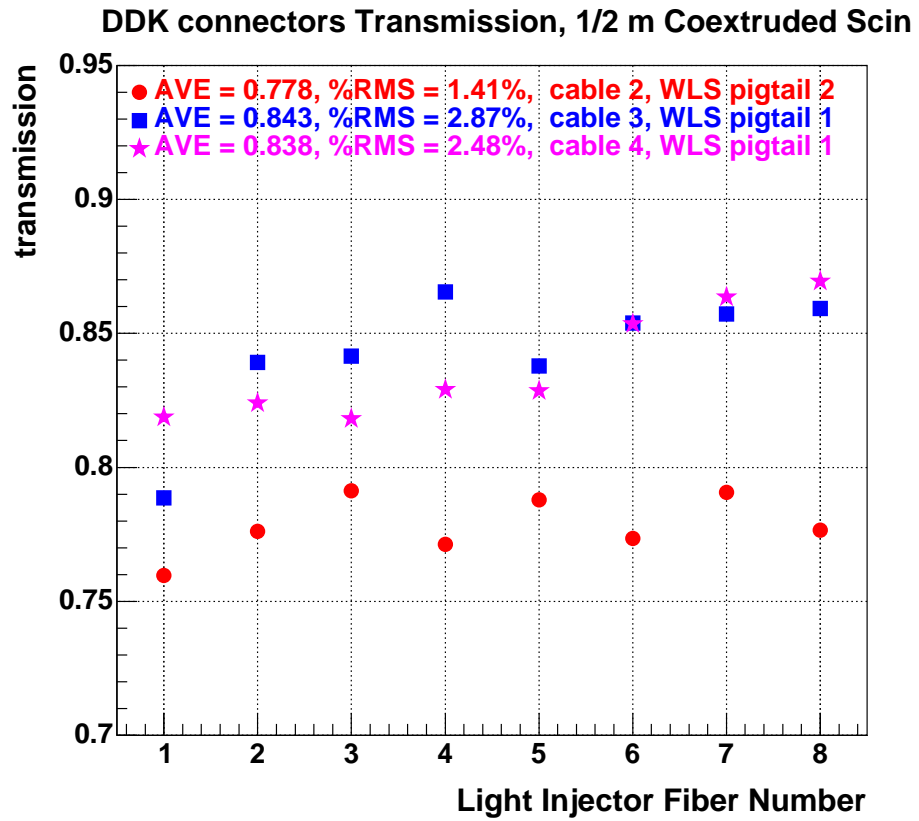


Figure 16: The light transmission for 3 DDK connectors.

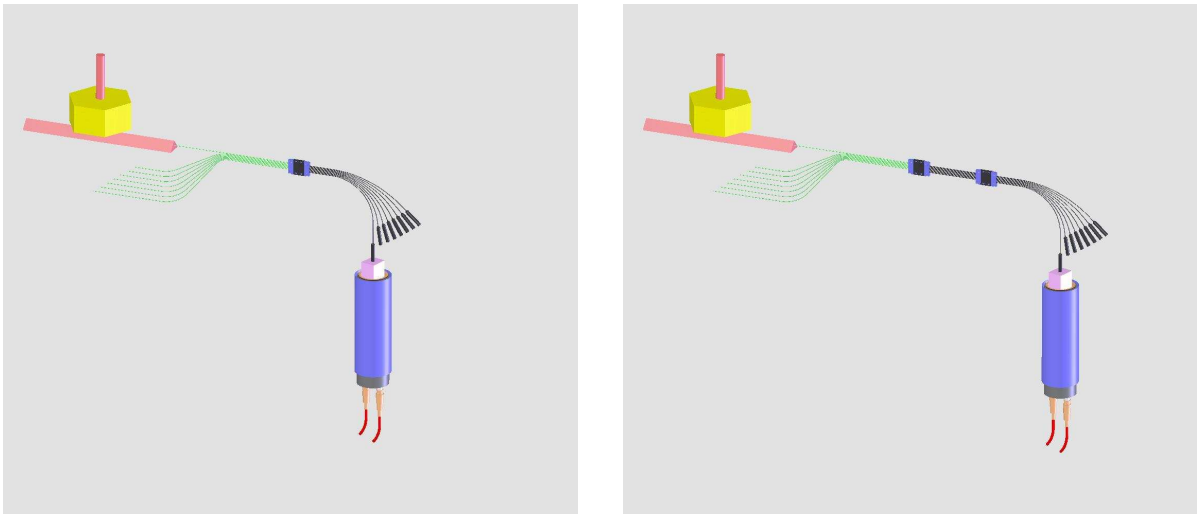


Figure 17: Schematic of the apparatus used to measure loss from a 1 m cable. The left picture shows the light being measured before the insertion of the cable. The right picture has a cable inserted between the 2 pigtails.

The fabrication and polishing procedure we plan to adopt was used by the CDF collaborations on DDK cables. Initially, the fibers are cut to the correct length. Then, the fibers are inserted into a ferrule oriented vertically and taped in place, with the mating end pointing down. The top of fibers are taped against a horizontal piece of metal. BC600 epoxy is then placed in the pocket of the ferrule with a syringe. After the epoxy cures (the next day), two clips are placed on the fibers, one for the ferrule that was just epoxied and the other to fit over the ferrule yet to be fixed to the other end of the cable. A light-tight tube is placed over the entire length of the fibers except for approximately 5 cm near the ends where the fibers enter the ferrules. The end of the fibers not glued in the first ferrule are then placed in a second ferrule and epoxied in place. After curing, the fibers on both ends of the cable are trimmed to about 1/8" at the connector in anticipation of the polishing. After the ferrules and fiber ends are polished, the clips are pushed up onto the two ferrules.

For the CDF Plug Upgrade, a significant Fermilab effort was devoted to developing a method to polish the DDK connectors [156]. Since then, Fermilab has developed a machine which can polish multiple optical connectors simultaneously. Fermilab has designed a fixture for this machine to hold 6 DDK connectors. We have used this machine to polish the R&D cables which have been used for a variety of measurements, including the transmission measurement described above.

We have developed a light-tightening scheme similar to one developed by the Michigan State University nuclear physics group, who used DDK connectors in a large electromagnetic calorimeter. The fibers are surrounded by an 1/4" opaque sheath, INSUL #4900/3. We have developed a mold to surround the region at the connectors with a light-tight urethane boot. Figure 19 shows a light tight cable. Both the boot material and the tubing have passed the FNAL fire safety review. The urethane boot takes about 1/2 hour to cure, so that only ~ 5 molds are needed for production.

The final QC measurement tests the light transmission for each fiber in the connectors. This

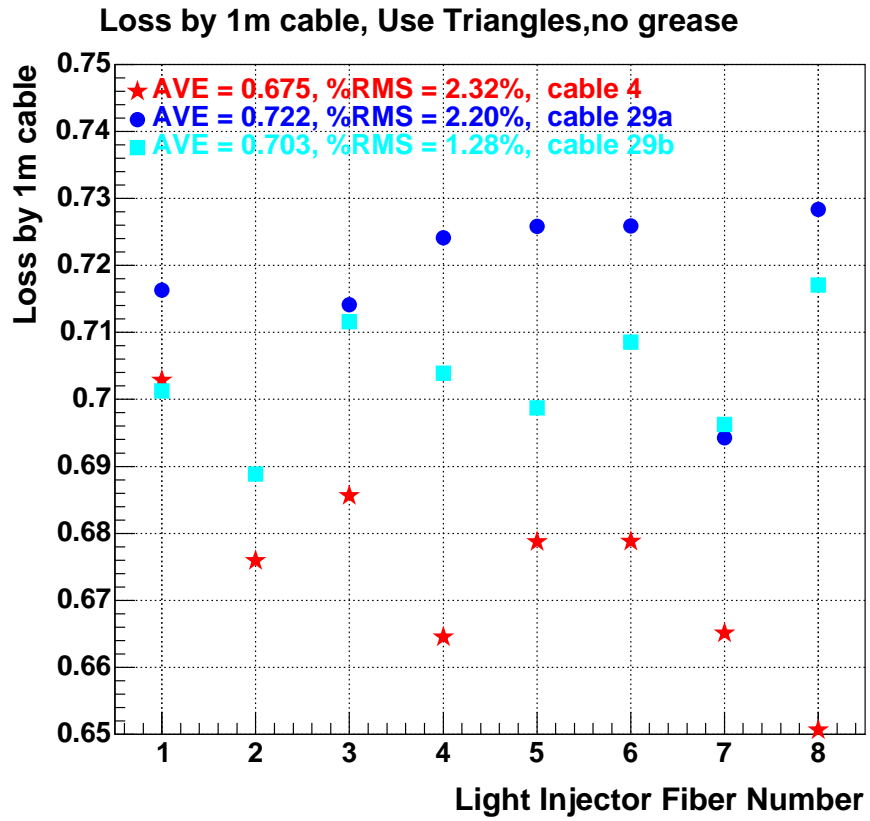


Figure 18: The measurement of the light loss from a 1 m clear cable. The average light loss from a 1 m cable is 30%



Figure 19: The light-tight boot for DDK connectors.

test uses a light injector box. This box has a LED with a pin diode for normalization. The LED shines on the fibers in a consistent way which can be normalized by the pin diode. Each cable is connected from this box to a readout box using optical jumper cable on both boxes. The jumper cables help to preserve the optical surface of both boxes by reducing the number of box connections. Fibers in the readout box go to individual pin diodes which are read out using a Keithley 6485 digital picoammeter. In order to bring the individual pin diodes to the Keithley we will use the Keithley 7001 high density switch system and a Keithley 7058 low current scanner card. A LabView program controls the automated readout procedure. Figure 20 shows the output of the cable QC for 14 R&D ODUs. The average of each channel is set to 1. Fibers varying more than certain amount from the average will have their cable rejected. In this case all fibers were fine. Note that, measuring 2 jumper cables connected together without the test cable will give us an additional handle. Fibers will be visually checked for breaks or cracks during and at the end of assembly.

For cables, two additional QC procedures are done. We check that the cables are light tight and check the fibers are connected in the correct order. The box which checks the cables are light tight consists of a PMT inside a light tight box. The PMT is readout by a picoammeter. The box has connections for both ends of the cable. We check to see if the PMT sees any light. A box with 8 different color LEDs checks the fiber order. Each fiber is lit up by a different color LED. We visually check that the fiber order is correct.

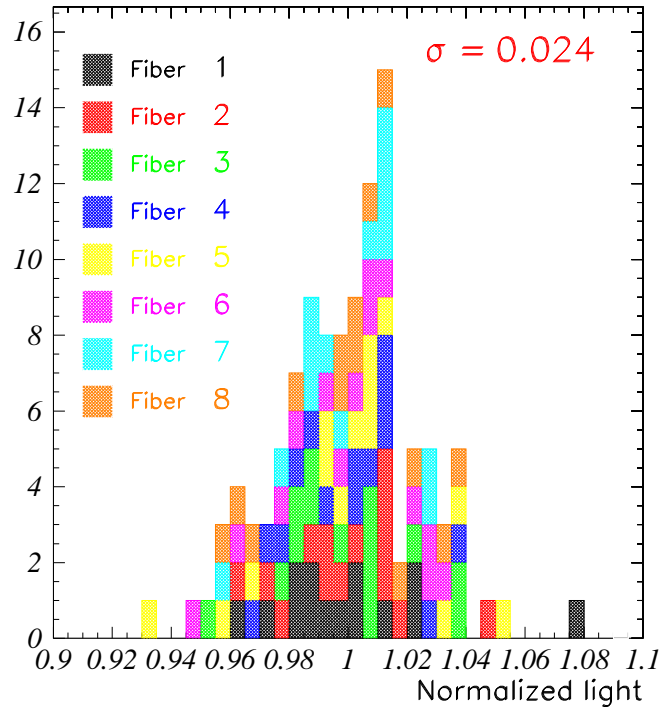


Figure 20: The QC results for R&D ODUs is shown. This uses the final Light Injector Box and Cable Tester Readout Box. A intermediate version of the final DAQ is used. Fourteen ODUs are tested. The normalization of the light for each fiber channel is determined by averaging each fiber channel and setting the average to 1 for each channel. The individual colors show the distribution of each fiber channel.

| Parameter | Description/Value | Unit |
|----------------------------------|-----------------------|------|
| Spectral Response | 300–650 | nm |
| Peak Wavelength | 420 | nm |
| Photocathode Material | Bialkali | |
| Photocathode Min. Effective Area | 18 × 18 | mm |
| Window Material | Borosilicate Glass | |
| Dynode Structure | metal channel dynodes | |
| Number of Stages | 12 | |
| Weight | 30 | g |
| Operating Ambient Temperature | -30–50 | °C |
| Storage Temperature | -30–50 | °C |
| Supply Voltage | 900 | V |
| Average Anode Current | 0.1 | mA |

Table 1: General properties of the R7600U phototube

3.3 Photomultiplier Tubes

Light from each of the $\sim 30,000$ scintillators in MINER ν A must be converted to an electrical pulse which carries accurate timing information and has an amplitude proportional to the energy deposited. This is done with photomultipliers (PMT's) of moderate gain and good linearity. To save cost, multianode PMT's with 64 pixels are used. The MINER ν A detector will require 473 PMT's. Each PMT sits in a steel tube called a PMT box (Sect. 3.3.1). The inputs to this box are the clear signal fibers (WBS 2) bringing light from the scintillators and 2 light injection fibers (Sect. 3.3.3) which will track the gain during the experiment. Fast analog signals are fed to front end boards (FEB's) which sit on top of the PMT box. There, the signals are amplified, digitized, and converted to a fast timing signal (WBS 7).

We will use the R7600-00-M64 multi-anode photomultiplier tubes from Hamamatsu Photonics. These are 2 cm x 2 cm, 8 x 8 pixel PMTs, i.e. 64 pixels with effective dimensions $2 \times 2 \text{ mm}^2$. The general properties of and manufacturer specifications for the R7600U PMT are listed in Tables 1 and 2. Additional specifications on the PMTs set for the MINER ν A application are listed in Table 3.

Since this is the successor to the PMT's used by MINOS, we have good experience on which to build. For the overall system, we require standard properties of mechanical strength, isolation from light, electronic noise, and magnetic fields, and excellent calibration techniques. Standard concerns with PMT's include dark current and gain uniformity. With multianode PMT's, linearity and cross talk must be carefully considered. Finally, alignment of the fibers with respect to the pixels is also very important. Selection criteria will be imposed based on the dark count rate, and pixel gain uniformity. Alignment methods and performance testing method will be discussed in Sect. 3.3.2.

3.3.1 PMT optical boxes of the MINER ν A detector

In MINER ν A, optical cables must carry the light signals from the inner and outer regions of the

| Parameter | Min | Typical | Max | Unit |
|---------------------------------------|-----------------|-----------------|-----|------------|
| Luminous (2856 K) Cathode Sensitivity | 60 | 70 | – | μ A/lm |
| Quantum Efficiency at 420 nm | – | 20 | – | % |
| Blue Sensitivity Index | 7 | 8 | – | – |
| Luminous Anode Sensitivity | 4 | 140 | – | A/lm |
| Gain | 5×10^5 | 2×10^6 | – | |
| Anode Dark Current | – | 2 | 20 | nA |
| Anode Pulse Rise Time | – | 1.4 | – | ns |
| Electron Transit Time | – | 8.8 | – | ns |
| Transit Time Spread (FWHM) | – | 0.26 | – | ns |
| Pulse Linearity ($\pm 2\%$) | – | 30 | – | mA |

Table 2: R7600U phototube characteristics at 25°C.

| Parameter | Min | Max |
|--|-----|---------|
| Single Anode Dark Rate | | 5000 Hz |
| Quantum Efficiency at 510nm | 12% | |
| Ratio of Gains of highest to lowest gain pixel | | 3 |

Table 3: Additional specifications for MINER ν A R7600U MAPMTs

tracking spectrometer and transport them to pixels of the the detector’s readout array of photomultiplier tubes (PMTs) [157]. Each PMT is housed in an individual light-tight cylindrical enclosure (“box”) made of steel. Each box provides the optical connection of fibers to PMT pixels in a way which ensures the crucial alignment. The boxes facilitate the routing of signal and voltage cables to-and-from the PMTs. Moreover they provide mechanical protection as well as significant shielding from ambient magnetic fields - the latter arising as result of proximity to the magnetized Near Detector of MINOS.

A new PMT box design has been developed for MINER ν A, the essential features of which are described below. The design incorporates features of two optical box implementations which have been serving the MINOS experiment very well. As will be elaborated, MINER ν A boxes accommodate one M64 phototube per box and so are more similar to “Alner boxes” of the MINOS Near Detector, rather than MINOS MUX boxes of the Far Detector (which serve three M16 PMTs per box). However, in contrast to Alner boxes, the MINER ν A design utilizes construction-standard steel extrusions to achieve fabrication economy and improved magnetic shielding. Fabrication and quality assurance testing of a total set of 550 optical boxes is required to fulfill MINER ν A’s immediate deployment need (473 boxes) plus its operational maintenance needs upon extended operation. (The latter includes the experiment’s need for hot spares and spare components, plus a small allowance for production wastage.) Manufacture of the optical box array and its delivery to the staging area at Fermilab will be carried out using two coordinated, independently operating assembly “factories” which are being set up at Tufts and Rutgers universities.

Functions of PMT boxes

PMT box functions addressed by the design developed for MINER ν A are listed below. Design aspects which relate to these functions are elaborated in the Sections following.

1. *Boxes provide precise alignment of signal fibers to PMT pixels:* Alignment is made using machined mounting cookies which capture the input fibers and press them onto the face of each M64 PMT; the PMT is held via a machined holder, to which the cookie mates in a precise way and with unique orientation.
2. *Boxes provide light-tight enclosures for the PMTs:* Each box consists of a hollow cylindrical steel hull with endplates at either end; each endplate is augmented with a gasket and RTV seals which ensure that no light can leak in from the outside.
3. *Boxes provide mechanical protection for the delicate and valuable M64 PMTs:* Construction-standard Fe extrusions are used to provide rugged and inexpensive enclosures.
4. *Boxes provide magnetic shielding for the PMTs:* Ambient magnetic fields exceeding 5 gauss can degrade PMT efficiency; ambient fields in spaces to be occupied by the detector have been measured and are in the range of 2 to 16 gauss. In the deployed orientation, axes of MINER ν A boxes will be nearly transverse to residual B-field from MINOS and will provide a factor ten field reduction from the box exterior to the inner, central location of the PMT.
5. *Boxes provide optical fiber and electronic voltage and signal routes to the PMT:* Routing of fibers and cables to/from the box interior is made via connectors and ports which breach the endplates.
6. *Boxes provide mounting surfaces for circuits of the Front-End Board (FEB):* Within a MINER ν A PMT box, a part of the FEB plugs directly into an electronics endplate feed-through board, while the remaining circuitry is housed in an aluminum tray positioned axially along the outside the the cylindrical hull.
7. *MINER ν A boxes provide the interface between the PMTs and the light injection (LI) calibration system:* Light from a reference LED is routed via optical fiber through the fiber feedthrough endplate of each box and terminates within the box in a diffuser piece. The PMT response to diffused light which is propagated through narrow area around the optical fibers as they threaded through the cookie, is used to monitor its performance.

MINER ν A PMT box mechanical design In the Alner boxes build for MINOS, the box enclosures were made from thin-wall plate, creased and welded into a rectangular box. In MINER ν A, an equivalent structure is obtainable more economically by utilizing construction-standard hollow steel extrusions of cylindrical cross-section. These can be capped by spot-welding of flanges onto each end, to which flat steel endplates can be screw-mounted.

A highly useful feature of the Alner boxes is that the metallic enclosure forms an outer shell from which the inner components can be separated. The latter are mounted on a rigid structural frame which is inserted along the axis of the rectangular enclosure. Using this arrangement, easy access to

all pieces which must eventually reside within the box, is available during assembly and alignment, e.g. the loaded cookie and its fiber bundle and the PMT-holder-base assembly. This same fabrication stratagem has been adapted for MINER ν A. In the latter implementation, four rigid mounting rods are attached to the interior side of the fiber feed-through endplate. The PMT-holder assembly has a receiving hole pattern which allows it to be slipped to the center of the rod frame. The unit thusly mounted can then be inserted axially into the cylindrical hull. These mechanical aspects are readily discerned in the photo of Fig. 21 which shows a partially assembled MINER ν A box prior to insertion of the frame.

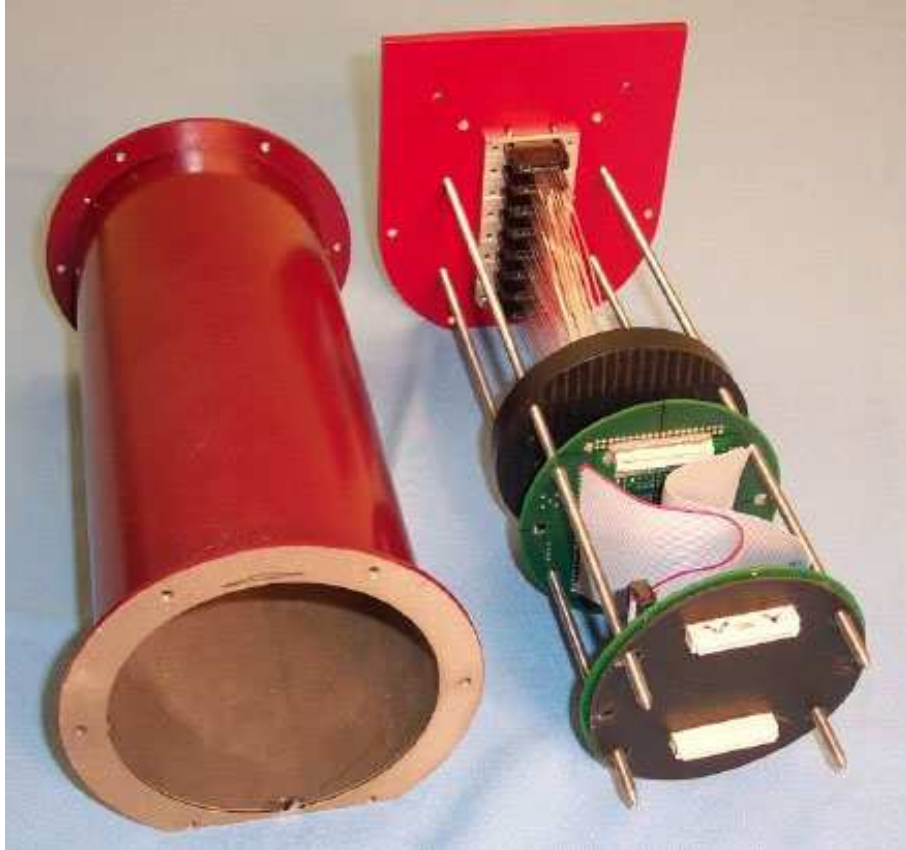


Figure 21: MINER ν A PMT optical box prior to assembly. The rod frame which holds the fiber cookie plus holder plus PMT (right) is inserted axially into the surrounding steel enclosure (left).

By using construction-standard steel extrusions, it is possible to have a relatively thick-walled box at modest cost; for MINER ν A boxes, wall thickness of 2.36 mm has been chosen. The result is a box which provides a useful degree of magnetic shielding for the inner region occupied by the PMT.

Alignment of fibers to pixels

Within each box, the enclosed PMT will be in optical contact with the polished ends of the bundled fibers which it reads out. This contact is made possible via termination of the fiber bundle with a precisely machined fiber mounting “cookie” - shown in Fig. 22 - which holds the polished

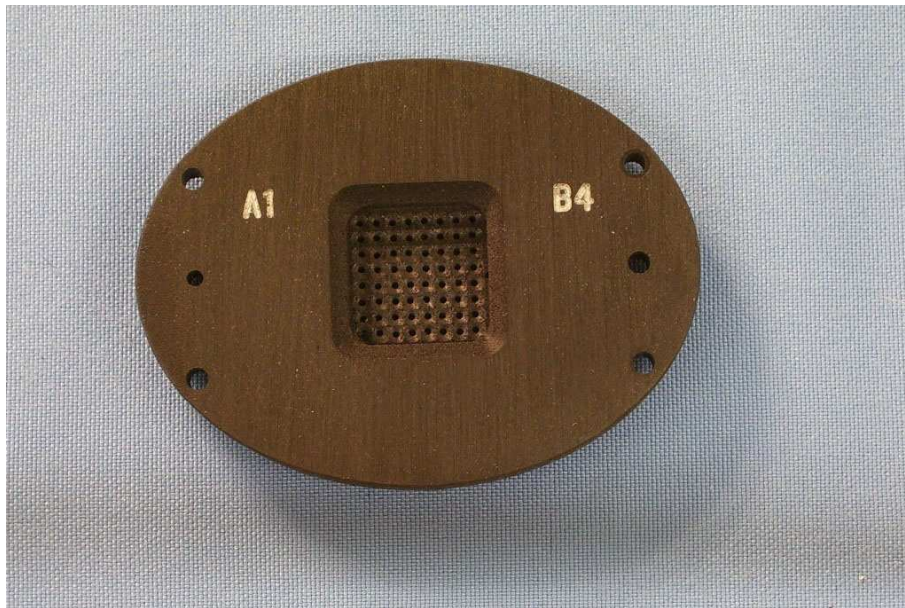


Figure 22: Optical fiber “cookie”. The hole pattern accommodates the sixty-four fibers which are routed to the box by eight fiber cables.

fiber ends. Registration of the fiber-loaded cookie to the PMT is mechanically precise. This is made possible by a precision mounting “holder” which captures the PMT and which receives the cookie; the correct positioning of fiber ends onto the PMT pixel pattern is assured via alignment pins on the holder. A holder piece is shown in Fig. 23. The fiber mounting cookie and the PMT holder are precision pieces CNC-milled from Noryl plastic. The cookie, precision holder, and their relation to the PMT, are indicated in the photograph of Fig. 24.

It is highly desirable to ensure that at the PMT pixel grid, signals originating at neighboring locations within the detector receive a degree of isolation; otherwise, pixel to pixel cross-talk can obscure the assignment of pulse heights to track hits. In order to provide a degree of isolation, a simple weave pattern is used in the routing of fibers onto the cookies. The weave pattern is a “row-pair interleave weave”; the fiber-to-pixel association which it introduces is shown in Fig. 25.

Box endplates

As indicated previously, each end of the box hull is closed off with a steel endplate. Connections to the box interior are made via various connectors and ports which breach the endplates. The box interior layout with endplate connections can be seen in the cutaway view of Fig. 26.

All of the electrical connections are brought through one endplate (the “electronics endplate”), whereas the optical fiber connections and also the connection to the LI diffuser are brought through the opposite endplate (the “fiber feedthrough endplate”). Consequently the endplates are quite different, and the implementation of light-sealing is different. At the electronics endplate, the light seal is made via a thin-rubber gasket. The fiber feedthrough endplate however, is mechanically more complicated due to the port arrangement needed for eight separate fiber cables. On the interior surface

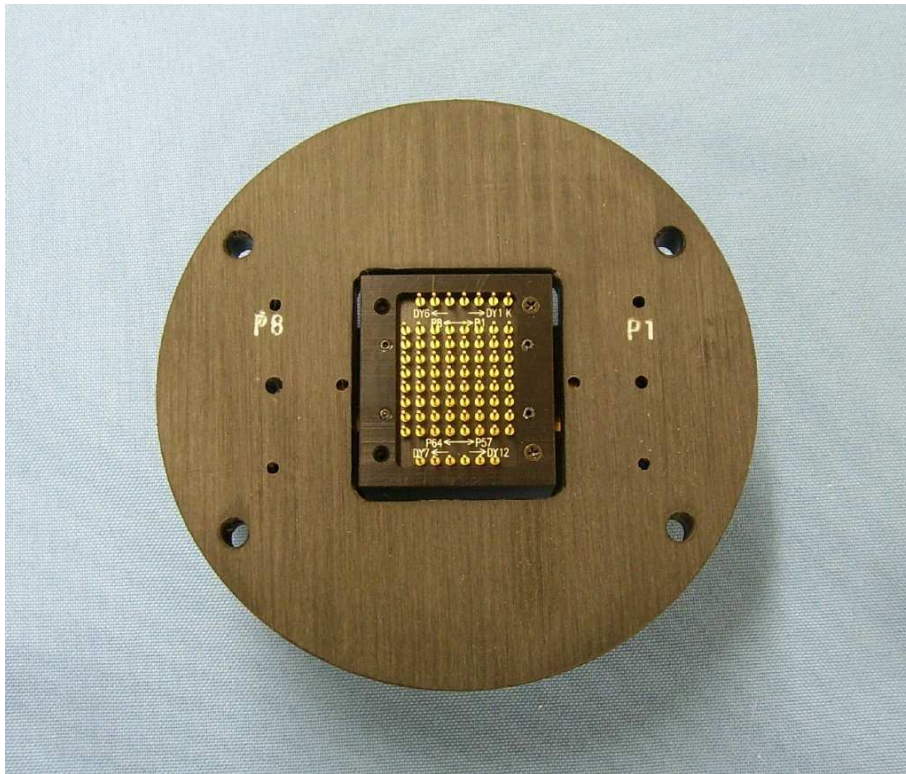


Figure 23: The precision PMT holder. The PMT is held so that its pixel grid relates to the holder locating pins in a precise and reproducible way.

of this endplate, sets of small aluminum clips with pins are used to secure the eight plastic box connectors. Light sealing of the plate is accomplished using a sealing compound which is poured into a cavity on the outside of the endplate. The feed-through box connectors can be seen in the foreground of the photograph of Fig. 27. The sealing cavity, prior to epoxy-loading, is also clearly visible.

Box magnetic shielding of the PMT Measurement of the magnetic fields in Near Hall regions immediately upstream of MINOS was carried out by M. Bonkowski [158]. An ambient magnetic field of five gauss exists throughout the area to be occupied by the MINER ν A detector. In the space immediately downstream of MINER ν A and in front of the first magnetized plane of MINOS, the ambient field will be larger; the measurements show ten gauss at the downstream end of MINER ν A, increasing to 21 gauss within a few inches of the MINOS front plane. Ambient field of the latter magnitude, if it were to pervade the volume occupied by MINER ν A's M64 PMTs within their optical boxes, could be deleterious to phototube performance. Measurements of M64 response to magnetic field are provided by Hamamatsu; it is observed that PMT output is reduced to 92% in the presence of an axial magnetic field of five gauss (Hamamatsu curves are reproduced in Ref. [159]. Consequently it is required that MINER ν A PMT boxes provide, in addition to a light-tight enclosure, an environment for the PMT which is well shielded magnetically.

This goal is achieved in the MINER ν A design as the result of two features: Firstly, the wall of the



Figure 24: Photograph shows a fiber-loaded cookie, oriented towards the face of the precision holder onto which it is to be mounted using alignment pins. The PMT plus its holder - shown on the right - is affixed into the holder (at the PMT testing sites) in a way which relates the PMT pixel grid to the locating pins of the holder.

box cylindrical hull is made of 2.36 mm steel; this is distinctly thicker than either of the MINOS box implementations which have adequately provided magnetic shielding for PMTs deployed in environments similar to MINER ν A's Near Hall location. Secondly, cylindrical containers are especially effective in shielding from ambient fields provided that the cylinder axis is transversely oriented relative to the ambient field direction. The latter situation is in fact the case for deployment configuration planned, wherein the cylindrical box axes are oriented transversely and radially with respect to the spectrometer's central axis. In this orientation, PMT box axes are everywhere roughly transverse to the ambient toroidal field arising from the MINOS coil current. An additional design feature, which has been thoroughly explored using Hall probe measurements (see below), is the capability of each box to readily accommodate a mu-metal foil insert should it prove necessary. The foil insert is to be wrapped cylindrically, so that it defines an interior volume within which each PMT resides. The foil acts like a conducting path for B-field lines, drawing them away from the PMT and routing them around it.

Magnetic shielding capabilities of the MINER ν A PMT box were examined by placing an assembled box in various orientations within 20 gauss ambient B-fields created using Helmholtz coils. A Gaussmeter with axial and transverse Hall probes was used to measure the leakage field pervading the box interior. It is observed that the MINER ν A box provides a field reduction factor (outside/inside-center) of about ten when the box axis is oriented transversely to the external B-field; in the most unfavorable orientation - box axis parallel to ambient \vec{B} - the reduction factor drops to four. With the introduction of a mu-foil inner surface, the reduction factor with unfavorable box orientation is increased from factor four to factor ten. Fortunately, the magnetic shield provided to MINER ν A

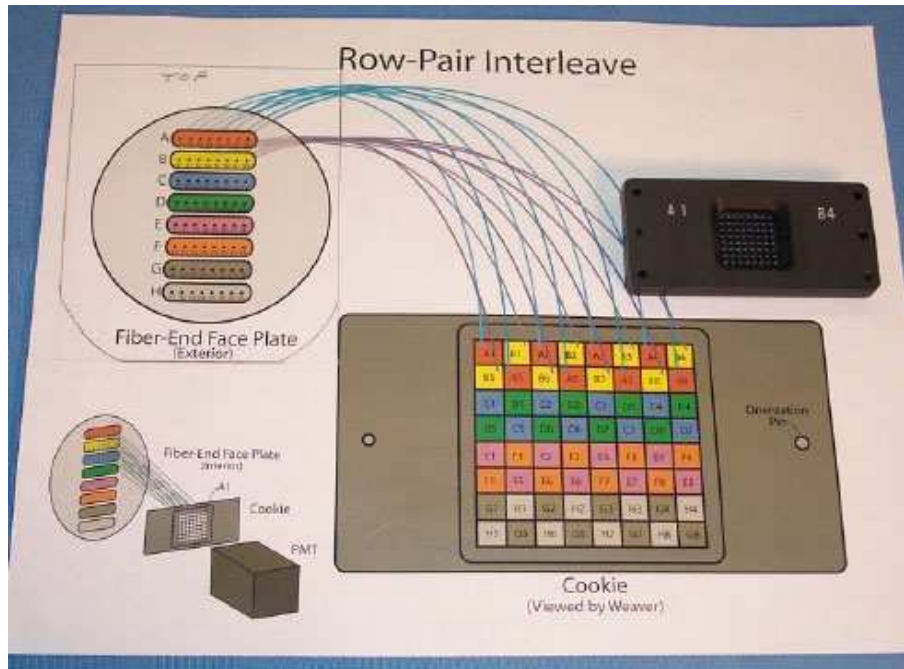


Figure 25: The weave used in placing optical fibers into the cookie grid. The resulting row-pair interleave pattern is designed to minimize signal reconstruction confusion arising from pixel-to-pixel cross-talk.

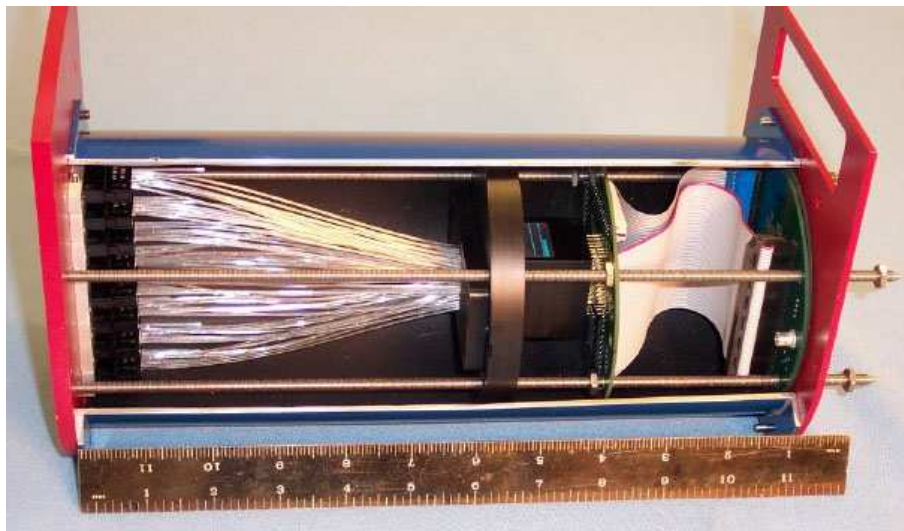


Figure 26: Interior structure of an optical box: Optical fibers enter from the outside via connectors through the fiber feedthrough endplate (left side) and terminate on the cookie. The pixel grid of the M64 phototube is registered to the cookie hole pattern via precision mounting pins which are part of the PMT holder. Cables provide voltage and signal connections to the PMT from connectors which breach the electronics endplate (right side).

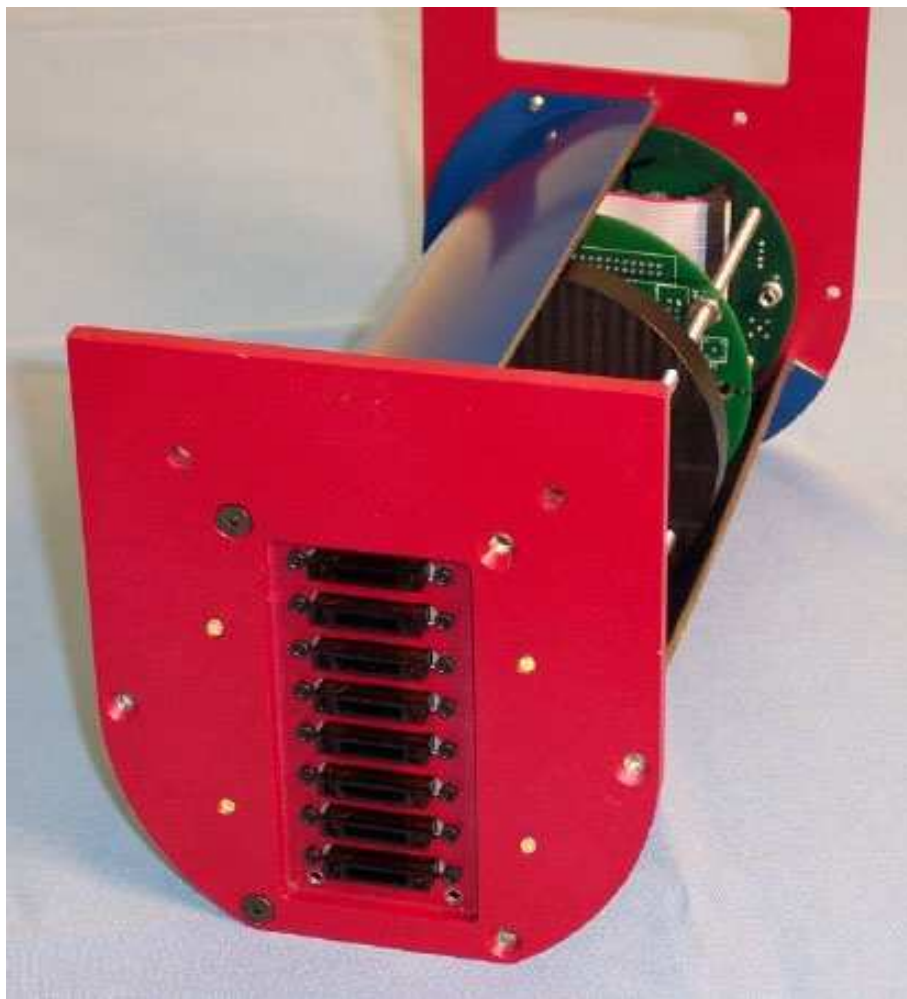


Figure 27: Fiber feed-through endplate - exterior view.

PMTs appears to be sufficient in either orientation and without the mu-foil augmentation, provided that the MINER ν A detector is operated without its own magnetic field. Details of magnetic shielding measurements with the MINER ν A box design can be found in Ref. [159].

Mounting the box array on the detector Each MINER ν A box has two steel mounting pins which are welded to the fiber-feedthrough endcap. The pins allow each box to be loaded - with fiber connectors radially inward, electronics endcap radially outward - into a structural framework mounted atop the spectrometer's two upper/outer surfaces. The framework provides a standoff space from detector surfaces to facilitate fiber cable routing and their connections to the PMT box array. The mounting arrangement positions the circuits and connections of the signal Front-End boards on the elevated, outer surfaces of the boxes, thereby facilitating access to them for diagnostic work and for repair. The layout is designed to allow rapid removal and replacement of individual PMT boxes, should that be needed during running of the experiment.

Factory production Mass production and checkout of PMT boxes requires that dedicated factory fabrication areas be set up. Moreover, frequent utilization of modern, staffed machine shops is a prerequisite for timely box array manufacture. In MINER ν A these resources - in the form of dedicated university shops - are available at two factory sites which are being developed at Tufts and Rutgers universities. The factory sites will operate concurrently and independently. In steady-state operation, each factory will produce functional boxes at a rate of approximately one box per working day. Workstations are being deployed at the factories which will carry out the following:

1. Machining of precision PMT holders and fiber mounting cookies (Tufts).
2. Machining of box endplates and flanges.
3. Spot-welding of endplate flanges to cylindrical hulls.
4. Electrostatic painting of box cylinders and endplates.
5. Optical fiber weaving into cookies and epoxying.
6. Cutting and polishing of fiber-loaded cookies.
7. Quality assurance (QA) testing of assembled PMT boxes.



Figure 28: A loom rig is used to thread optical fibers into cookies according to the weave pattern of Fig. 5. The central assembly is mounted so as to maximize hand access. Vertical struts on either side accommodate stabilizing supports (preferred by some operators).

Instrumentation has been designed for each workstation to facilitate execution of the task at hand. For example, the weaving and epoxying of optical fibers into cookies (task 5 above) is greatly facilitated by use of a “loom rig”; the current prototype is shown in Fig. 28. The rig holds a set-of-eight ODU cables and their fibers optimally for ease in implementing a weave.

Tasks which involve weaving of cookies, mounting of components into the endplates and onto the internal frame, final assembly of boxes and their QA testing, will be carried out in clean room assembly areas. Factory daily operations, from arrival of parts to shipment of completed boxes, will be monitored and progress will be recorded in a web-accessible database.

Assembled optical boxes will be shipped by commercial trucking to Fermilab. For this purpose, shipping containers will be built which accommodate forklift handling and which will hold a convenient (large) number of boxes.

3.3.2 PMT Alignment and Testing

The Hamamatsu multianode PMT (R7600U-00-M64) was selected for use in MINER ν A. This type of multianode PMT is an incremental design improvement from the R5900-00-M64 phototubes used in several high energy experiments, including the MINOS near detector. The R7600U-00-M64 PMT meets the design requirements of the experiment (to be elaborated below); the high density maximizes the channel/\$ ratio.

Alignment The first task of the James Madison University (JMU) group is to align each PMT channel with its corresponding optic fiber. The actual part number delivered by Hamamatsu is H8804-MOD2, which consists of the actual PMT epoxied in a rigid jacket or housing. This packaging, while saving a couple of manufacturing steps (manufacturing the jacket and gluing the PMT in it), does not eliminate the need of aligning the PMT pixels with respect to the optical fibers. The MINER ν A PMT optical boxes (see Sect. 3.3.1) contain precision-machined mounting cookies which capture the 8×8 array of optic fibers and press them on the face of the PMT. The optical fiber cookies are precision-mounted to the PMT holder using alignment pins. To ensure the unambiguous orientation of the cookie with respect to the PMT holder, different diameter pins are used. The only degrees of freedom allowed are between the PMT holder and the jacketed PMT.

Each PMT has 4 alignment “dots” provided by the manufacturer. Regular cookies are opaque making difficult to use for alignment purposes. A special, transparent cookie outfitted with cross-hairs will be used instead. A schematic of the alignment stand built at JMU is shown in Fig. 29. The PMT is held by the (green) holder shown in the middle of the picture, mounted on top of a set of X-Y- ϕ stages. The alignment cookie is fixed to the top plate of the device (shown in gray). The PMT can be moved using the stages with respect to the cookie-PMT holder assembly. A high resolution digital camera (Nikon...) is used to visually check the alignment. Based on the resolution of the camera we estimate that we can obtain a $10 \mu\text{m}$ alignment precision. The PMT holder has holes drilled and tapped for 4-40 screws that are used to “lock-in” the alignment once the PMT is properly positioned. These screws pass through slightly oversized holes drilled through the “ears” of the PMT jacket. A picture of the alignment station at JMU is shown in Fig. 30.

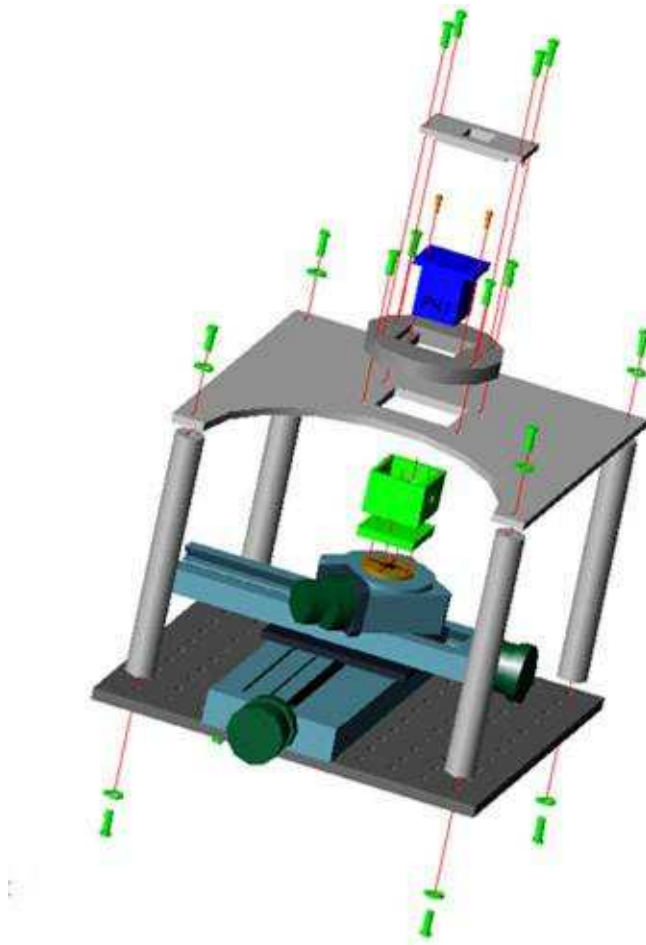


Figure 29: Schematic of the Alignment Stand

PMT Testing Once aligned, each phototube will be subjected to a series of tests to determine its suitability for use in the experiment. These tests are designed to complement and augment the testing done “in-house” by Hamamatsu and are driven by the physics requirements of the experiment.

To further understand the real meaning of some of the figures listed in Tables 1 and 2 we asked the Hamamatsu representatives to elaborate on the tests they conduct prior to delivery of PMTs. Hamamatsu tests all PMTs shipped and provides a data-sheet for each PMT that includes S_k (cathode sensitivity in $\mu\text{A}/\text{lm}$), S_p (anode sensitivity in $\mu\text{A}/\text{lm}$), dark current, Blue Sensitivity Index, and Gain (calculated from S_k, S_p). Dark current information is provided on our final test data sheet shipped with the PMTs and at no additional cost/delivery time. But, the dark current value is a total value and is not specific for each anode. Gain is calculated using the S_k and S_p values provided on the final test data sheet. $\text{Gain} = S_k/S_p$ and this value is provided as well. Hamamatsu will provide a relative gain versus channel map and will guarantee no deviation outside the MINERvA specification of 3:1.

As seen from the above, Hamamatsu Photonics is mostly concerned with obtaining numbers that globally characterize their product. While this type of information is suitable for rejecting defective

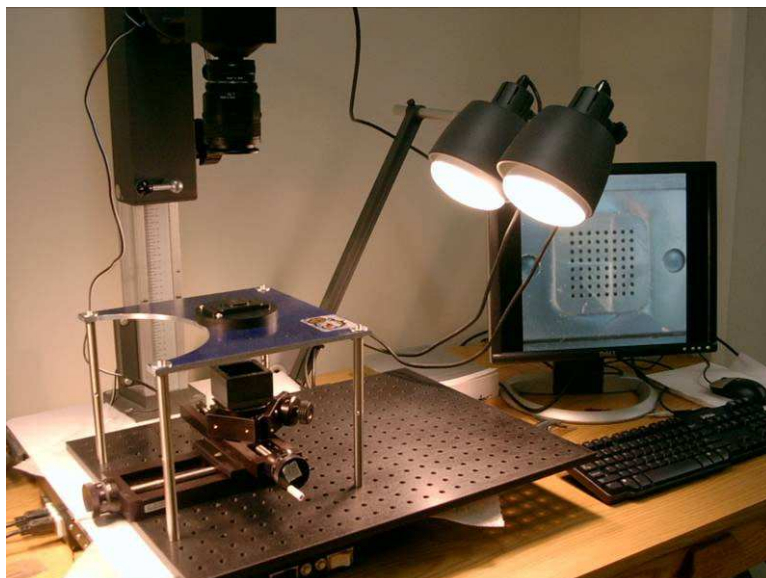


Figure 30: JMU Alignment Stand

PMTs, it does not provide the channel-by-channel data needed for MINER ν A use. As outlined in the next section, the MINER ν A collaboration will build a test stand enabling us to perform these more detailed tests.

The Test Stand The MINER ν A test stand will be designed to test 5 PMTs at a time. Automation will allow a complete series of tests which will last less than 24 hours for a batch of 5 PMTs. The test stand will use 448 (= 7 x 64) channels of MINER ν A electronics, and will assume a DAQ rate of 500 Hz and integration time of 12 microseconds. The conceptual design of the test stand is shown in Figs. 31 and 32.

The test stand will consist of:

- a) Frame: A relatively light frame which will consist of two separate sections that fit precisely together. Fig. 33 shows two views of the frame. The upper part will hold the light injection manifold. The lower one will have a plate on which several parts will reside: the traveling stages, the LED, the filter wheel, and the monitoring PMT. The relative alignment of the two frames is important to ensure that the light pen travels in x-y-z directions matching the positions of the fiber bundles. This arrangement of the support structure in two sections allows for easy transportation of the assembled test stand.
- b) Fiber optic light injection manifold: this is placed in the upper section of the frame. It will provide light from an LED to 6 M64s, one of which will be permanent and will serve as a reference PMT. The concept is shown in Fig. 32. The upper plate will hold 6 cookies+PMT's and the lower plate will route fibers illuminated by the LED to the PMT's. Each cookie will accept a bundle of 64 clear fibers, each 1.2 mm in diameter (same as will be use for scintillator

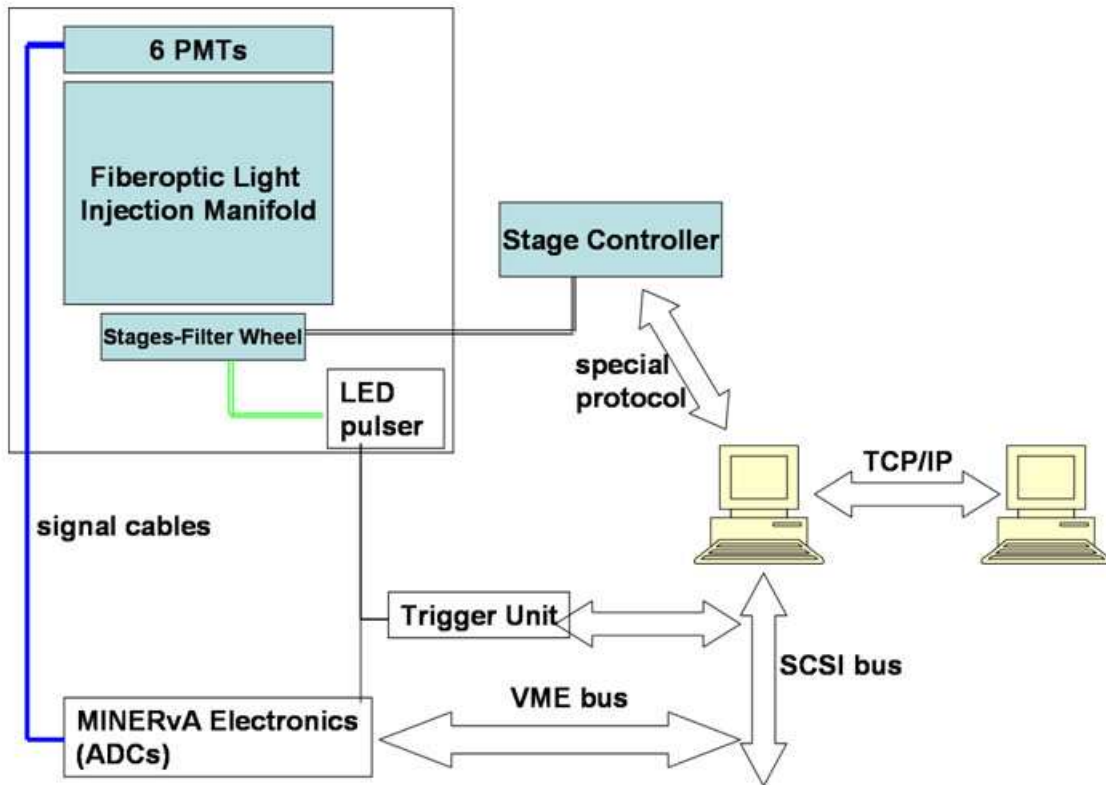


Figure 31: Schematic of the Test Stand

signals in the experiment). The lower plate has 64 holes, each of which can be illuminated by the LED. Each hole holds 6 fibers which are routed to the same pixel in each PMT in the upper plate. Thus, 64 bundles of 6 clear fibers each will emerge from the lower plate and they will get reorganized into 6 bundles of 64 fibers to match the PMT. Each LED position will send light to 6 pixels and when the LED has been in all 64 positions all 6×64 pixels will have been illuminated.

- c) A system of x - y - z stages carrying an LED light pen which injects light sequentially to all 64 fiber bundles. The LED travels with the system, so that no changes to the optical readout system (e.g. fiber bending) occur during the movement from bundle to bundle. The stage motion will be controlled by the DAQ PC. The LED light will go through several feet of WLS fiber to emulate the frequency distribution from the real detector. A light diffuser in each hole in the lower plate will send light uniformly to all 6 clear fibers. Before the light reaches the light pen it goes through a set of 7 neutral density filters mounted on a filter wheel controlled by a moving ϕ stage. This enables the study of the PMT response versus light intensity. A light monitoring PMT will sample the light intensity prior to injection.

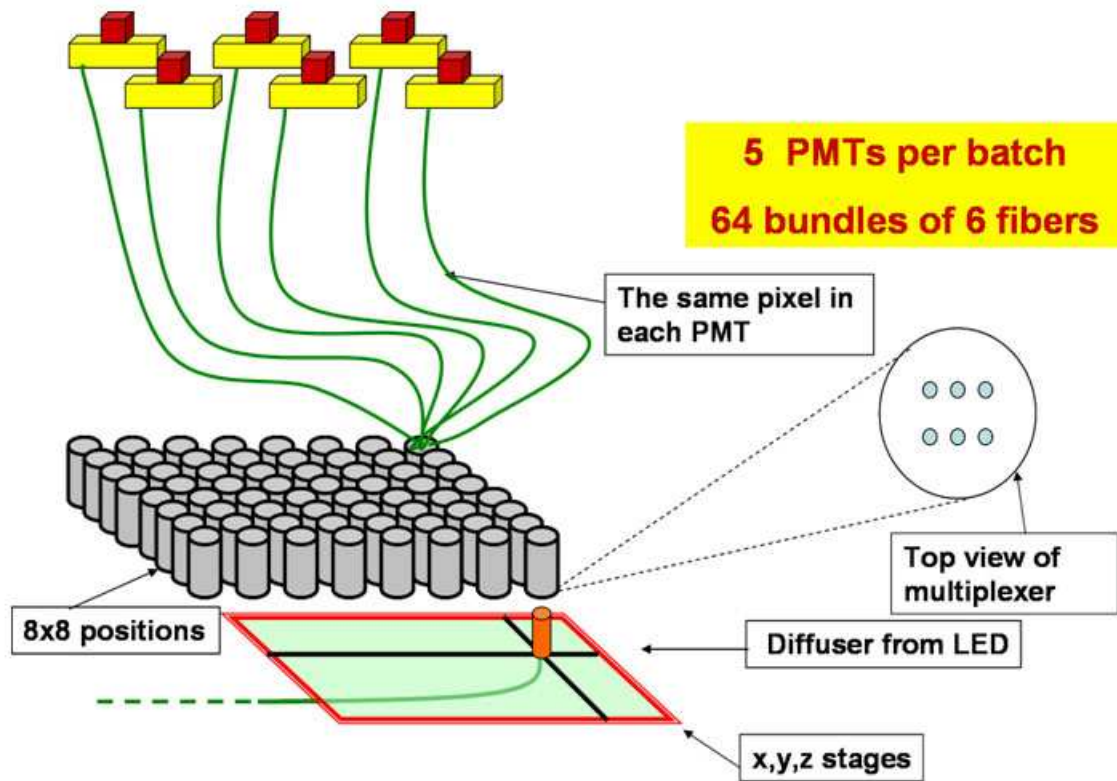


Figure 32: Schematic of the fiber optic injection manifold.

- d) MINER ν A Electronics: The signals from the M64s are amplified and digitized in the same front end boards (FEB's) as will be used in the experiment. The data is then read out through VME. to the DAQ computer.
- e) Trigger: A computer controlled trigger unit will trigger the LED pulser and will provide an integration gate for the ADCs.
- f) Data analysis PC: this computer will receive the data from the DAQ computer via TCP/IP connection. Analysis done here will provide monitoring data, histograms, tables, and summaries; it will build the information that will be stored the data base.

Athens and Fermilab are responsible for the design of the test stand. The frame was constructed at Fermilab. The mounting plates and cookies were done by Tufts. The fiber-optic 64 to 6 distribution is will be done by Rutgers and is expected to be complete by the end of October, 2006. . The overall assembly of the system, including MINER ν A electronics, DAQ, software, and commissioning will be done by Athens. After successful initial operation the test stand will be installed at JMU for the testing of the MINER ν A PMTs. The PMT alignment will be done at JMU before the PMT's are



Figure 33: The test stand frame.

mounted to the test stand.

Initial Tests Each PMT will be subject to a series of short/quick tests. These tests will determine the optimum operating point via a high voltage scan. The optimum operating setting will have a gain of about 3×10^5 and a good one photoelectron resolution. Also at this stage we will look for dead pixels as well as grossly misaligned PMT assemblies.

Dark current The main concern is that high dark noise leads to unacceptable dead time and/or large event size. A dark noise pulse (defined as the signal produced by the PMT when no light input is present) produces a ~ 300 ns dead time, evenly split between the integration time and the reset time. This represents a 3% dead time for the whole PMT (assume $10\mu s$ beam pulse). For a 1 kHz dark noise rate the probability of having a dark noise pulse during the $10\mu s$ beam pulse is 1%. Overall this amounts to a 0.03% dead time, assuming all tubes have the same dead time rate. Past experience (MINOS) with M64 phototubes shows that only 5% of tubes exceeded the 1 kHz rate. For MINER ν A we propose to test/reject tubes that have a dark noise rate of 5 kHz in any pixel. The summed rate for the full PMT will have a higher limit.

Testing procedure The high voltage on the PMTs will be set to the nominal operating point and the system will be kept in the dark for 1 h. During this time (and the rest of the test) the temperature will be monitored/kept constant to within $2\text{ }^{\circ}\text{C}$. The DAQ will be pulsed and $\sim 10\text{ M}$ events will be accumulated. Counting how many times the integrated charge was greater than the $1/3$ p.e. threshold will provide a measure of the dark current.

Linearity Non-linearity in the PMT response (energy vs. npe curve) leads to inaccurate energy measurement, possibly affecting particle identification. Observable non-linearities of the signal may result from space charge effects due to the small size of the M64 dynodes. One should expect to see non-linearities in the PMT response for large input signals. The MINOS experiment found non-linear effects starting at 70–300 pe, phototube dependent. Hamamatsu Photonics quotes a 5% deviation at 0.6 mA, which corresponds to ~ 87 pe assuming typical MINER ν A conditions (~ 7 ns pulse width and 3×10^5 gain). The typical MINER ν A signal will produce ~ 5 photoelectrons/MeV. Electromagnetic showers deposit about 20 MeV per detector element (extruded triangular prism), for a total of ~ 100 photoelectrons. The largest non-linear effects documented by MINOS were of the order of 10% at 300 pe. Even assuming a worse case scenario of 10% non-linear effects at the expected 100 pe, a modest measurement (20% accuracy) will help keep this uncertainty at a 1-2% level.

Testing procedure A remotely controlled filter wheel will vary the light intensity received from the LED. The data set will comprise of 10,000 pulses/pixel for each light intensity level. By first measuring the tube's response to a preselected reference level, say 12 p.e., the expected response, based on an assumption of linearity, may be calculated as a product of the incident light intensity, the gain, and the pixel efficiency. The incident light level is determined from the relative opacities of the filters between the reference and current points. The ratio of the measured/expected charge, when plotted over the expected dynamic range for MINER ν A, will indicate the PMT's linearity.

For this test to be useful, the test stand setup must be a good match to the actual experiment. We will use the same cookie, PMT, and electronics as the experiment. The blue LED will be triggered with a fast pulser to match the experiment and a few meters of WLS fiber will shift the frequency spectrum to approximate what we will see in the experiment.

Phototubes are expected to be linear within 1% up to 80 pe. The accepted PMTs will be further tested up to 400 pe and the best tubes will be selected for the central region of the detector.

Inter-pixel cross talk For the purpose of this document cross talk is defined as the process in which one pixel of a PMT provides a measurable output when other/adjacent pixel(s) is/are illuminated. This mechanism gives incorrect energy measurements and deteriorates the position resolution (if between adjacent detector elements). Both of these affect pattern recognition/particle identification and further complicate tracking. The origin of cross talk are either electrical (charge leakage during amplification from one channel to another) or optical (light from one fiber ends up on a different pixel).

The MINOS experiment found the electrical cross talk to be small, consistent with the 2% value quoted by Hamamatsu Photonics. The amount of electrical cross talk to nearest neighbors is less

than 0.5%.

Optical cross talk is potentially more damaging, as it affects the position resolution and thus tracking. Misalignments between the PMT and its holder would result in large cross talk effects, although gross misalignments should be easy to spot. This type of effect is more important for minimum ionizing particles, where the overall number of photoelectrons is small (10 pe for MINER ν A). For these kind of yields an extra pe causes an error of about 10% in position resolution (about 2 mm). Optical cross talk is minimized in MINER ν A using the weave-pattern described in Sect. 3.3.1 (adjacent triangles are mapped to diagonals on the PMT face).

Testing procedure Each individual pixel will be pulsed with an amplitude of about 30 pe for 10,000 pulses. The cross talk observed should be less than 5% of the primary signal for diagonally opposite pixels and less than 10% for adjacent pixels. The procedure will be repeated (with less counts/setting) for two more intensity levels.

Pixel-to-Pixel Uniformity The average gain for MINER ν A will be around 3×10^5 . Individual pixels will exhibit larger or smaller gains. These variations need to be contained so as to not exceed the dynamic range of the MINER ν A electronics. It is anticipated that the MINER ν A electronics could accommodate a 3:1 range. Previous testing done by MINOS found very few tubes exceeding this limit. The 3:1 pixel-to-pixel gain variation limit is explicitly requested in the contract with Hamamatsu Photonics and will be tested for each tube.

Efficiency Low efficiency tubes will adversely affect the photon statistics. This is especially important for minimum ionizing particles where the experiment cannot afford significant decreases in efficiency. Hamamatsu Photonics gives a typical value of $70 \mu\text{A}/\text{lm}$, with a minimum efficiency of $60 \mu\text{A}/\text{lm}$. Our preference would be to request that all tubes have at least $70 \mu\text{A}/\text{lm}$ luminous cathode sensitivity.

The MINER ν A PMT test stand does not provide a method for measuring the absolute quantum efficiency (QE) of the PMTs. However, the procedure outlined below can measure an “effective efficiency”, i.e. the product of the QE and charge collection efficiency, integrated over the whole light spectrum of the diode/fiber combination.

Testing procedure The monitor PMT will be used to correct for variations in the light input to 1 % or better. This correction will make possible comparisons between the numbers of photoelectrons detected on a pixel/phototube basis. These effective efficiencies can be subsequently normalized to one/few PMTs for which the manufacturer provides an absolute efficiency curve(s).

Summary The tests listed above will take an estimated 24 hours for 5 PMTs, including setup (loading and unloading PMTs) and data analysis.

3.3.3 Light Injection Calibration System

Any particle physics experiment with a large scintillator system such as MINER ν A needs a rapid, simple, cost effective monitoring system. MINER ν A has over 30,000 scintillators that must be installed, monitored, and at times replaced. The scintillators are read out with wavelength shifting (WLS) fibers which are joined to clear fibers that direct the light to Hamamatsu M64 phototubes. The PMT's sit in an iron PMT box. Confronted with the same problem, MINOS chose to inject LED light into the WLS fibers at the detector [160]. When injecting light directly into scintillators, nitrogen lasers are also used, e.g. at CDF. Our plan is to inject LED light into the PMT box, a simple and robust light injection (LI) calibrations system. The LI system is presently in the prototyping stage. Although we have a preliminary design, features are still being defined.

Function of Light Injection System

- The main application will be during installation and maintenance periods. A rapid check for dead channels and an accurate measurement of the gain of each PMT will be an important requirement.
- We also anticipate regular tests while taking data to supplement the calibration data coming from muons traversing the detector. In the MINOS near detector hall (where MINER ν A will be located), the temperature is held constant to within a 6.5° range and the diurnal variation of about 1° is seen [161]. Thus, monitoring doesn't need to be continuous, but will be important whenever detector conditions change significantly (e.g. during detector maintenance, certainly when replacing phototubes.)
- A system such as this could also be used to measure the absolute gains non-linearities of each pixel in situ. This property will be measured as part of the PMT testing at JMU and Athens. The cost and complexity of doing a similar test with this system were deemed too large.
- As this is a moderate resolution experiment, the physics requirements are not thought to drive the design at present.

LI System Design Our design is a simplified version of the MINOS system. To keep costs down, we choose to inject LED light directly into the PMT box, some of which will be captured by the multianode PMT. Each PMT is serviced by 2 fibers to ensure that each pixel is uniformly illuminated. The light is spread out in the PMT box with a diffuser (see Fig. 34). This will enable a rapid and accurate gain check for the entire PMT.

The LED's sit in a Pulser Box near the detector; it is the most expensive part of the system. This box is presently being designed. It contains optical fanouts, the LED's and associated electronics. PIN diodes will be used initially to monitor the LED light output. They will be close to the Pulser Box. The output of this box will be $2 \times 500 = 1000$ fibers funneling light to the PMT boxes and the PIN diodes. The light from each LED will be fanned out to 50 PMT boxes in a cone/collar assembly similar to what MINOS used [160]. Thus, 20 LED's are expected to be enough to cover the full set

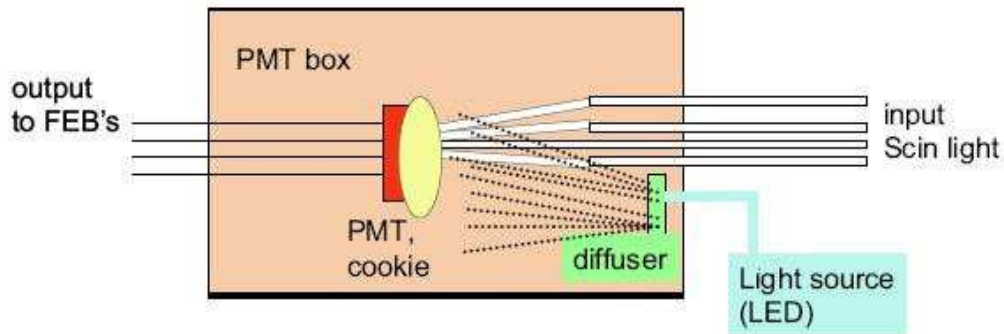


Figure 34: Conceptual picture of the way light will be injected into the PMT box. A simple prototype of this technique is discussed.

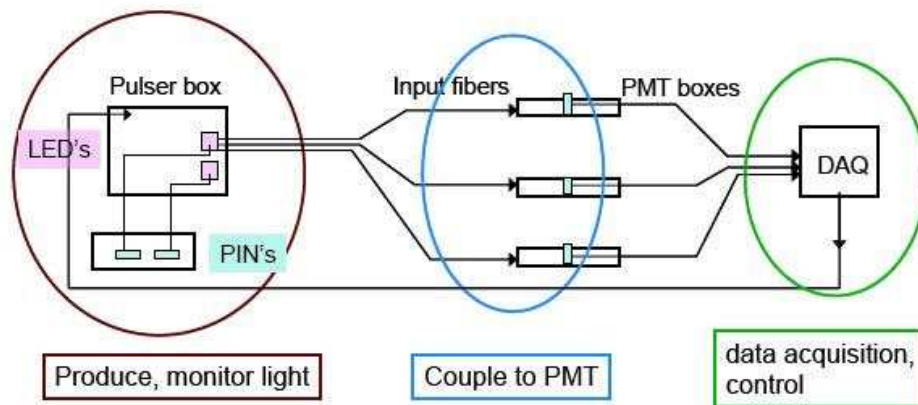


Figure 35: Design of the LI system. The DAQ computer will control the pulser box which will send out short pulses to each PMT. The response will then be read out.

of 473 PMT's and the PIN diodes with a sufficient number of spares. It is clear that the mechanical stability of these components is essential.

A diagram of the system is shown in Fig. 35. The entire system will be controlled as part of the MINERvA experiment data acquisition program. Groups of PMT's will be pulsed together (like MINOS) and all PMT's and the PIN diodes will be read out each time the calibration system is triggered.

The electronics required to control the LED's are not complicated. MINOS made 3 cards for power, LED driver, and control functions. A microprocessor on the control card will determine how the LED is fired - e.g. pulse height and width. We will start with the MINOS electronics and adapt to our needs. A very fast pulser (width stable at ~ 10 ns) will be required to simulate the scintillator output signals. The overall cost is low when compared with the MINOS system.

The MINOS light injection system achieves $\sim 2\%$ accuracy with careful attention to construction details and a PIN diode to monitor the LED output. Although we don't need as much accuracy, we

can easily obtain few percent accuracy with the system envisaged. The main usage for this system will be to monitor the overall gain of each PMT. At present, we plan to inject green LED light into the ends of a clear fiber. This will provide a moderately good match to the frequency spectrum of light from the scintillators.

Construction Prototyping efforts to date have measured the ability to inject LED light into clear and WLS fibers. Green LED's couple well to either kind of fiber when the light is directed into the end of the fiber. For this test, the light transmitted through the fibers was measured with a PIN diode. We have also used the LED to trigger an M64 PMT in 2 realistic situations in a dark box (see Figs. 36 and 37). In the first test, light from the green LED triggered with a $4V \times 100ns$ pulse produces a few pe signal in each PMT pixel using a prototype cookie. We have verified that at least 95% of the light reaching the PMT comes through the cracks between fiber and cookie. This test showed the need for small changes in cookie and PMT mount design to better protect the PMT from light other than what comes through the cookie. The second test (see Fig. 37) takes light from the same green LED as used in the first test. Using a cone/collar assembly from MINOS[163] (seen at the left side of the photo), light was fed through a clear fiber and aimed at the PMT in the approximate position the fiber will be located on the input plate to the PMT box. The light has to find its way through a 'forest' of 64 fibers simulating the real situation. The response for pixels on the far side of the forest was about a factor of 3 less than for pixels on the near side. When we added a diffuser (as seen on the right side of the photo), the response of all pixels showed less than 20% variation. This proves the concept in Fig. 34. Modifications to the PMT box are now complete.

Preliminary versions of the cone assembly are now being tested with the goal of defining properties of the LED and the density of clear fibers in the collar. We have purchased a fast pulser and will investigate LED's for speed, intensity, and stability. The light reaching the PMT's should not vary by more than a factor of 2 across the full set. We plan to complete prototyping efforts by end of 2006.

3.3 Calorimeters and Targets

One of the main goals of MINER ν A is to improve the estimate of the incident neutrino energy based on the visible energy. The physics goals of MINER ν A require measurement of the energies of charged (p , $\pi^{+/-}$, $K^{+/-}$, $\mu^{+/-}$ and neutral π^0 , K^0 particles with energies up to a few GeV. The best way to do this would be with a fully active detector with 100% containment of the energy, but cost and location constraints prohibit a fully active detector of the required size. Instead, we have chosen a mixture of detectors with fairly standard elements.

The elements of MINER ν A are: a central fully active detector, an array of alternating lead and scintillator downstream and surrounding the active detector for electromagnetic calorimetry, an array of alternating steel and scintillator downstream and on the outside of the detector for hadron calorimetry, and plates of lead, steel, and carbon upstream of the central detector for upstream electromagnetic and hadron calorimetry.

Another goal of MINER ν A is to study the A dependence of neutrino interactions. The main detector is scintillator, which will serve as a carbon target. The upstream targets of iron, lead and some pure carbon, which serve as the upstream calorimetry, will do double duty as the nuclear targets.

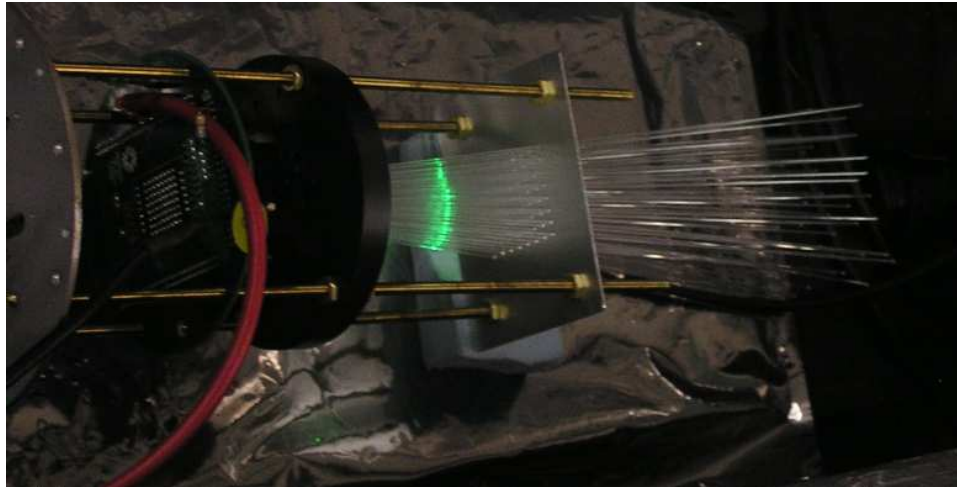


Figure 36: Prototype test of the light injection transmission to the PMT. The MINER ν A PMT and prototype base (left) and cookie (hidden) are used. All 64 pixels have a fiber attached; the final design has a complicated weave, not used here. The green LED is in the approximate position of the light source for the final system. The frame, but not the iron shell, of the PMT box is used.

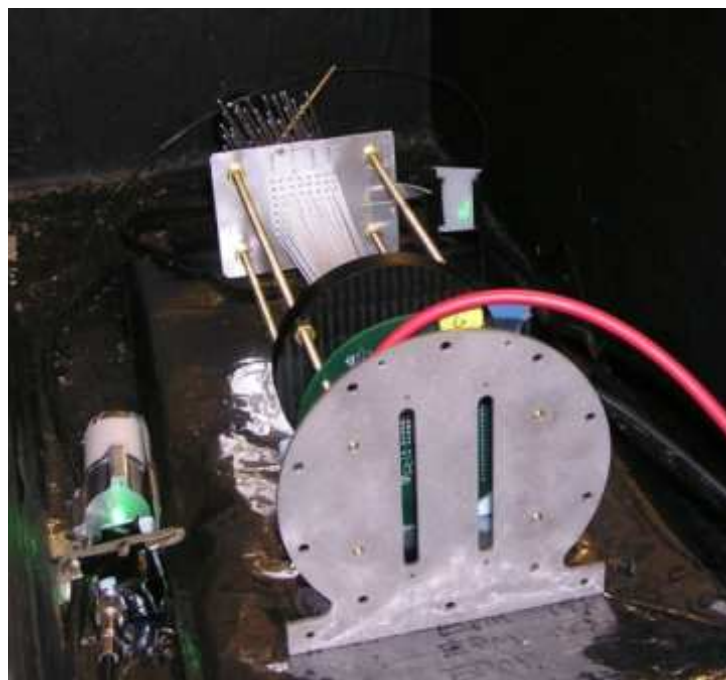


Figure 37: Prototype test of the light injection transmission to the PMT, an extension of the test shown in Fig. 36. Light is now injected into a clear fiber in a cone/collar assembly on the left of the photo. This assembly was borrowed from MINOS and is very similar to what will be in the full design. The fiber (not seen) loops around the apparatus and is aimed at the PMT (right). A diffuser is shown.

The general criterion for the calorimetry is that hadronic energy and electromagnetic showers originating in the central tracking region should be fully contained. This is most critical for the downstream calorimetry because for the neutrino energies of interest the particle production is strongly peaked in the downstream direction and those particles have the highest energy.

The requirement that the upstream elements do double duty as both calorimeters and nuclear targets, means that care must be taken to allow them to serve effectively in both roles.

3.3.1 Electromagnetic Calorimeters

The detection of high energy photons is through the pair-production/bremsstrahlung process leading to a shower of e^+ , e^- and γ . Because the pair production cross section is proportional to Z^2 , lead sheets are generally used to produce a shower of reasonable length. The characteristic length of the shower varies with energy, but for photons up to a few GeV, as expected in our energy regime, 99% of the energy will be contained within 4 cm of Pb (about 7 radiation lengths).

The downstream electromagnetic calorimeter will consist of 20 layers of Pb, each 2 mm thick, interleaved with one layer of scintillator, consisting of the standard 1.7 cm thick layer of triangular strips. Arrangements such as this have been widely used in the past. The expected energy resolution is approximately $6\%/\sqrt{E}$, with E in GeV.

The side calorimetry is quite similar. Trapezoidal sheets of Pb, also 2 mm thick, will be interleaved with each layer of scintillator. The sheets will extend 15 cm into the active area. Photons entering the side calorimeter will be fully contained for angles less than about 25° with respect to the neutrino beam axis. At larger angles the shower will not be fully contained, but will penetrate into the outer hadron calorimetry, where the remainder of the shower will be fully contained, but less well sampled, leading to a decline in resolution.

Because the primary purpose of the upstream Pb/Fe/C plates is to serve as nuclear targets, the design does not allow as efficient calorimetry as the downstream and side modules. The sampling is more coarse because the Pb/Fe/C plates are thicker than in the downstream calorimeter. The arrangement of targets means that the number of radiation lengths the shower sees before escaping from the upstream end will vary from 5 to 10. However, since the backward going photons will generally be much lower energy, showers starting in the active central region will be fully contained.

3.3.2 Hadron Calorimeters

The downstream hadron calorimetry will consist of 20 layers of iron, each 2.54 cm thick, interleaved with one layer of scintillator between plates, downstream of the electromagnetic calorimeter. The combined thickness of the 4 cm of Pb and 50 cm of Fe will stop muons up to about 600 MeV and protons up to about 800 MeV. One nuclear interaction length is 16 cm for Fe, so higher energy protons (or pions) will also generally be stopped.

The side hadron calorimeter consists of a plates of iron 55.9 cm thick, with five slots, each 2.5 cm wide, filled with scintillator. The total iron thickness is 43.4 cm, or 340 g/cm^2 , which can stop, from ionization losses alone, up to 750 MeV protons at 90° and nearly 1 GeV protons entering at an angle of 30° .

The resolution of the hadron calorimeter, based on studies by MINOS, is expected to be about $50\%/\sqrt{E}$ for hadron energies above 1 GeV. The resolution for lower energy particles is expected to be 50% or less, depending on the energy. The primary reason for the poor resolution is the likely interaction of the particle with a nucleus before stopping, which frequently produces one or more energetic neutrons whose energy is unobserved, making it difficult to get good energy resolution

As with the upstream electromagnetic calorimetry, the upstream hadron calorimetry relies on the nuclear targets, with a less efficient design than the downstream calorimeter. The upstream mass thickness is sufficient to stop protons originating in the active central region of at least 300 MeV.

Studies show that the visible hadronic component of quasi-elastic and resonant events originating in the fully-active central region of the detector are completely contained, apart from secondary neutrinos and low-energy neutrons. Figure 38 shows the fraction of escaping visible hadronic energy for deep-inelastic reactions in several hadronic energy ranges, and figure 39 shows the probability that a deep-inelastic event will leak visible energy as a function of the true hadronic energy. Only for hadronic energies greater than 8 GeV is there any significant probability of leakage and only above 15 GeV is the average fraction of escaping energy greater than 10%. The fraction of deep-inelastic interactions with hadronic energies over 15 GeV in the low-energy, medium-energy, semi-medium or semi-high energy beams is $< 1\%$, and so visible energy leakage should be insignificant. These estimates ignore downstream components beyond the forward hadron calorimeter, such as the MINOS detector, and are therefore conservative.

To study MINER ν A's calorimetric E_h resolution, the detector response to a neutrino sample generated throughout the inner detector by NUANCE, on carbon and hydrogen targets, was simulated using GEANT3. From this simulated sample, events where all hadronic fragments were contained within MINER ν A were used. Hits from lepton tracks in charged-current interactions are excluded from the following analysis.

In a fully-active scintillator calorimeter, the total light yield should be essentially proportional to E_h . (The proportionality is not unity due to escaping neutrinos, rest masses of charged pions, nuclear binding energy in the initial and secondary reactions and other nuclear effects such as pion absorption.) While the central inner detector volume is fully active, there are also regions with passive iron or lead absorber sandwiched between scintillators. In these sampling calorimeter regions, not all energy deposited results in scintillation light, so the light yield is corrected accordingly.

3.3.3 Nuclear Targets

The MINER ν A nuclear targets will consist of carbon, iron, and lead. Hydrogen is also present as a component of the scintillator in the active target. However, separating reactions on hydrogen from those on carbon will be extremely difficult and dominated by systematics. Iron is chosen both as a relatively inexpensive medium mass target and as the absorptive material used in many neutrino detectors, such as MINOS. Lead is the highest nuclear mass material that is easily obtainable.

There are a number of criteria that determined the nuclear target design. The ideal arrangement of nuclear targets would have many thin targets with several tracking layers in between each target in order to determine multiplicity of final states and the amount of energy going into relatively low energy particles. There are a number of factors which limit the number and size of targets, as well as the number of tracking layers.

Energy Leakage for DIS events

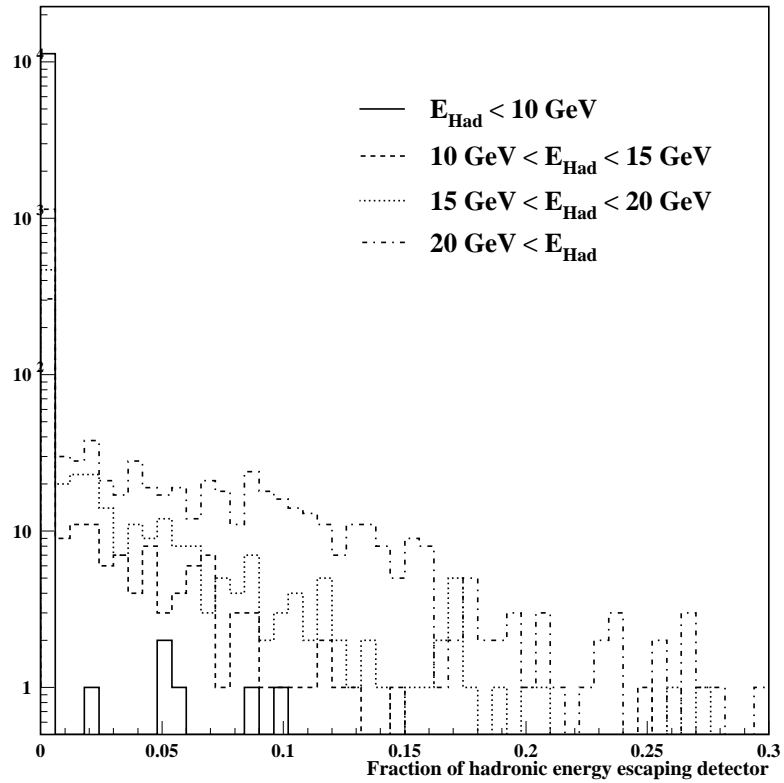


Figure 38: Fraction of hadronic energy escaping the detector for deep-inelastic scattering in the fully-active central region.

The intrinsic spatial resolution of the detector is of order 1 cm, so thinner targets will be inefficient. MINOS used 2.5 cm iron plates, so plates thicker than this will not allow significant improvement of the knowledge of the low energy particle spectrum, which is one of the goals of MINER ν A. In order to get sufficient statistics over a wide range of kinematics, we would ideally like of order 1 ton of each target. The number of frames required to determine a single stereo point is two (an XU and an XV). We would at least two of these points, or four frames, between targets in order to determine the trajectory of short tracks before they enter the next detector. A thickness of 4 frames will stop a straight going proton of 200 MeV. However, because we wish to use MINOS for muon identification, we cannot put too many tracking planes between target plates or use too many plates since the upstream target will then be too far from MINOS a large fraction of the muons will miss MINOS. In addition, we would like to have similar detection configurations for each of the three materials.

The design we have decided on his shown schematically below, with the most upstream section on the left. Each “F” represents one frame, either an XU or XV, and an “FF” pair will be a set of XUXV.

FF Pb/Fe [1] FFFF Pb/Fe [2] FFFF Pb/Fe/C [3] FFFF Pb[4] FFFF Pb/Fe [5]

Targets [1] and [2] will be 2.5 cm thick Pb and Fe mounted in one plane. The areal coverage will

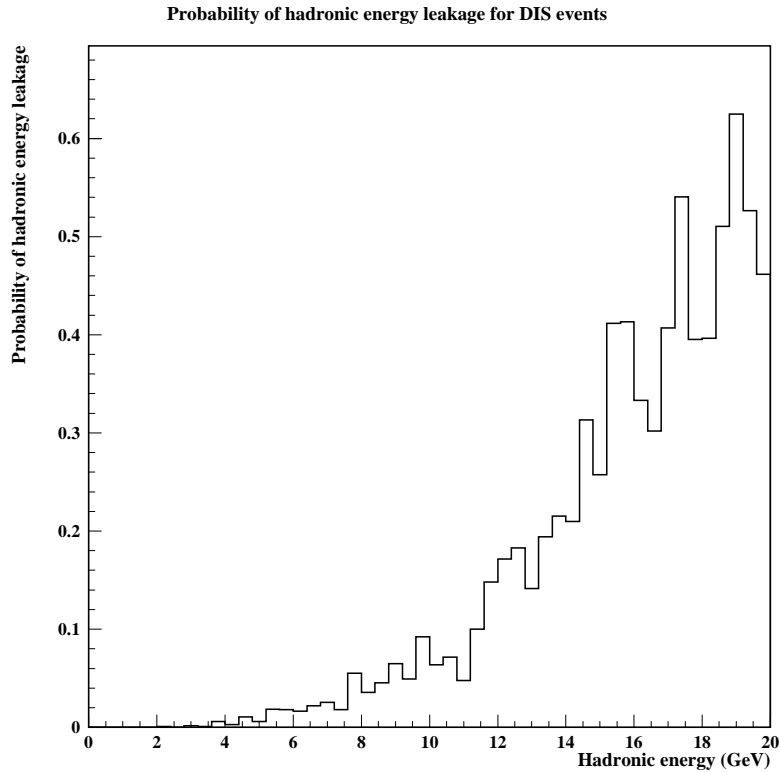


Figure 39: Probability that visible hadronic energy from a deep-inelastic event escapes undetected vs. total hadronic energy.

be 60% Fe and 40% Pb, which gives about 230 kg of Pb and Fe in each target within a radius of 80 cm. Target [3] will have areal coverage of 50% C, 30% Fe, and 20% Pb, which gives 140 kg of C and 110 kg each of Pb and Fe. The Pb and Fe targets will again be 2.5 cm thick, and the C target 7.5 cm thick. Target [4] will be 0.75 cm thick pure lead, with a mass of 170 kg. Target [5] is 1.25 cm thick Pb and Fe, again 60% areal coverage in Fe and 40% in Pb, with a mass of about 115 kg each. To illustrate the feasibility of these hybrid targets, Figure 40 shows engineering drawings of Targets [1] and [3].

The total mass of Fe and Pb are 685 kg and 855 kg, respectively. The expected number of CC events are about 2.0 million for Fe, 2.5 million for Pb, and 400,000 for C.

The first two frames will allow us to determine if a particle going through the upstream veto detectors originated in the first nuclear target or outside the detector. Targets [1] and [2] will have the Pb and Fe rotated with respect to each other to allow checks for differences in detection. Target [3] contains all three nuclei with essentially the same detection capability to allow detailed studies a the A dependence of interactions. Target [4] is pure lead to insure that any produced photons, either from the upstream or downstream targets, begin to shower. The Pb sheet is about 1.5 radiation lengths thick, which is enough to begin the shower but not enough to contain it. Target [5], directly upstream of the fully active central detector, will give allow us to study multiplicities and distributions of lower energy particles with good tracking and energy resolution.

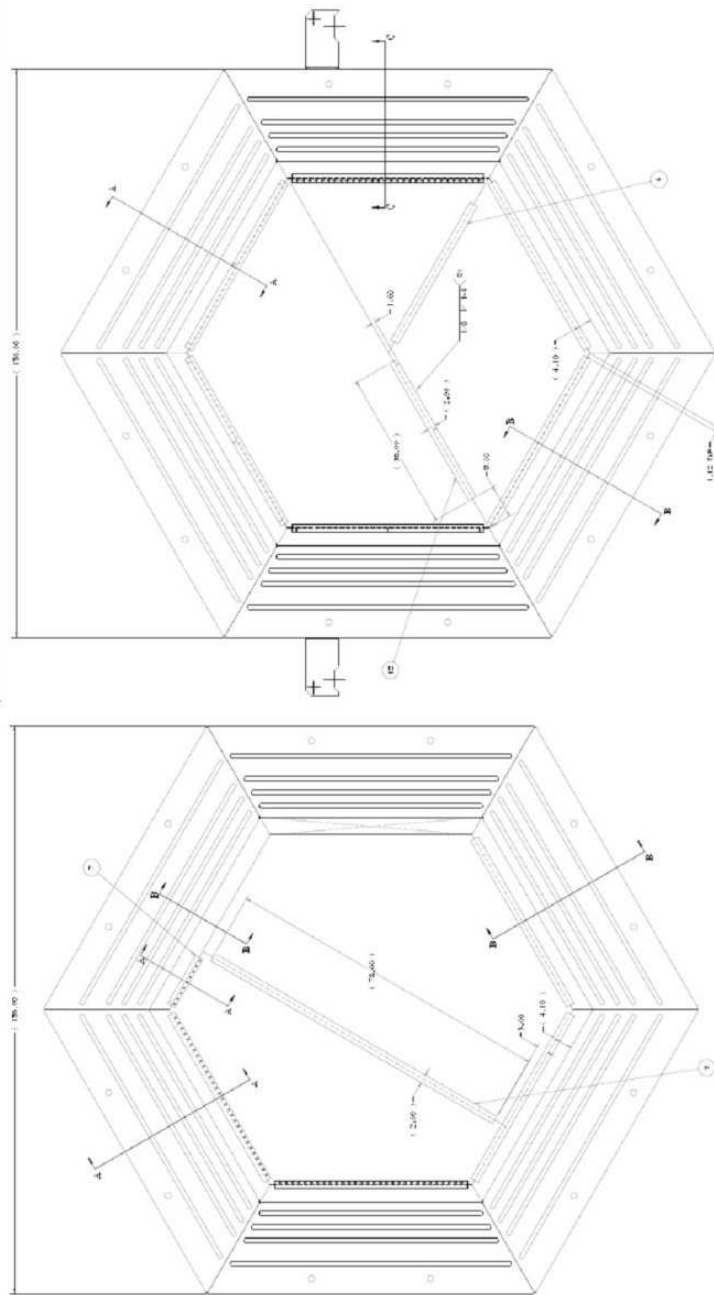


Figure 40: Engineering design of nuclear targets #1 and #3

We have studied this arrangement with our standard Monte Carlo. We find that it satisfies most of our requirements. Most importantly, energy containment for events originating in the central detector is good for upstream (backward) going particles despite there being less material, due to the fact that the backward going particles are lower energy. The energy of charged hadrons and photons from neutral meson decay resulting from quasi-elastic and resonance reactions is almost 100% contained, due to the very forward peaked nature of these reactions. For the most upstream nuclear target, energy confinement is worst for DIS reactions. The high multiplicity of these events produces some lower energy particles going upstream. However, over 90% of produced protons and charged pions are fully contained. Only photon containment is significantly worse than the central region. For incident neutrino energies above 2 GeV about 80% of the photon energy is contained. Thus we conclude that all targets can be used for studies of all interaction types at all energies with only moderate loss of resolution due to lack of confinement.

3.4 Electronics, DAQ, Monitoring and Slow Control

The requirements for the MINER ν A electronics are summarized in Table 4. These requirements are motivated by the experiment's physics goals, which include:

- Fine-grained spatial resolution, exploiting light-sharing between neighboring scintillator strips,
- Identification of π^\pm , K^\pm and p using dE/dx information,
- Efficient pattern-recognition, using timing to identify track direction and separate interactions occurring during a single spill,
- Ability to identify strange particles, and muon decay, using delayed coincidence, and
- Negligible deadtime within a spill.

The average data rate expected for MINER ν A (~ 100 kByte/second) and the relatively modest duty-factor of the NuMI beam (one ~ 10 μ s spill every 2 seconds) are far from demanding, by the standards of modern high-energy physics experiments.

Electronics and DAQ systems are needed not just by the full MINER ν A detector but in a number of other testing and measuring subsystems which will be commissioned earlier. The needs of the complete detector, the photomultiplier tube testing station and the module mapper are:

- PMT Boxes: All(473) Transition boards/cables (Interface between PMT base and FEB)
- PMT Testing: All(473) PMT bases, 7 FEB/FESB, 1 CROC, and stand-alone DAQ system for PMT testing
- Module Assembly/Mapping: 7 PMT bases, 7 FEB/FESB, 1 CROC, and stand-alone DAQ system for module scanning

3.4.1 Front-end Electronics

The front-end boards digitize timing and pulse-height signals and provide high-voltage for the photo-multiplier tubes (PMTs), and communicate with VME-resident readout controller modules over an LVDS token-ring. For easy access in connection, testing and replacement, the boards are mounted *outside* the light-tight PMT housing assemblies. Pulse-heights and latched times will be read from all channels at the end of each spill.

The front-end board for MINER ν A is designed around the D0 TriP-t ASIC which is a redesign of the readout ASIC for the D0 fiber tracker and preshower. The TriP-t chip has suitable capabilities for use in MINER ν A. The most significant technical risks have already been addressed by our successful 2004 R&D program, using a prototype board fabricated using available TriP chips from D0.

Requirements and design features Each front-end board (FEB) will service one PMT (64 channels) which will require 6 TriP-t chips per board. The TriP-t chips will be controlled by a commercial FPGA (Field-Programmable Gate Array) using custom firmware. A prototype of this firmware has already been developed and successfully operated during our R&D studies. In addition to digitization of charge and timing information, the front-end boards will also supply high-voltage to the associated PMT and communicate with the downstream readout system over an LVDS (Low-Voltage Differential Signaling) link. The FEB will attach to the PMT box via the transition board that is mounted to the rear of the PMT box. Figure 41 shows the basic design of the board and the main components. Table 5 summarizes the channel counts for the final design.

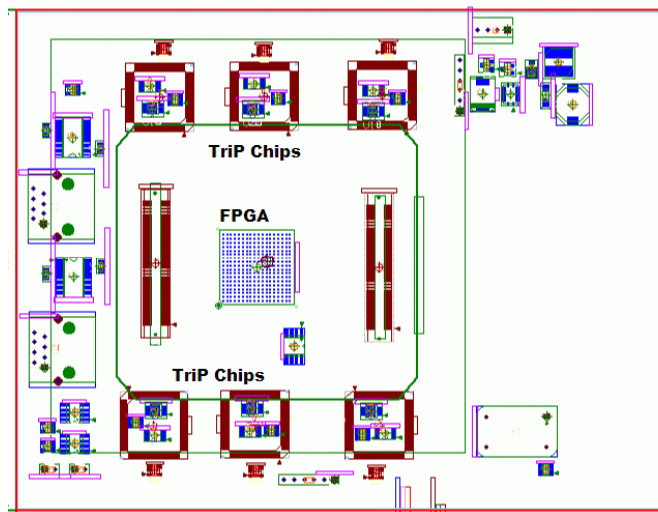


Figure 41: Simplified schematic of the front end electronics 2nd prototype board.

The TriP-t chip and digitization The heart of the system is the D0 TriP-t ASIC. The TriP-t chip was designed by Abder Mekkaoui of the Fermilab ASIC group and has undergone extensive testing by D0 [164]. Its analog readout is based on the SVX4 chip design. Each TriP-t chip supports 32

| Parameter | Value | Comments |
|-------------------------------|--------------|--|
| Active spill width | 12 μ sec | Spill plus $2\tau_{\mu}$ |
| Repetition Time | > 1.9 sec | |
| Number of channels | 30272 | |
| Occupancy per spill | 2% | LE beam, 2.5E13 POT/spill |
| Front-end noise RMS | < 0.2 PE | |
| Photo-detector gain variation | 4.5 dB | Extremes of pixel-to-pixel variation |
| Minimum saturation | 350 PE | Proton range-out or DIS event |
| Maximum guaranteed charge/PE | 50 fC | Lowest possible charge at highest gain |
| Time resolution | 3 ns | Identify backwards tracks by TOF Identify decay-at-rest K^{\pm} |

Table 4: Electronics design requirements and parameters for MINER ν A

| Item | |
|---|-------------------------------|
| Number of FEB boards including spares(15%)) | 545 |
| Number of PMT's serviced per board | 1 |
| Number of PMT channels serviced per board | 64 |
| Number of ADC channels per board | 192 (Low, Middle, High Gain) |
| Number of TDC channels per board | 64 |
| Number of HV channels per board | 1 |

Table 5: MINER ν A front-end board channel summary.

accurately, the RF/2 reference clock from the Tevatron (approximately 25Mhz) is multiplied by four in a PLL and phase shifted by 90deg to form a quadrature clock that is used inside the FPGA to form a digital TDC with least bit resolution of 2.5ns. This feature has also been tested on the prototype board and a timing resolution consistent with the 2.5 ns least count timing resolution of the TDC's has been achieved. The reset time for the latch is only 15 ns, so inside a spill the latch will be in the ready state by default. When the signal exceeds a threshold of 1.5 PE, the latch will fire. After storing the time, the latch is reset, incurring minimal downtime.

Each board includes its own high-frequency phase-locked oscillator, which provides a local clock signal for the FPGA logic. Global synchronization is provided using an external counter-reset reference signal distributed over the LVDS interface from the VME readout boards once every second, and originating with a MINOS timing module which is, in turn, synchronized to the NuMI beam.

High-voltage and Front-End Support Board (FESB) A Cockroft-Walton(CW) high-voltage base supply will provide power to each board's PMT. The Cockroft-Walton high-voltage supply will be split between two boards: one that resides in the PMT box and contains passive components and a second board (Front-End Support Board - FESB) that will be attached to the outside of the PMT box and contain the CW oscillator elements. The CW card that resides in the PMT Box will also map the analog PMT pixel signals to connectors on the transition board. The auxiliary card (FESB) design will allow a malfunctioning high-voltage supply to be easily replaced without changing the main readout board. In addition the FESB will physically separate the CW oscillator elements from the incoming analog signals from the PMT to reduce noise pickup and by reducing the physical size of the FEB improve its cooling capabilities. An existing Cockroft-Walton controller design (developed at Fermilab) will allow the PMT voltage to be monitored, adjusted or disabled over computer control, using the LVDS interface.

LVDS interface As detailed in Section 3.4.2 each front-end board will be a member of a chain (or token-ring) connected by LVDS to a VME-resident readout controller. As such, the front-end boards require two LVDS connections, one to receive data from the previous member, and another to transmit data to the next. The LVDS interface transmits all information to and from the board, including:

- Transmission of digitized timing and charge data from the front-end board to the VME readout controller,
- Write access to the front-end memory buffers, for diagnostics,
- Configuration of the TriP-t chip registers (thresholds, gains, etc) for data-taking,
- Reprogramming of the flash ROM containing the front-end board's FPGA firmware, and
- High-voltage control and monitoring messages.

The first prototype front-end board used in our 2004 R&D studies was designed to accommodate an LVDS interface, was commissioned and tested in late-2004/early-2005.² This subsystem represented the most significant remaining technical risk in the electronics (now that the TriP-t digitization and timing scheme has been successfully tested), as the latency in propagating signals from one front-end board to another via LVDS limits the number of boards that may be linked in a single chain, and hence the number of chains (and VME readout boards) required to service the full detector. The latency tolerance is constrained by the need to transmit a global timing synchronization signal to all front-end readout boards. As explained in Section 3.4.2, pending prototype testing we estimate approximately 100 ps jitter may be introduced by each link in the chain. As the least count of our TDCs is 2.5 ns (which is itself considerably better than required, since each track will have numerous timing measurements) we have conservatively limited the design length of each LVDS chain to 12 boards, which represents a factor of two safety margin ($12 \times 100 \text{ ps} = 1.2 \text{ ns}$) from a single TDC count. As LVDS is a mature technology, used in many consumer applications, this risk is a relatively mild one, which in the worst case would require fabrication of a small number of additional VME readout boards and/or a modest compromise in timing resolution which will not noticeably degrade the experiment's physics capabilities. Based on results from the first prototype, the final version of the LVDS interface will be designed and incorporated into the second (64-channel) prototype, and the full token-ring communication protocol defined, for testing together with a prototype of the VME readout controller.

FPGA and firmware The internal behavior of the front-end board is supervised by an FPGA operating as a finite-state machine, making the system programmable and highly flexible. As noted, during commissioning of the first prototype version of the board during 2004 R&D, the most mission-critical and timing-sensitive elements of the firmware (controlling the TriP-t chip's buffering and TDC functionality) have already been developed and successfully tested. For the production boards, logic to interpret commands and exchange data over the LVDS interface, and control the Cockcroft-Walton high-voltage supply will also be required. This additional logic can be developed and tested using the full 64-channel prototype version to be built in the summer 2006.

Persistent storage for the firmware is provided by an onboard flash PROM, which is read by the FPGA on power-up and can be re-written under computer control. As such, it will be possible to reprogram the FPGA logic of all boards remotely even after they are installed, if necessary.

3.4.2 Data acquisition and slow control

MINER ν A's data acquisition (DAQ) requirements during data taking are relatively modest, as the average data rate expected in the NuMI beam is only a few 100 kByte/second and a two-second window for readout is available after each $\sim 10 \mu\text{s}$ spill. The most demanding requirements from the DAQ arise from calibration (module mapper) and testing (PMTs). The predictable timing of the beam obviates the need for a complicated trigger - instead, a gate is opened just prior to arrival of the beam, and all charge and timing information from the entire detector is simply read-out after the

²For testing and commissioning the board's core digitization functionality, an alternative parallel-port interface was used during initial R&D studies.

spill is complete. The slow-control system is also relatively simple, with each PMT powered by its own local Cockcroft-Walton HV supply and uses the same hardware as the DAQ.

The DAQ and slow-control system is therefore essentially a communication network for distributing information (synchronization, high-voltage commands, and exceptionally, updated firmware) to the front-end boards and funnelling event data collected from them to the main data acquisition computer. The system consists of the following components:

- The main DAQ computer (Dell Power Edge), including a VME interface board (CAEN V2718+A2818 Kit),
- A VME crate (CAEN VME8010) containing a total of 12 custom-built Chain Read-Out Controller (CROC) modules, with each CROC controlling four LVDS chains, There are no CPU processors in the VME crate.
- 40 LVDS chains (CAT-5e network cable), with each chain linking 12 front-end boards, and
- A third VME crate, containing timing, diagnostic and logic modules.

Due to the distributed nature of the front-end digitizer/high-voltage boards, the central DAQ and slow-control system itself can be easily accommodated in a single electronics rack.

LVDS token-ring chains As explained in Section 3.4.1, the front-end digitizer boards are daisy-chained into 40 LVDS token rings of 12 boards each. Both ends of a chain terminate in a custom built VME chain read out controller (CROC) module described below. The number of digitizers on a chain is limited by the allowable jitter in the high-precision timing information transmitted to each digitizer board over LVDS. As LVDS is a one-way protocol, each digitizer board must receive the period global synchronization signal from the previous member of the chain on one connection, and re-transmit it to the next member on a second connection. From tests using our prototype boards we estimate that each board in a chain will introduce approximately 100 ps of jitter; thus a chain consisting of 12 boards would translate into roughly 1.25 ns timing jitter (worst case). This represents a factor of two safety margin over the 2.5 ns least-count timing resolution of the front-end TDC's. In the unlikely event the jitter introduced by a chain of 12 front-end boards proves unacceptable, even with this large safety factor, the number CROC modules (and hence chains) could be increased, allowing each chain to have fewer members.

LVDS signals will be transmitted around a ring on standard, commercially-available fire-resistant and halogen-free CAT-5e network cable approved by Fermilab safety division for underground use. The LVDS chains will also be used to transmit configuration and slow-control messages to the cards.

Chain read-out controller (CROC) modules Each CROC module, shown in Figure 43 will control four LVDS chains, requiring a total of 12 CROCs (plus spares) for the entire detector. These modules will reside in a VME crates alongside a crate controller and a MINOS timing distribution module. The CROCs also pass timing and synchronization signals from the NuMI/MINOS module to the FEBs without computer intervention.

The readout controller modules have the following functions:



Figure 43: Photo of Prototype CROC 6U VME module.

1. Prior to the arrival of a NuMI spill, as signaled by the VME-resident MINOS timing module, to reset the timing counters of each front-end board and open a $10\mu\text{sec}$ gate to collect data from the spill.
2. Upon completion of a NuMI spill, to initiate readout of front-end digitizer data over the four associated LVDS rings, into internal RAM.
3. Upon completion of the parallel readout of all four chains, to raise an interrupt with the main DAQ computer, indicating that event data is available. The PVIC/VME interface/crate controller allows VME interrupts to be received directly by the main computer.
4. The internal RAM of each CROC is memory-mapped to the host computer's PCI bus, allowing block transfer of event data via the PVIC/VME interface/crate controller. The relatively long NuMI duty cycle (~ 2 seconds) and low data rate (under 1MB per spill for the entire detector) ensures that no deadtime will be associated with the readout itself.
5. Once per second, to globally synchronize the detector's TDCs over LVDS using a high-precision refresh signal from the MINOS timing module. The need for this synchronization drives the choice of LVDS for the readout chains, as opposed a less performant alternative such as Ethernet.
6. Upon command of the main data acquisition computer, to control and monitor the Cockroft-Walton high-voltage power-supplies and to configure the firmware of these boards at run-startup.

VME backbone Communication between the main data acquisition computer will be via commercially available PVIC/VME link, allowing block data transfers to and from VME and interrupts to be received by the computer in response to the NuMI spill gate.

Ancillary electronics A trigger scaler and TDC to monitor the NuMI timing signals, and a programmable pulse generator to simulate them during beam-off periods, along with other any additional logic needed for monitoring and calibration, will reside in the third VME crate. All VME components will be installed underground, within about 20 meters of the detector.

Data acquisition computer The main DAQ and slow-control computer will be located near the VME electronics, in the NuMI hall, with two high-speed TCP/IP links (one for data, one for monitoring and control messages) to the Fermilab network. A relatively modest, dual-CPU server model will be more than adequate for our purposes. One CPU will be dedicated to real-time data acquisition, and the other will handle control messages and monitoring. An on-board, RAID-5 disk cluster with sufficient capacity to store several weeks of data will serve as a buffer for the data, pending transfer to offline processing nodes and permanent storage.

DAQ Software The MINER ν A DAQ software will make significant use of existing packages. The default choice for the client(control room)/server(Near Detector Hall) infrastructure is the GAUCHO package and related software developed by LHCb and the LHC Joint Controls Project. The LHCb package is integrated with GAUDI, PVSS (process visualization and control system(German acronym)), and DIM (Distributed Information Management). This enables data exchange between GAUDI-based (offline software system) jobs running on different processors. LHCb uses this system to control and monitor their high-level trigger processor farm, with PVSS-based user-interface components subscribing to and displaying counters and time-trend data, and controlling and monitoring individual jobs.

While MINER ν A's requirements are far simpler (we have only a data provider, the DAQ computer, instead of a farm of hundreds), it appears to meet our needs and is attractive as it allows online monitoring software to be developed and tested seamlessly within the offline framework, and also because it will spare MINER ν A the need to develop such a system itself.

Event building and buffer management will utilize the MBM(Memory Buffer Management) package from LHCb which includes the GAUDI offline interface. The producer task reads raw data from the detector and registers RawBank data into the buffer. GAUCHO-based consumer tasks then read data from the buffer allowing control of monitoring jobs and display of accumulated counters, histograms, *etc* over the network. The DIM package allows each task to be controlled as a finite state machine and expose this information to control room client displays (see figure 44) .

MINER ν A specific software includes CROC and FEB device control libraries. This will involve a high-level interface for LVDS message building and to hide the VME interface from clients. In addition device management to synchronize hardware access, manage device dependencies, and maintain configuration database will be required. Specific producer/consumer jobs using the MBM package templates will need to be developed. The manpower needed to produce this software will come from UC Irvine, Northwestern, PUCP Lima, and UNI Lima.

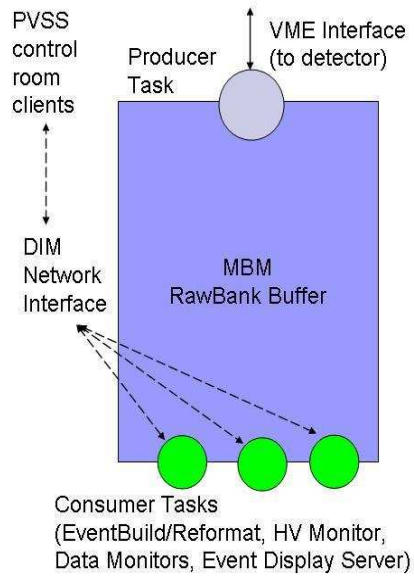


Figure 44: Simplified Flow Diagram of Event Building and Buffering.

| Component | Number | Comments |
|-------------------------------|--------|-------------------------------|
| Channels | 30272 | WLS Fibers |
| Front-end boards | 473 | One per PMT, plus 15% spare |
| Readout Token Rings | 40 | 12 PMTs/ring |
| VME Readout Cards | 12 | 4 rings/card, plus two spares |
| VME Crates | 3 | Plus one spare |
| VME PVIC Interface | 3 | One per crate, plus one spare |
| PVIC/PCI Interface | 1 | Plus one spare |
| DAQ Computer with RAID system | 1 | Data rate is 120 kByte/spill |

Table 6: Parts count for MINERvA electronics design

3.4.3 Control Room Monitors and Displays

In addition to the DAQ computer, which handles the controls and data flow for the DAQ system itself, independent systems which allow physicist operators to monitor and diagnose errors in the apparatus are also required.

Subsystems include:

ACNET Beam Parameter Monitor This subsystem gathers information from the accelerator and associates it with spill data to ensure that the beam flux can be monitored. The MINOS experiment already has such a system in place. MINER ν A will either duplicate this system or receive data from the existing MINOS server.

Data Processor This processor will read in data as it is taken and run it through simple versions of the offline algorithms. Quantities such as plane occupancies, pedestals, signals for straight through muons, timing would be accumulated, as well as physics quantities from full reconstruction of interactions. Due to the low data rate, each spill can be read from disk as it is logged. No network event server will be needed. This data processor will be a simple instance of the offline MINER ν A data processing code.

Histogram Evaluator and Viewer A separate process will provide a user interface to the updating histograms from the **Data Processor**. Many HEP experiments already have such systems, which can display and compare online histograms with reference sets, flag discrepancies and alert the operator. We propose to reuse one of the existing systems.

Event Display One or more instances of the MINER ν A event display need to be available to monitor data as they arrive. The offline event display will run on either the raw data or reconstructed data written out by the **Data Processor**.

Alarm and Message System This system will gather error message from the other online systems, including the slow controls and rack monitors and alert the operator in the event of a serious error. MINOS has an existing system, Distributed Control System, which performs this function. Another alternative would be a SCADA system such as PVSS.

Logbook An online logbook will be available to the operator, the run control and alarm systems should be able to write to this log book to automatically flag begin and end run and serious alarms.

Database The online system will need access to the experiment conditions database, both to obtain hardware information and to store information about running conditions. This can either be the same as the offline database or a separate instance if required by computer security.

We anticipate that during the prototype and testing phases, where data rates are lower and failures will not result in irrevocable loss of data, these functions may be performed by one or two machines. However, the system for beam operations will probably require one machine per monitoring function, as is currently the case for the MINOS experiment.

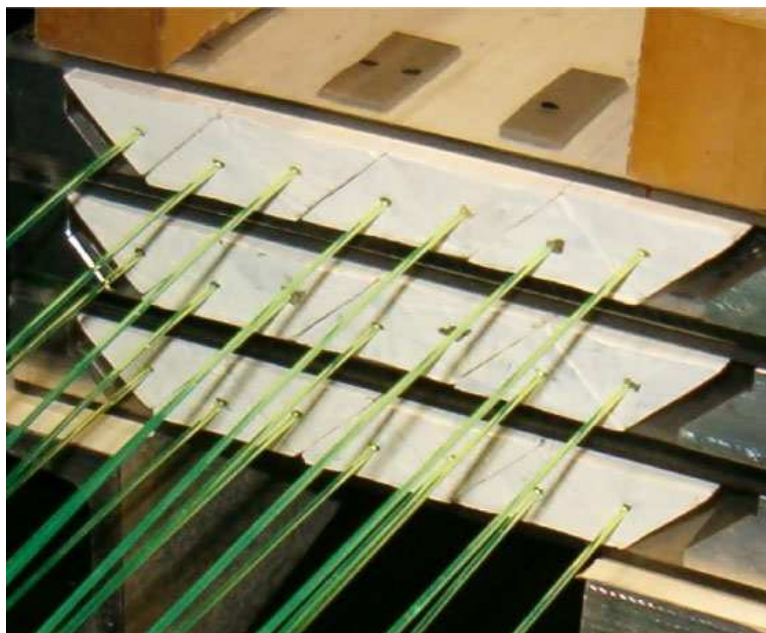


Figure 45: Picture of the VST showing the 3 layers. Scintillator paddles above and below the array serve as the DAQ trigger.

3.5 Vertical Slice Test, VST

We have done a complete test of the MINER ν A system. The Vertical Slice Test (VST) approximates the MINER ν A detector by including every stage of the eventual detector, except for the clear fiber cables and their connections. Figure 45 shows the optical components of the VST. The VST consists of 3 layers of scintillator bars 0.5 m long. Each layer consists of 7 scintillator bars. The scintillator bars are readout by mirrored WLS fiber (Y11 from Kuraray, 3.5 m long, 1.2 mm diameter), identical to the WLS fiber used in MINER ν A. The WLS fibers are glued into the scintillator bars using the production MINER ν A glue, Epon 815C epoxy with TETA hardener (Epi-Cure 3234). The WLS fibers are glued into optical connectors used by MINOS which are connected to a MINOS CALDET PMT box. The box contains a 64-channel multi-anode PMT. (The CALDET PMT box was used by MINOS for their CERN testbeam.) Coincidence counters are put above and below the array and cover the array to ensure that only cosmic ray muons that pass through the array trigger an event. In addition, a counter some distance from the array insures the muons are perpendicular to the array.

The VST electronics is serving as the first prototype for the MINER ν A electronics, see Figure 46. The VST prototype boards were designed to be compatible with the MINOS CALDET PMT box and to serve as proof of principle for the proposed daisy-chain LVDS readout system. The VST electronics is composed of four identical boards, each of which plugs into the four 16-channel connectors at the back of the MINOS CALDET PMT box. Since these prototypes were produced before TriP-t chips were available, the TriP chip is used - but this is a nearly identical chip and the additional timing feature, which distinguishes the TriP from the TriP-t is not used by MINER ν A. The key

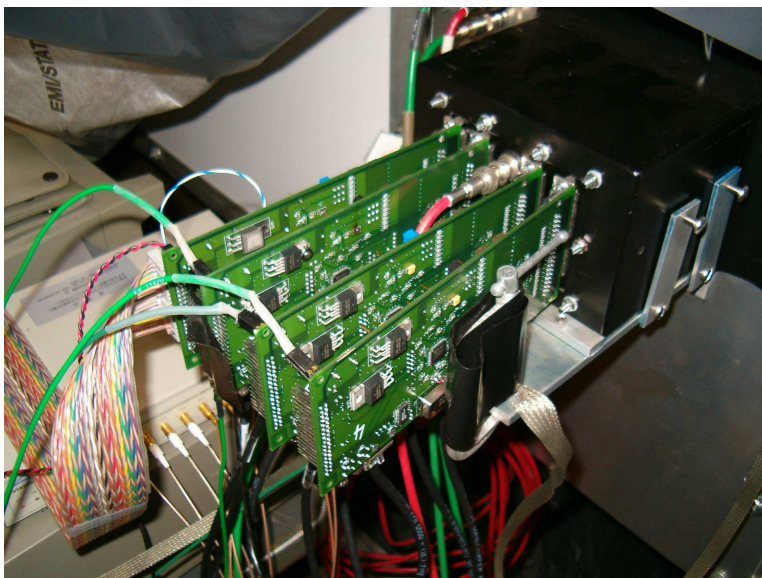


Figure 46: Picture of the MINOS CALDET Box and the prototype MINER ν A electronics which was designed to be used with the MINOS box.

features required by the final electronics are present on this first prototype. The VST boards are interconnected by an LVDS link using the same protocol as that proposed for the final MINER ν A electronics. Each TriP chip is split with 16 channels used for high gain, and 16 channels used for low gain. The discriminator outputs are routed to an FPGA and the TDC function is implemented in the same way as proposed for the final design. One key feature of the final design that has not been tested with the VST boards is the integration of the CW HV generator with the electronics, because this is precluded by using a MINOS CALDET PMT box, which already has an integrated resistive divider base. However, this has been tested using a separate CW generator prototype.

Figure 47 shows the pulse height distribution for cosmic ray muons. In order to determine the single photoelectron (PE) peak, each WLS fiber was pulsed with a LED at a very low light level. Each layer was found to yield roughly 6.2 pe/MeV or an average of 20.7 PE/MIP for a cluster of hits associated with a muon..

We can use the light measured from the VST to estimate the light for the MINER ν A detector by correcting for the losses in the clear fiber cable, the expected phototube quantum efficiencies and the fiber length. From this we derive a worst-case estimate of 18 PE/MIP for the inner detector light yield. If we assume the quantum efficiencies (QE) of the MINER ν A PMTs similar to the QE of the MINOS PMTs we get an additional 9% of light. According to the MINOS documentation the QE of VST tube is 9% below the mean of the MINOS PMTs. The light loss from a 1.4 m cable is 0.66. We determined this by measuring the light loss from a 1 m cable, as described earlier, and using the measured clear attenuation length of 6.8 m. We measured that optical grease increases the light by 16% for each connection. The WLS length for the VST is 3.5 m while the longest length in the detector is 3.2 m. This increases the expected light by 6%. Putting all these factors together gives

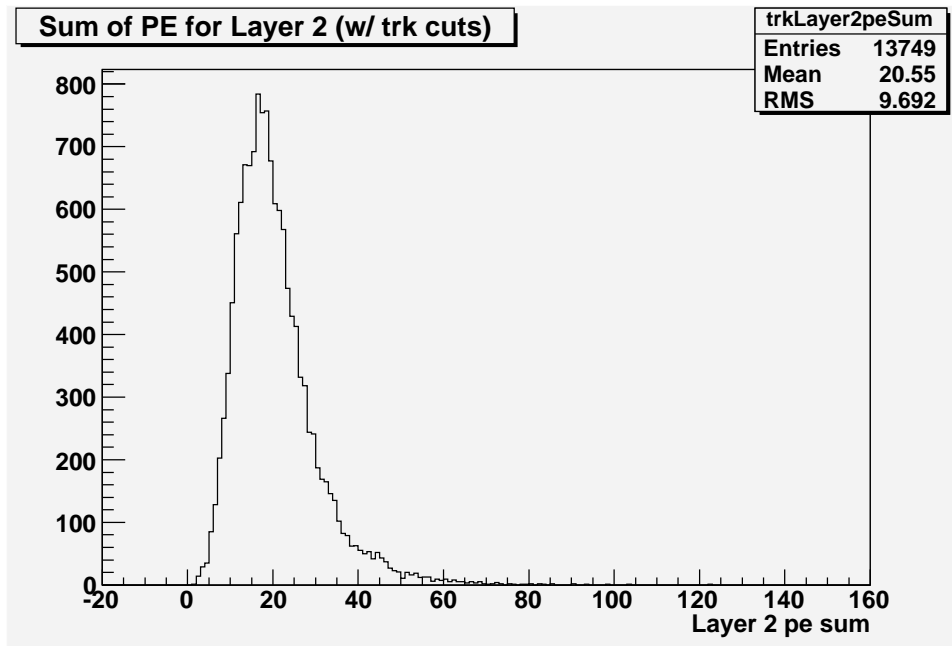


Figure 47: Plot of the pulse height distribution for muons for Layer 2. The average of all 3 layers gives 20.7 pe/layer.

| Filter | Effective Transmission | # PEs | Resolution(mm) |
|--------|------------------------|-------|----------------|
| 0.5 | 0.43 | 8.9 | 3.7 |
| 0.63 | 0.59 | 12.2 | 3.2 |
| 0.80 | 0.75 | 15.5 | 2.8 |
| 1.00 | 1.00 | 20.7 | 2.5 |

Table 7: Measurement of the position resolution vs light level. A Wratten neutral density filter is inserted in the optical chain and the position resolution is measured.

21.3 pe/layer.

Approximately 1/8 of the detector is readout using 3.1m clear cables, instead of the 1.1 m or 1.4 m clear cable. For this portion, the longest WLS fiber in this section is 2.9 m instead of 3.2 m, compensating for some for the light loss from the longer clear cable. For the configuration of 3.1 m clear cable and 2.9 m WLS fiber, there is an approximately 15% reduction in the light. This gives 18.0 pe/layer. We note that this 18.0 pe/layer is calculated at the geometric point in the detector which gives the lowest amount of light.

We determine the position of the resolution using the VST. The positions are found by weighting strips by photoelectron deposit within a layer. Resolution is found by first averaging layer one and three positions to get a projected position. Next, layer two position is subtracted from that projected position to give a residual. The RMS of the residual for all events divided by $\sqrt{3/2}$, which comes from statistics, gives the actual resolution. Figure 48 shows a resolution of 2.5 mm.

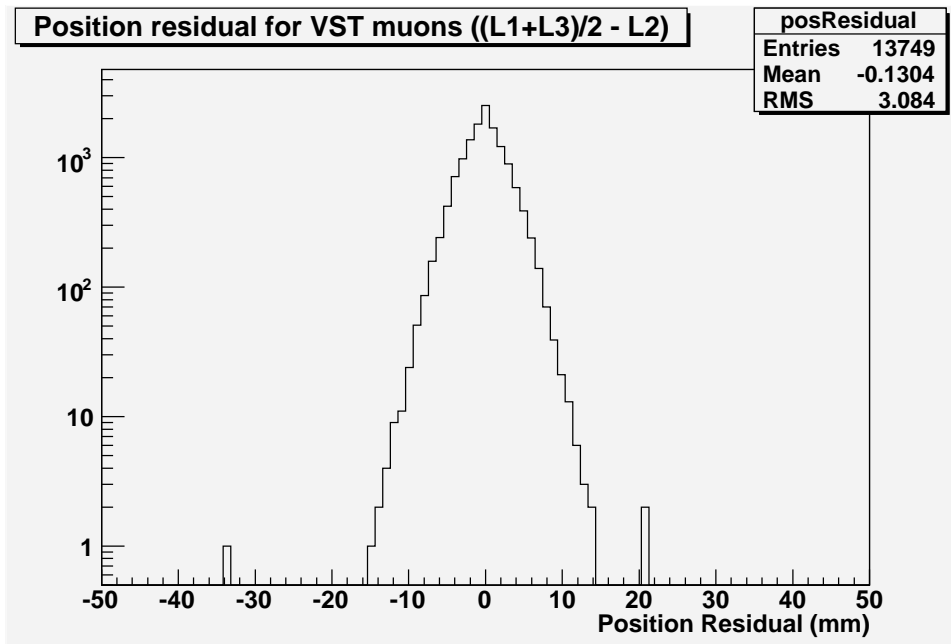


Figure 48: Plots of the $((L1 + L3)/2 - L2)$ where the "L#"s are the position determined in that layer. The tracking resolution is 2.5mm which comes the width of $((L1 + L3)/2 - L2)/\sqrt{3}/2$.

We studied the position resolution vs. light level. To change the light in the array we inserted Kodak Wratten neutral density fibers between the optical connector on the WLS pigtail and the optical connectors on the MINOS PMT box. The Wratten filters are 4 mil thick so the optical connectors cannot quite be mated flush. This causes a little more light loss besides the optical attenuation of the filter. Next the resolution is measured with the Wratten filters in place. Table 7 gives the resolution vs light level. We see that the resolution is still quite good for our requirement of 13.2 pe/layer.

Finally, we have used the VST to determine timing resolution. We specifically used hits on different front-end boards to verify the synchronization of timing across the LVDS chain. For cosmic ray muons, we determine a timing resolution of 2.6 ns. A plot of the residual between two seed strips in the cosmic ray track is shown in Figure 49.

4 Assembly and Installation

Once the detector components, discussed in the preceding chapter, have been constructed, then these components must be assembled to create the MINERνA detector.

The basic functional unit of the detector is called a "module". A module consists of a hexagonal steel frame which, depending on the type of module, contains various scintillator packages or absorber material. Overall, the detector will consist of 108 modules.

The assembly of the MINERνA modules is handled in three steps. First, the scintillator is shipped from the extrusion facility at Fermilab to Virginia where it is packaged into units that can be easily

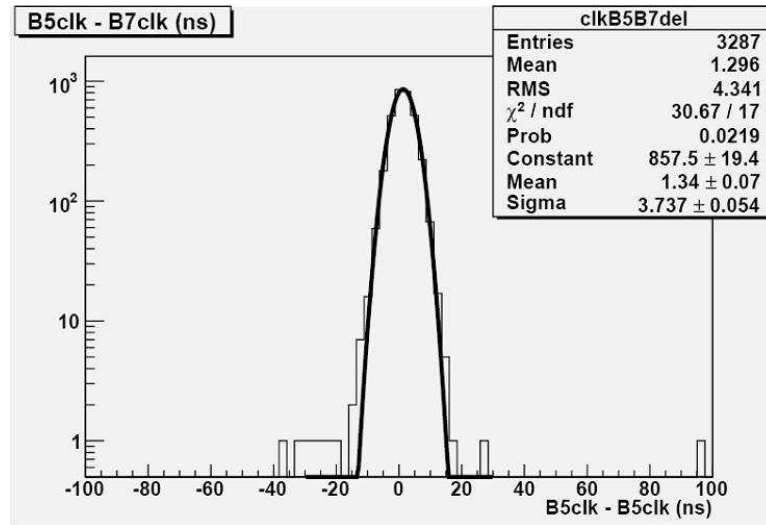


Figure 49: Plots of the time difference between two hits on different layers in the same muon track. The timing resolution is determined to be better than 3ns.

installed into the detector modules. To do this, the raw extrusions must first be cut to length and glued together into a structurally-robust and light tight package. The mirrored wavelength-shifting fibers must be inserted and glued into each extrusion. The final package must be light-tightened and tested. All of this work will take place at two factories located at the College of William and Mary (W&M) and at Hampton University (HU). This task has been named WBS 3 and is being managed by Jeff Nelson of William and Mary.

The second step of assembly involves fabrication of the steel frames, which are the main structural unit of each module. These frames are assembled from six steel segments (or “wedges”) which are individually cut from 1.25” thick steel plates. These segments must be welded together to form the frame. This work will be done at Fermilab in the Wideband Hall. The task has been named WBS 8 and is being managed by Jim Kilmer of Fermilab.

In addition to fabricating the steel frames and absorber material for the detector, WBS 8 will also prepare a number fixtures required for the detector assembly and installation. This includes the detector stands, strongbacks and a number of related items.

Finally, once the steel frames and scintillator units have been prepared, the modules themselves will actually be assembled. The scintillator units will be shipped back to Fermilab from Virginia. Scintillator units and nuclear absorber material will be installed into the OD frames. The final units must be scanned with a radioactive source to determine the local performance of the scintillator. This step, known as “mapping,” will also be the main quality control step before the detector installation.

The module assembly task has been named WBS 9 and is managed by Robert Bradford of the University of Rochester (UofR). While module assembly will take place in Wideband Hall at Fermilab, most of the preparatory work is being done at the University of Rochester. In addition to the module assembly and mapping, WBS 9 also is responsible for the veto wall, commissioning the tracking prototype, and fabrication of the PMT racks.

Once assembled, the modules will be stored in Wideband Hall until the detector is installed in the NuMI experimental hall. While it would be ideal for the modules to be installed as they are completed, the feasibility of this, however, is not well understood. The main concern here is that the installation procedure could interfere with the operation of the MINOS near detector. Currently, the collaboration has planned an installation procedure that is minimally invasive for MINOS (during a shutdown), but we are still investigating the feasibility of a prompt installation. Because installation may take place during an accelerator shutdown, it has not been included as part of the Project. Nonetheless, installation related activities are being managed by Jim Kilmer, and this task has been named WBS 11.

This chapter, then will be divided into four sections, one for each of the major tasks addressed in this chapter. Section 4.1 will detail construction of the scintillator modules while Section 4.2 will discuss the OD steel frame construction and physical facilities. Final module assembly will be covered in Section 4.3. Not being technically part of the Project, installation will not be discussed in as much detail as the other three tasks. However, an overview of the detector installation will be presented in Section 4.4. Each section will include a more detailed introduction to the scope of the task, a discussion of required resources, and a breakdown of the main tasks within each WBS structure.

4.1 Scintillator Assembly

WBS 3 designs and constructs all scintillator units for the detector. Of these, there are two kinds: The large hexagonal planes of scintillator for the inner detector, and the smaller “towers” of scintillator for the OD HCAL. This section will begin by defining the scope of WBS 3, including an overview of both scintillator assemblies, and a discussion of the construction process. We will then discuss facilities and resources required for the construction, interfaces with other WBS tasks and outside vendors, major tasks included in the WBS 3 schedule and end with a short section on the R&D effort.

4.1.1 Task Objectives and Overview

The specific tasks for which WBS 3 is responsible include:

1. Design the components of the scintillator assemblies.
2. Purchase the construction supplies, component materials and fabricate the components of the scintillator assemblies.
3. Assemble all MINER ν A scintillator units. These include assemblies for the MINER ν A detector, the tracking prototype, and the full module prototype. The final MINER ν A detector will require 196 ID planes and 648 outer detector assemblies. Once production waste, spares, and prototyping efforts are included, we plan to construct 253 ID and 820 OD assemblies.
4. Test the assemblies for dead readout fibers and light leaks.
5. Package and ship the assemblies to the module assembly site at Fermilab.

4.1.2 Design of the scintillator assemblies

WBS 3 will design and construct two types of scintillator modules - the ID planes, and the OD towers.

Details of the ID planes are shown in Figure 50. The main body of the plane is largely composed of 128 triangular scintillator extrusions, each containing a green WLS fiber. The scintillator extrusions will range in length from 123 to 246 cm and will be glued edge-to-edge using 3M Scotchweld DP190 adhesive to form a large solid hexagonal plane of scintillator. The outer edges of the planes will be treated with a rigid PVC foam, shown as white, yellow, and pink bars in the figure. The yellow bars run parallel to the length of the extrusions and provide structural reinforcement for the plane. At the top of the plane (white bars in the figure), the PVC pieces contain precisely machined grooves which will be used to route the WLS fibers out of the plane for readout purposes. To form a light-tight package, the entire assembly will be wrapped in an outer skin of 0.010" thick Lexan film. A sheet of Lexan, called the "web," will also be woven through the scintillator plane to provide a convenient gluing surface. A drawing depicting a cut-away side view of a plane is shown in Figure 51.

The plane design builds on the success of the MINOS detector scintillator module assembly [165]. The two assemblies are conceptually very similar - large planar structures composed of extruded scintillator. However, a few modifications are required to meet the needs of MINER ν A. Most significantly, the aluminum skins from the MINOS modules were replaced with Lexan; the aluminum skins would have presented too much high-Z material for the MINER ν A target region. In addition, the MINER ν A triangular strip design uses an axial hole to house the WLS fiber, rather than a groove for better dimensional tolerances.

The readout end of the WLS fibers extends beyond the edge of the planes. In the final assembled module, these fibers must be routed across the face of the OD steel frame. The fiber routing scheme has been carefully planned so that there is appropriate clearance around assembly hardware and other module structure that could damage the fibers. Figure 50 shows the fiber routing for a plane. At their extreme ends, these fibers will be arranged into groups of eight and terminated in a DDK connectors. These connectors will provide an optical connection between the WLS fiber and the clear fiber cables that will carry light signals to the readout PMT's. The fiber bundles will be encased between two layers of an opaque fire-retardant polyester-reinforced extruded LDPE plastic sheet sold under the band name of "Tuff-Scrim." The DDK connectors will be installed onto the WLS fibers, polished, and mounted onto a steel strip.

Each assembled detector module will require six OD towers. The OD towers are a scintillator package that will be installed into channels in the steel OD frame and will form the active component of the OD HCAL. Each OD tower consists of eight scintillator extrusions, with a rectangular cross section. The scintillator will be packaged into four individual bundles of two bars, and each bundle will have its own light-tight outer Lexan skin (0.010" thick). Four bundles will be mounted to steel cross pieces that will form an assembly that mount easily into the channels in the OD frame. The WLS readout fibers will be light-tightened with Tuff-Scrim sheeting and will terminate with a DDK connector. An engineer's drawing of an OD tower assembly is shown in Figure 52.

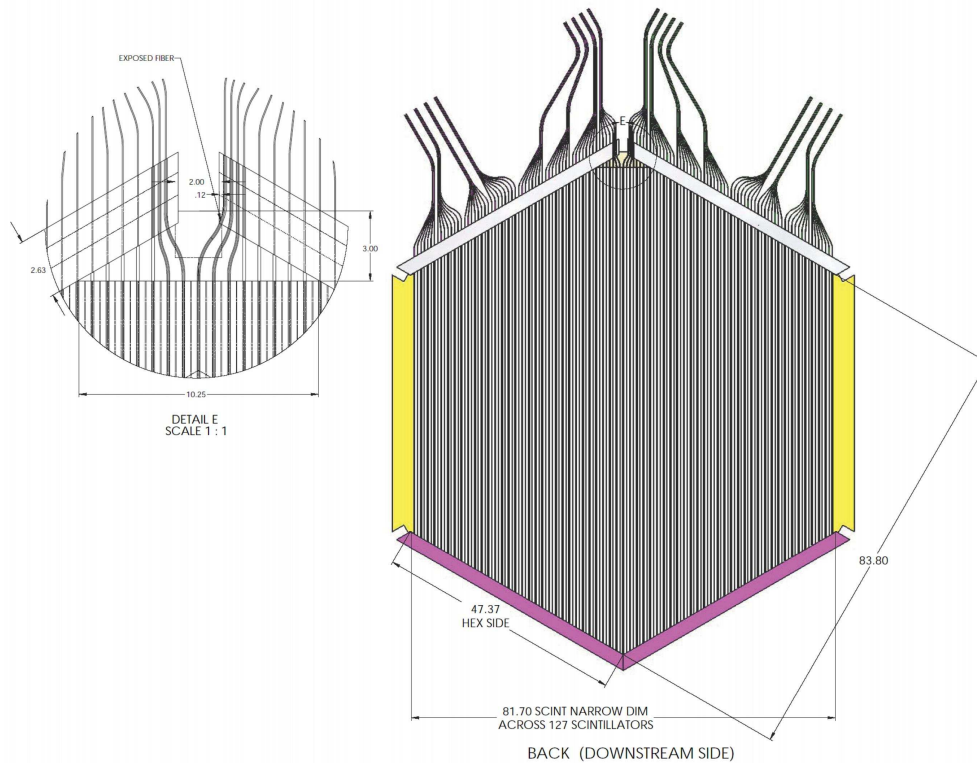


Figure 50: Engineer's drawing of an ID scintillator plane. The WLS readout fibers, shown in a typical routing pattern, are drawn at the top of the plane. The white, yellow, and pink bands at the edge of the plane represent rigid PVC pieces which will be added to reinforce the plane's structure and aid in the fiber routing. Image courtesy of Robert Flight.

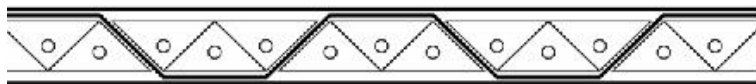


Figure 51: Schematic cross-section of an ID scintillator plane assembly. The scintillator is shown as a plane constructed of triangles. The Lexan web piece is shown as the heavy black line moving through the triangles, and the Lexan outer skins are the thin black lines above and below the plane of scintillator.

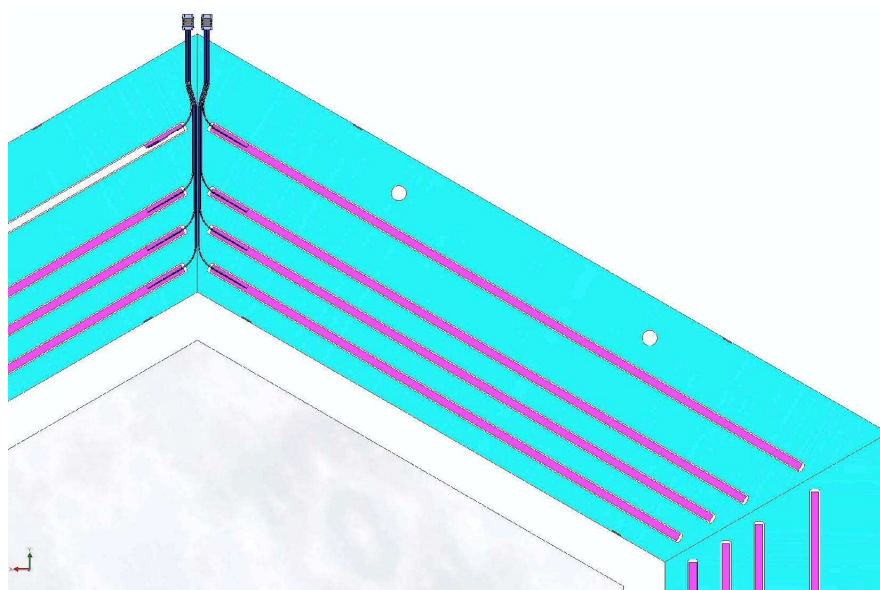


Figure 52: Engineer's drawing showing OD towers (in purple) inserted into the OD steel frame (in blue). The WLS fibers and DDK connectors are shown near the peak in the OD frame toward the left of the picture.

4.1.3 The ID Plane Assembly Process

The assembly of a MINER ν A plane is a multi-step process. The following is a brief overview of the assembly procedure. Many of the figures in this section are photographs we took during assembly of the first MINER ν A inner detector plane prototype completed in July, 2006. This prototype was built at William and Mary by members of the Hampton and William and Mary groups.

Receive and Unpack Scintillator The scintillator extrusions will be manufactured at the Fermilab-NIU extrusion facility. The extrusions will be crated and shipped to the scintillator assembly factories in Virginia. As neither the William and Mary nor the Hampton University physics builds have sufficient room to store a truckload of scintillator, a central warehouse will be used for receiving and storage. This warehouse will be climate-controlled. As need dictates, crates will be and transferred to the assembly factories.

Cut Scintillator to Length As manufactured, the extrusions will all be roughly 4 meters in length. Construction of the hexagonal plane, on the other hand, will require scintillator bars of ranging from 123 cm to 256 cm in length. The first step, then, in the manufacturing process will be to cut the extrusions to the proper length. Each of the 4 meter bars will be cut to yield two bars.

A cutting table has been developed to aid in the cutting. The table incorporates a system of rails with stops used to properly position a cutting fence. The scintillator will be cut by a saw equipped with a carbide-tipped blade used for cutting plastics. As plastics are best cut with a slow blade speed, the saw blade will be slowed down using a Variac controller. One quarter



Figure 53: A photo of the ID scintillator cutting table.

of the scintillator required for each plane will be cut in a single pass. A photograph of the prototype cutting table is shown in Figure 53.

During the cutting process, a modest fraction of the waste scintillator removed by the saw blade, called flashing, can melt, adhere to the extrusions, and obstruct the fiber holes. After cutting, the ends of the scintillator are cleared of flashing and painted with reflective paint to improve the light collection uniformity along the ends of the strips. The holes used to hold the WLS fibers will also be inspected and cleared using dental tools as needed.

Assemble Lower Half of Plane The lower Lexan skin will then laid out on a large work surface. A layer of glue will be applied to the skin, and the lower scintillator bars (those lying below the Lexan web) will positioned on top of the skin. More glue will be applied to the scintillator, and the Lexan web piece which runs through the plane will be positioned on top of the scintillator. At this point, the PVC edge pieces will also be positioned on top of the lower skin. Figure 54 shows a photograph of the lower half plane assembly. A vacuum seal will be applied, and the assembly will be left to cure overnight. Figure 55 shows an plane (with lower extrusions having been positioned to provide a smooth surface) while it vacuum cures.

Assemble Upper Half of Plane The next day, more epoxy will be applied to the top of the web, and the upper scintillator bars and top skin will be added. The plane will then be left to vacuum cure for another day.



Figure 54: Photo showing main components of the lower half plane. The PVC edge pieces are visible toward the top of the photograph. The scintillator extrusions are shown lying under the Lexan web.



Figure 55: The first prototype MINERνA scintillator plane while it vacuum cures.

Insert and Route Fibers After the structure has been assembled, the mirrored WLS fibers will be inserted into the scintillator bars. The readout end of the WLS fibers must follow an appropriate path across the outer OD steel frame in order to avoid damaging the fibers. A sheet of opaque Tuff-Scrim will be used as a routing substrate; the fibers will be fixed into position on the Tuff-Scrim with carpet tape.

Install and Polish DDK Connectors The readout ends of the WLS fibers will be mounted in a “ferrule” which will allow the fibers to plug into a DDK connector. The fibers will be glued into the ferrule, and the entire assembly will be polished using a fly-cutter. 16 connectors will be installed for each plane. The connectors themselves will be mounted to a piece of 1/8” thick aluminum stock. During module assembly, this aluminum stock will be installed on connector mounts on the outer edge of each module’s steel frame.

Glue Fibers and light seal To increase light yield, an optical epoxy will be injected around the fibers in the scintillator. This process will use a commercial two-part epoxy mixing and dispensing machine to inject optical epoxy into the fiber hole in each extrusion. After gluing, an upper Tuff-Scrim cover will be added. The edges of the two layers will be heat sealed and taped together to form a light-tight seal for the fibers.

QA and Light-Leak Testing The final assembly step will be a QA procedure. Planes will be inspected for light leaks and damaged fibers.

Ship to Fermilab Finished scintillator planes will be placed in plywood shipping crates and stored at the central warehouse facility. Once a shipment is complete, the full crates will be sent to the module assembly factories at Fermilab by flat-bed truck.

There will be three assembly periods. First, we will assemble two planes plus a spare and 6 towers plus a spare for the full module prototype in 2006. A year later, we will assemble 40 planes plus spares and 120 towers for the tracking prototype. Finally, we will construct the production assemblies for the final detector in 2008 and 2009.

Using the MINOS manpower requirements as guidance, the expected production rate one plane every six days from each workstation at each assembly site with 45 hours of labor per plane.

OD Tower Assembly The outer detector assembly is significantly simpler. The process begins by cutting the scintillator extrusions to one of four prescribed lengths. Once cut, grooves must be machined in the end of each extrusion to permit routing of the WLS fiber out of the scintillator. Two extrusions of the same length will be glued together, and fitted with a Lexan skin to form a “doublet.” WLS fibers will be inserted into each extrusion in the doublet and glued into place with optical epoxy. Steel straps will be fixed to four bundles to form the basic structure of the OD tower.

The readout end of each fiber will be covered with Tuff-Scrim sheeting, and one DDK connector ferrule will be installed and polished on each OD tower.

Using the MINOS manpower requirements as guidance, the expected production rate is ten OD towers per 35 hours of labor.

4.1.4 Facilities and Resources

The construction of the MINERνA scintillator assemblies will be undertaken at both Hampton and William and Mary. Both programs have extensive experience in detector production. Since the two institutions are located less than 25 miles from each other (and less than 15 miles from Jefferson Lab), they provide a natural team for undertaking a joint detector production program. This team will benefit from a collaborative prototyping program, and the joint set-up costs are minimal for this project. Bulk purchasing responsibilities will be shared by the two institutions, according to the particular strengths and experience of each.

Each university will provide suitable laboratory space to run an assembly factory. The space must be large enough to safely accommodate the construction of the hexagonal ID planes, which are roughly 256 cm in their largest dimension. The fabrication sites must also have appropriate clearance to permit the planes to pass in and out of the building.

Aside from the basic lab space, both assembly sites must be appropriately outfitted for the construction tasks. The required resources will include:

1. Id and OD Scintillator cutting stations.
2. Lexan cutting templates
3. Folding stations necessary to produce the Lexan web pieces and OD doublet covers.
4. Work surfaces to accommodate both ID plane and OD tower assembly. The surfaces must suitably flat and air-tight to facilitate vacuum curing of the epoxy.
5. Vacuum pumps and bags required for vacuum curing.
6. Adhesive mixing and dispensing equipment (required for structural epoxy).
7. Fly cutter (used to polish DDK connectors)
8. Gluing machine (used to dispense optical epoxy for gluing WLS fibers into scintillator).
9. Facilities and rigging to permit overhead lifting. This will be required to load the scintillator assemblies into shipping crates.
10. Appropriate ventilation and safety equipment.

The William and Mary site will be partially outfitted with a fly cutter obtained from the MINOS scintillator assembly factories.

Both sites will be staffed with a mix of full-time technicians and student labor. Graduate students and technicians will be used to supervise teams of undergraduate labor. Each assembly site will require the equivalent of five full-time laborers. Most custom machining will be done at the William and Mary machine shop.

A shared off-campus facility will be used for storage, shipping and receiving. This facility must be climate controlled to prevent damage to the scintillator during storage, and must have necessary materials handling equipment to permit movement of the large crates used to ship the ID planes.

This facility will be used to receive shipments of scintillator from Fermilab. The shipping facility will be used to store the raw extrusions before they are dispatched to the assembly factories. As scintillator assemblies are completed, they will be packaged for shipping and loaded into crates at the factories. Loaded crates will then be moved to the shipping facility, where they will be stored until a full truckload is assembled. Then, the completed assemblies will be shipped to Fermilab.

4.1.5 Interfaces with other WBS Tasks

WBS 3 will receive supplies and materials from three other WBS tasks: WBS 1, WBS 2, and WBS 4. WBS 1 will provide the scintillator extrusions. These will be produced at the NIU-Fermilab extrusion facility, and then shipped to Virginia. WBS 2 will provide the WLS fibers. This effort is being lead by a group from the University of Rochester working at Fermilab. WBS 2 will acquire the fiber from the vendor, verify the fiber quality, mirror one end, and then ship the fiber to Virginia. The fibers will be supplied to WBS 3 pre-cut to their appropriate lengths. WBS 4 will supply the optical connectors and fly cutting bits required to polish them. WBS 4 will perform the majority of connector-related R&D, spec the connectors to the vendor (DDK), and handle the procurement.

The final WBS interface is with WBS 9, module assembly and mapping. The completed scintillator assemblies will be shipped to the module assembly factories at Fermilab, where WBS 9 will use the ID planes and OD towers to build the final detector modules.

WBS 3 will also maintain a number of minor interfaces with private vendors who supply material required for the scintillator assemblies. Epoxy, Lexan, opaque plastic, and PVC foam will all be supplied by private vendors.

4.1.6 Major Tasks

This section will give an overview of the tasks that we have scheduled for the next several years. The subsections will each refer to a specific task or group of tasks in the MINER ν A Project file.

- WBS 3.1.1 - WBS 3.1.3: These tasks cover initial R&D and design work for the scintillator assemblies during 2005-2006. The scintillator units will be designed and prototype assemblies will be constructed. Issues relating to the integration of the planes and towers into the MINER ν A detector modules will be resolved. The majority of the design and integration work was carried out by Robert Flight, a mechanical engineer from the University of Rochester in collaboration with Hampton and William & Mary. Connector polishing techniques will be tested and practiced.
- WBS 3.1.4-5: These tasks cover outfitting of the scintillator assembly factories at both Hampton University and William and Mary. Workstations will be constructed, and tooling will be purchased during the summer FY 2006 and FY 2007.
- WBS 3.1.6-9 - Full Module Prototype Scintillator Assemblies: In the fall of 2006, a prototype detector module will be build at Fermilab. These tasks cover production of three ID planes and seven OD towers for the prototype module.

- WBS 3.2 - Tracking Prototype: The tracking prototype will consist of 20 detector modules that will be built in the fall of 2007. Tasks under WBS 3.2 cover production of the ID planes and OD towers for the tracking prototype. Tasks cover procurement of the materials for the factories, construction of the assemblies, and shipping of the complete assemblies back to Fermilab.
- WBS 3.3.1-4 Detector components and materials: After the tracking prototype is completed, the assembly factories will prepare for the construction of the final (production) detector. WBS 3.3.1-4 cover procurement of materials for the production detector. This work will take place in FY 2008 and early FY 2009.
- WBS 3.3.5-6 Detector assembly: The scintillator assembly factories will open for their third and final time in mid 2008. These tasks are the construction of the ID planes and OD towers for the production detector.
- WBS 3.3.8 - Storage and shipping: The last step in the process will be to package the final assemblies in shipping crates, store them, and then ship them to Fermilab. This work will be completed in early FY 2009.

4.1.7 R&D and value engineering

A significant amount of R&D has already been completed. In the summer of 2005, a W&M undergraduate researched techniques for injecting optical epoxy into the fiber holes of the scintillator extrusions. Optical epoxy improves the optical contact between the WLS fiber and the scintillator, improving the light collection efficiency of the system. Two different glues were tested, 815C and Eljen optical epoxy. 815C was chosen because it produced the highest light yield. Glue mixing and injection techniques were also researched. In the production factory, glue will be injected into the fiber hole with an air driven glue machine. Final techniques were used to glue WLS fiber into the vertical slice test, a small array of scintillator used by WBS 2 to test detector optics and tracking.

In 2006, significant amounts of time were spent interfacing with WBS 8 and 9 to resolve fiber routing issues. In the final detector modules, the WLS fibers will be routed across the OD steel frame. The fiber path across the steel frame is where the WLS fibers will be least protected and most susceptible to damage. Hence, the path must protect the fibers as much as possible, while being consistent with the overall module design.

With assembly of the prototype plane in the summer of 2006, there was significant development of the cutting table and other factory workstations. These early tests have demonstrated that the labor estimates are reasonably valid.

As planes and towers are developed for the full module prototype, factory outfitting and production techniques will be refined in late 2006 and early 2007.

4.2 OD Steel Frame Construction and Physical Facilities

WBS 8 is responsible for fabrication of the detector module OD steel frames and steel fixtures to be used in Wideband Hall during the detector assembly. In addition, WBS 8 procures all nuclear absorber material for the detector calorimeters and assembles the upstream nuclear targets.

is suitable for use as a magnet and preserves the possibility of a magnetic field as a future upgrade. The most important parameter of the steel plates is its flatness. In the specification, the upper limit is required to be 1/2 of the ASTM standard limit for flatness in plates; for MINER ν A, this translates to a flatness of less than 3/16". For the MINOS project a steel mill was able to routinely provide material that was within the specification. Less than 1% of the over 4000 plates in MINOS were out of spec.

Cutting the steel is specified in [167]. In this specification are the tolerances for the part dimensions, flatness of the finished pieces, and fabrication methods. The vendor will evaluate the flatness of the finished pieces on a case-by-case basis. Parts will be flattened as required by the specification. Contingency for the steel pieces is sufficient to cover any additional costs associated with flattening.

2. OD Frame Assembly: The steel wedges previously described must be welded to form the OD frames. This work will be done by Fermilab technicians and welders just before each detector module is assembled. Six wedges will be clamped into place on a strongback. The strongback will be held vertically, and the wedges will be welded together to form the frame.
3. Detector Stands, Bookends, and Axial Bolts: WBS 8 supplies all fixtures required to mount the detector. The detector stand will hold MINER ν A modules much like a hanging file system in a file drawer. The first module will be anchored to a bookend structural element at the end of the stand. This bookend will keep the modules stable and plumb. Axial bolts will then be used to anchor each succeeding module to the one previously installed. Six axial bolts will be used for each module. Figure 57 shows a drawing of an axial bolt and Figure 58 shows a drawing of the detector stand. MINER ν A will require two detector stands in the NuMI experimental hall (one holds the detector in the beam, while a second is used to stage modules during installation) and three smaller detector stands to be used in Wideband Hall during module assembly. Each detector stand must be outfitted with a bookend.

Fermilab uses the American Institute of Steel Construction, Manual of Steel Construction as the safety code for all structural steel fabrications such as the stand and lifting fixtures.

4. Strongbacks: A strongback is a steel framework that supports modules during assembly and protects them during lifting operations. WBS 8 will procure three strongbacks for use in Wideband Hall during the production frame welding and module assembly periods.

For WBS 8's specific interests, the strongbacks will serve as a welding jig during frame construction. The six wedges of steel will be placed on the strongback in the correct position and clamped down by a series of holding bars. These bars will keep the frame from distorting as it is welded together. After tacking the wedges together the strongback will be moved to a vertical holding fixture that allows the frames to be welded on both sides.

As a lifting fixture the strongback allows the frames to be built on the floor horizontally and then raised to vertical for hanging on the support rails. The pick point on the strongback is chosen so that the frame never hangs in a truly vertical position but always has a slight tilt so the load is stable with the load's center of gravity on top of the strongback.

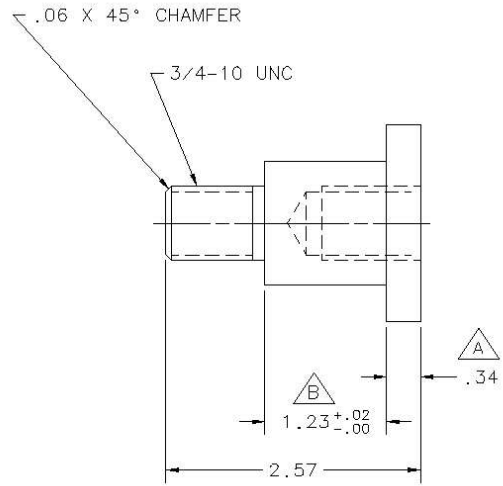


Figure 57: Engineer's drawing of an axial bolt.

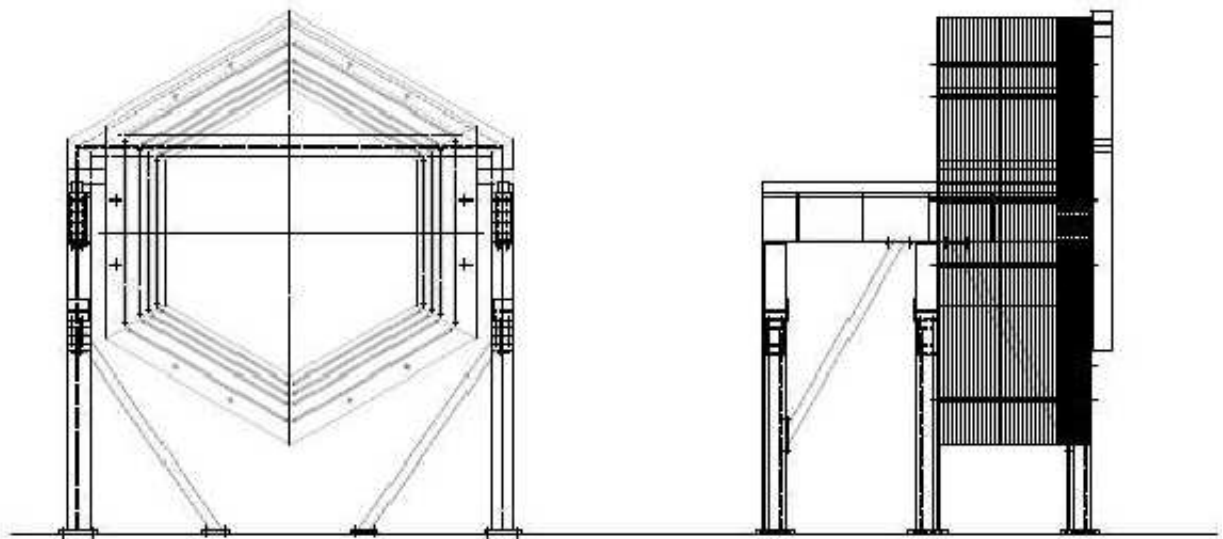


Figure 58: Engineer's drawing showing front and side view of the MINERνA detector stand.

Finally the strongback is used as the transport fixture for moving the frames from the Wideband hall to the MINOS cavern. Frames are kept on the strongback as they are loaded on the truck for hauling to the surface building.

For lifting fixtures, the “ANSI/ASME B30.20, Below-the-Hook Lifting Devices” safety standard will be used.

5. Procure nuclear absorber material: WBS 8 is to procure lead for the MINER ν A OD and DS ECAL and steel for the DS HCAL.

The OD ECAL is constructed by mounting a lead collar to the outer edges of the scintillator planes which make up the tracking volume of the detector. The collars are constructed from six wedge shaped pieces of lead. In the DS ECAL modules, the entire face of the scintillator planes are to be covered with a hexagonal sheet of lead. In the DS HCAL modules, hexagonal sheets of steel replace one of the scintillator planes.

6. Construct US Nuclear Targets: WBS 8 is to procure lead, steel, and graphite for the US nuclear targets. While these materials will be supplied by outside vendors, the nuclear targets will be assembled by FNAL technicians.
7. PMT Access Platform: The phototube access platform is needed allow a technician to service the the phototubes and the front end electronics, which are mounted above the detector. This will be a rolling platform mounted on rails above MINER ν A. The platform will not have drive motors, however a technician should easily be able to push it along the beam axis of the detector to reach any phototube box or fiber cable.

4.2.2 Facilities and Resources

The work required by WBS 8 will be accomplished by a mix of FNAL resources and an array of outside vendors. All of the WBS 8 design work will be accomplished by FNAL engineers and drafters, with some support from Robert Flight of the University of Rochester. The resulting drawings will then be taken to local vendors for fabrication work. Fermilab technicians and welders will also be used during times of OD frame construction. The Fermilab technicians that will be working on the MINER ν A project are the same crew that assembled all of the detector planes for the MINOS Near Detector. They have experience with the procedures and the material handling facilities available in the buildings. They also have training for using the cranes, forklifts and working with lead.

The major construction of the MINER ν A experiment will occur in the Wideband Experimental Hall. This is where the OD frames and nuclear targets will be assembled. This building has two 15 ton cranes available for assembling the frames and moving materials in the building. Wideband Hall has sufficient electrical utilities for welding and power tools required and will be equipped with an electric forklift for material handling in the building. The north end of the building will be used for storing, preparing and handling the steel parts of the detector and the south end will be used for storing and handling the active scintillator elements. The far south end of the building will have a cage securing access to the frame mapper and its radiation source. Figure 59 shows the proposed configuration of Wideband Hall as it will be used for frame and module assembly activities.

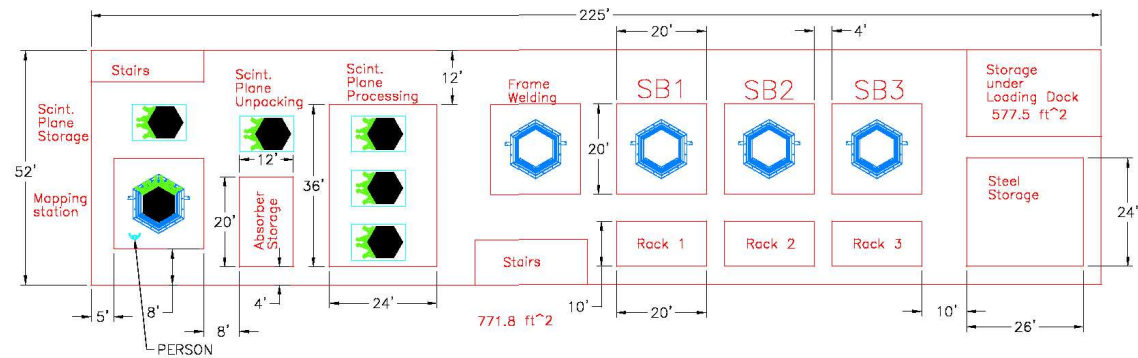


Figure 59: Engineer’s drawing showing an initial concept of the Wideband Hall layout. Most frame assembly and module assembly activities take place on the strongbacks, labeled “SB1”, “SB2”, and “SB3” in the drawing. Areas for scintillator preparation and module mapping are found to the left in the drawing. Drawing courtesy of R. Flight.

4.2.3 Interfaces

WBS 8 maintains a large number of interfaces, both with other WBS task groups and also with private sector vendors.

WBS 8 relies on vendors largely for supply and fabrication tasks. Because of the MINOS project, WBS 8 has past experience with many of the vendors who will be handling MINER ν A tasks. The most important, and involved, vendor interface will be with the suppliers of the OD wedges. The MINER ν A steel order is large enough that it will be supplied directly from a steel mill. Once a vendor is selected, MINER ν A will be assigned a place in the mill's work schedule, so procurement of the steel will have a large lead time. Since the critical specification of the steel is the flatness of the wedges it will be most important to monitor the quality of the steel parts with a quality assurance plan. Besides regular measurements of the parts as they are received it will be necessary to make some visits to the factory during production startup and periodically thereafter if the parts go out of tolerance.

The second interface is with WBS9. Once finished, OD frames will be delivered to WBS9 who will use the frames to construct detector modules. As frame assembly and module assembly will proceed in tandem, frames will be delivered to WBS9 individually as they are assembled. WBS9 will receive each frame sitting on a strongback in Wideband Hall. WBS 8 will also supply WBS 9 with all of the strongbacks and detector stands required to outfit Wideband Hall for module assembly.

The third interface is with the Installation and Infrastructure task WBS11. WBS 8 supplies WBS11 with a number of fixtures required for the detector installation, including the detector stand, axial bolts, bookends, PMT access platform, strongbacks, and the MINER ν A nuclear targets. There is substantial overlap between WBS 8 and WBS11; many of the installation tasks will be handled by the same FNAL crew and technicians that will assemble the OD frames.

4.2.4 Major Tasks

The major tasks required to complete WBS 8 include:

- WBS 8.1.1 and 8.1.2 - Prototype Design Work: These tasks include all of the design and engineering work for items such as the detector stands, axial bolts, strongbacks, and the PMT access platform. While the bulk of the work is to be done by FNAL engineers and drafters (WBS 8.1.2), Robert Flight at the University of Rochester, will give assistance with some tasks (WBS 8.1.1).
- WBS 8.1.3 - Procure Prototype Materials: This task completes procurement of all materials needed for early prototyping efforts, including the full module prototype. For the full module prototype, WBS 8 will deliver a prototype detector stand and bookend, one OD frame, a strongback, and a set of axial bolts.
- WBS 8.1.4 - Assemble Prototype Stand in Wideband Hall: This task covers installation of the prototype detector stand in Wideband Hall, which must be completed before the full module prototype is built.

- WBS 8.1.5 - Outer Detector Frame Prototyping: This task covers assembly, welding, and testing of the OD frame for the full module prototype.
- WBS 8.2.1 - Procure Tracking Prototype Materials: These are all the procurement tasks for the tracking prototype.
- WBS 8.2.3 - Tracking Prototype OD Fabrication: This task is construction of all the OD frames for the tracking prototype.
- WBS 8.3.2 - Procure Production Materials: These are the final procurement tasks required for the production detector assembly. Final OD steel wedges, strongbacks, detector stands and axial bolts will be purchased.
- WBS 8.3.3 - Production OD Fabrication: This task covers construction of the OD frames for the production detector assembly period.

In general, tasks falling under WBS 8.1 will occur during 2006, tasks under WBS 8.2 will happen during 2007, and tasks under WBS 8.3 will occur in 2008-2009.

4.3 Module Assembly and Veto Wall

The main tasks of module assembly are to construct and map all MINER ν A detector modules, and build the veto wall. These are the last construction steps before the detector is ready for installation. In addition, we are also responsible for a number of related tasks, such as construction of the PMT racks and the module mapper.

While the final module assembly and mapping for the detector will take place at Fermilab during a period of approximately six months in 2009, the preparations for module assembly require a multi-year effort that is being lead by the University of Rochester, with contributions from Fermilab and collaborators from Peru. The preparatory efforts entail an extensive program of building prototypes, development of assembly protocols, designing custom hardware, procurement, and fabrication. Because module assembly involves the integration of components built by other WBS task groups, our preparations also must emphasize communication with the other L2 managers responsible for these systems.

This section will begin by presenting an overview of WBS 9. This will include an overview of the module assembly and mapping process and some discussion of the less obvious aspects of WBS 9, such as the fabrication of PMT racks. We will then move on to a discussion of how WBS 9 plans to meet these objectives. This will include an overview of resources required both from Fermilab and the university groups, a discussion of the interfaces with other WBS tasks, and an overview of the specific activities that we have scheduled for the next few years.

4.3.1 Task Objectives and Overview

The specific tasks that WBS 9 is responsible for include:

1. Assemble all MINER ν A detector modules and map the local response of the scintillator. These include modules for the final detector, the tracking prototype, and the full module prototype.
2. Design and construct the module mapper.
3. Install and commission the tracking prototype.
4. Fabricate mounting racks for the PMT's and develop tools required for PMT maintenance.
5. Develop routing scheme for clear fiber cable routing.
6. Construct the veto wall.

The following subsections will discuss the specifics of each task.

Module Assembly and Mapping Procedure Assembling a MINER ν A module is a multi-step process. The following is a brief overview of the module assembly procedure as we currently envision it. Many of the figures in this section are based on photographs we took during mock assembly exercises that were conducted at the University of Rochester using prototype modules constructed from wood. More details about the module assembly procedure are contained in [168].

Receive and prepare materials WBS 9 receives scintillator modules from WBS3. Once these modules arrive at Fermilab from Virginia, we will receive the materials and store them in Wideband Hall.

Once the assembly factory opens, the first step will be to unpack and prepare the scintillator. ID planes and OD towers will be inspected for any obvious shipping damage and broken WLS fibers. If the schedule calls for active target modules or DS ECAL modules to be assembled, then sheets or collars of lead absorber material will be applied to the US face of the scintillator planes. Layout and identification marking will be applied to the modules.

Steel frames will be provided by WBS8. These frames will be inspected and deburred to ensure that rough edges do not damage scintillator or fibers. Markings identifying the type of module to be built will be applied. A traveler providing more specific instructions will also be affixed. After work on the OD frame has finished, the assembly area will be cleaned.

Figure 60 shows a model OD frame mounted on a strongback.

OD scintillator installation The scintillator towers will be installed by hand into the slots cut into the OD steel frame. We will use silicone caulk to secure the scintillator towers to the frame. A bead of caulk will be applied to the sidewall of the frame channels that house the scintillator. As the scintillator bars are installed into these channels, the caulk will fill the gap between the scintillator and the steel frame. Installing the caulk before the scintillator minimizes any mess. Figure 61 shows a picture of an installed OD scintillator assembly.



Figure 60: At this point, the steel frame has been welded and is mounted on the steel frame. It is inspected, cleaned, marked, and prepared for assembly.

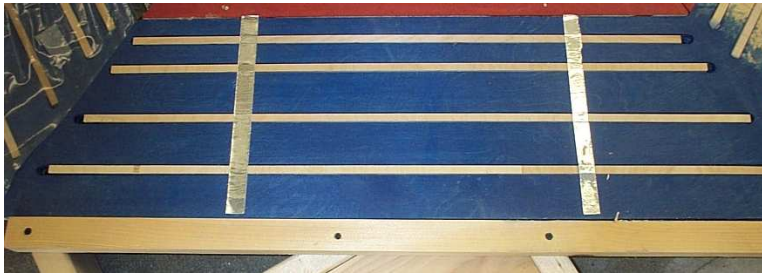


Figure 61: The OD scintillator fits in a series of channels in the OD steel frame. The metal bars, which are perpendicular to the scintillator bars, will be a structural element of the assembly. On an actual module, the scintillator assembly will be held into place with silicone caulk.



Figure 62: *Left:* Close-up photograph shows the load-bearing spacer (in red) mounted on the OD frame (in blue). *Right:* Angle stock for ID scintillator clear fiber connector mounting attaches to the outer face of the OD steel frame. Note pieces located above and below the module mounting hook.

Load-bearing spacer and connector mounting installation The load-bearing spacer will consist of four blocks of material which bolt to the inside surface of the bottom two sectors of the steel frame. This material will bear the weight of the scintillator planes or absorber material that will later be installed into the inner detector. These blocks will be held into position by studs which will have been welded to the OD frame by WBS8.

The connector mounting consists of aluminum angle stock that will mount to the outside surface of three OD sectors. The clear fiber cable connectors will later mount to this angle stock. Like the load bearing spacer, these pieces will be held by studs which will have been previously welded to the OD frame.

Pictures of the load-bearing spacer and connector mounting on our model are shown in Figure 62.

US plane or absorber material installation The first ID material will then be installed. For most modules, the first scintillator plane will be installed at this point. The scintillator plane will be moved into position with the aid of the Wideband Hall overhead crane and a vacuum lifting fixture. This plane will be installed in a “u” or “v” orientation, depending on the assembly schedule. The WLS fibers from this first scintillator plane will be routed across two sectors of the OD steel frame and the clear fiber connectors will be attached to the mounting stock.

Downstream HCAL modules do not have an US scintillator plane. In these modules, the US scintillator plane is replaced with a large steel plate. These plates will be installed during frame assembly by WBS8.

DS plane installation All module types incorporate a DS scintillator plane. In most modules, this plane will always be installed in an “x” orientation. However, the DS plane in the DS HCAL modules may have an “x,” “u,” or “v” orientation. Once the plane has been moved into position, the fiber packages will again be routed across the OD steel frame and the connectors will be installed.

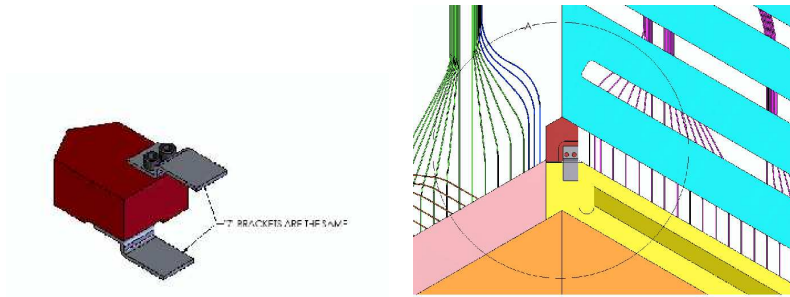


Figure 63: *Left:* Engineering drawing showing proposed h-clip. *Right:* Drawing showing an h-clip installed in a MINERνA module. The triangular end of the h-clip will be welded to the OD frame by WBS8 during frame assembly. The smaller metal pieces will clamp the scintillator planes into position. Images courtesy of R. Flight.

H-clip installation The scintillator planes will be fixed into position by a hardware piece we have called an “h-clip.” A picture of an h-clip is shown in Figure 63.

Module mapping At this point, the module will be mapped. Mapping will be discussed in greater detail in Section 4.3.1. If the mapping procedure reveals that a module will perform unacceptably, then we will troubleshoot and remap the module at this point.

Alignment surveys Before being stored on the detector stands, the modules will be surveyed by the FNAL alignment group. The modules are mapped while lying horizontally on the strongback, but they will be moved into a vertical position for storage and installation. This initial survey will measure the effect of hanging the modules vertically, noting any changes in the position of the scintillator planes in relation to the OD frame.

Package module for storage The module will then be packaged to minimize the risk of damage during storage and installation. Lengths of 2”X4” lumber will be fixed to the OD frame through the axial bolt holes. These wooden “bumpers” will minimize the risk of crushing fibers.

Store module The module is then moved to the storage rack in Wideband Hall, where it will await installation into the NuMI Experimental Hall. A picture of a completed module is shown in Figure 64.

After a factory startup period, we are planning to assemble modules at a rate of one per day. There will be three assembly periods. First, we will assemble one module for the full module prototype that will be built in Fall of 2006. A year later, we will assemble twenty modules for the tracking prototype. Finally, we will construct the production detector modules in early 2009.

Design and Construct Module Mapper Every detector module will be mapped after it has been assembled. The purpose of mapping is to study the local response of the scintillator. The mapper



Figure 64: The completed module has been moved to a storage rack. The DS face of the module here is shown so that the WLS fibers can be viewed.

will scan the scintillator of all detector modules at pre-determined points with a radioactive source. The response of the scintillator as a function of position will then be recorded by computer. Mapping allows us to identify any irregularities in the scintillator that will affect the detector performance so that we can account for this while analyzing data. Mapping is also one of our main quality assurance measures for each assembled module.

In consideration of radiation safety, we have decided that the mapper will remain within a fenced area at one end of Wideband Hall at all times. Modules will be transported to the mapping area by use of the Wideband Hall overhead crane. The module and strongback will be positioned on the floor in the mapping area, and then the mapper will be moved into position above the module.

While we have not yet completed our mapper design, an initial engineer's drawing is shown in Figure 65. As shown in the Figure, the mapper will consist of a large, heavy steel frame and a scanning carriage that incorporates two scanning heads. The frame must be large enough to span an assembled module and rigid enough to withstand the stress of repeated lifting. Each scanning head will incorporate a 5-10 milli-Curie Cs-137 radioactive source shielded in a lead cone. The scanning heads will travel on rails and the motion will be provided by lead screws driven by electric motors. The motors will be controlled by a nearby computer.

As a module is mapped, the scintillator response will read out using M64 PMT's and a prototype electronics system controlled by a computer.

The design goal of the mapper is to safely scan one module within a period of 10-12 hours.

Assemble and Commission the Tracking Prototype WBS 9 has been asked to assemble and commission the tracking prototype. As the modules are assembled, our technicians will "install" the detector on a detector stand in Wideband Hall. This installation exercise, unlike the final detector installation, is part of the Project and has been assigned to WBS 9. As modules are secured on the

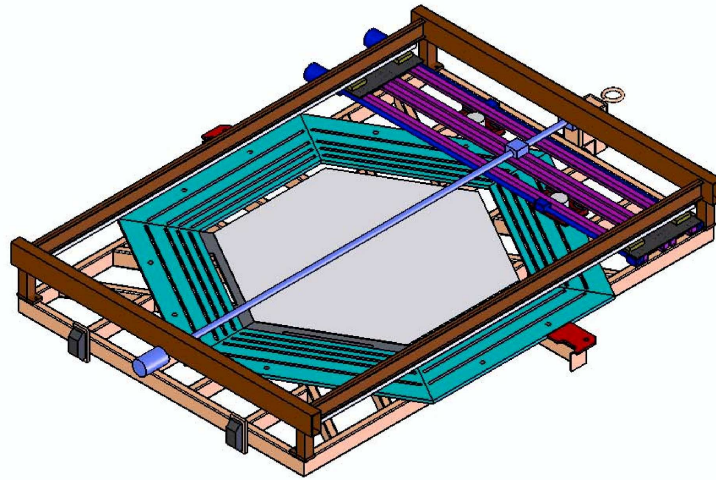


Figure 65: The module mapper incorporates a heavy steel frame and scanning carriage that will carry two Cs-137 radioactive sources. The mapper will be mated to the strongback so that the scanning heads are suspended above the module. Image source: [170].

stand, PMT's and readout cabling will also be installed.

Commissioning will be a busy time, and will involve input from more than just WBS 9. As the detector is turned on, there will be representatives from all levels of the collaboration interested in verifying the performance of specific systems. We will have expertise in the detector modules, but we will largely be reliant on experts from other tasks to handle problems with other systems, such as electronics and software. During this initial period, we will coordinate activities in the Wideband Hall and provide support to the various groups. We will ensure that groups have the tooling and resources they need to perform their work safely.

As the detector stabilizes and most of the immediate problems are solved, one of the major commissioning activities will be the collection of cosmic ray data over a period of 4-6 weeks. WBS 9 will ensure that the counting house is staffed with a shift crew. We will also verify that the shift crew has been properly trained, that necessary documentation has been provided, and ensure that the daily plan for shift workers is properly implemented.

PMT Racks and Clear Fiber Cable Routing WBS 9 will address certain issues related to the installation and handling of the PMT's and clear fiber cables. This responsibility was assigned to WBS 9 because our lab at the University of Rochester has the capacity to fabricate wooden models of detector components. We fabricated a full-sized model PMT rack based on early engineering designs and used this to study routing of the clear fiber cables and PMT box handling and maintenance issues.

The racks will be designed by a mechanical engineer at the University of Rochester. The final design will be based heavily on our experience with the wooden prototype rack. Racks will be fabricated in Rochester by an off-campus machine shop. Because the PMT's are to be mounted on

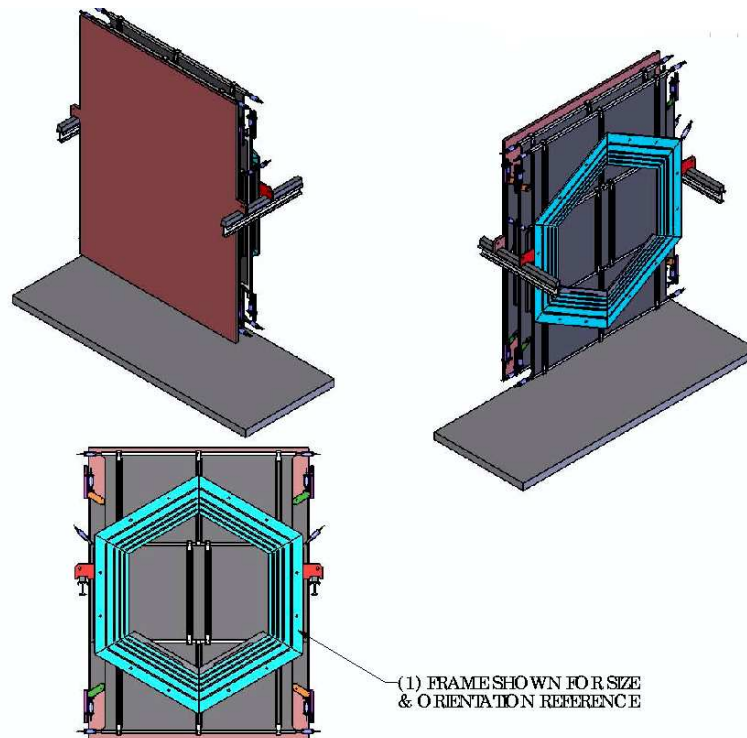


Figure 66: Initial engineer's drawing of the veto wall assembly. The veto wall consists of a large steel plate (shown in purple) followed by two tiled arrays of scintillator counters (in gray). The steel wall and scintillator arrays cover the front end of the detector. Image source: [169].

top of the detector, they must be accessed from an overhead platform that will be provided by WBS8. WBS 9 will also design and provide a lifting jig that can be used during PMT maintenance. Lifting a PMT must be done carefully in order to minimize the possibility of damaging the fiber optic cables used to convey light from the detector to the PMT's.

Finally, we will develop the connector-to-PMT mapping for the clear fiber cables. Because we have the prototype PMT rack, we have been able to experiment with various arrangements of the the clear fiber routing. We have also been able to spec the length of the clear fiber cables based on our experience with a scale model. While the cable lengths and routing scheme have not yet been finalized, details of the current scheme are available in [168].

Construct Veto Wall The veto wall will be constructed largely from recycled components. The large steel sheet on the US end of the veto wall will be scrap steel from Fermilab surplus. Just downstream of the steel plate will be two walls of scintillator. These walls will be tiled arrays of scintillation counters. The veto wall counters will be constructed with refurbished scintillator taken from the NuTeV experiment. Each panel will have its own WLS light guides and readout PMT's. An initial engineer's drawing of the veto wall is shown in Figure 66.

The scintillator panels will be refurbished as part of a summer research program for high school teachers at the University of Rochester. The teachers will re-wrap and test the NuTeV scintillator during the summers of 2006 and 2007. WBS 9 will coordinate with and provide some support to the summer research program, and take delivery of the refurbished panels. If any of the scintillator or light guides is found to be unusable, then WBS 9 will be responsible for procuring additional panels or light guides.

WBS 9 will design the support structure for the steel wall and scintillator arrays. We will have these parts fabricated and transport all veto wall materials to Fermilab.

4.3.2 Facilities and Resources

WBS 9 requires facilities from both the University of Rochester and Fermilab.

The R&D effort of WBS 9 is centered at the University of Rochester, where we have the core personnel and facilities required to efficiently complete the research effort. This R&D program covers such tasks as development of the initial assembly protocols, testing of materials and tools for use in the module assembly process, refurbishment of the veto wall scintillator, and all design, fabrication, and purchasing tasks. Much of these early tasks are being led by Robert Bradford (the L2 manager for WBS 9), Robert Flight (mechanical engineer employed by the UofR Physics Department), Kevin McFarland (MINER ν A spokesman), and Dan Ruggiero (UofR technician) with significant contributions provided by both graduate and undergraduate students. Our research group has been provided with laboratory space dedicated to MINER ν A.

While the R&D tasks will be well performed in Rochester, the heavier assembly tasks will require the use of Wideband Hall at Fermilab. Wideband Hall provides ample floor space required to safely assemble and map the detector modules, good overhead crane coverage, and a door large enough to permit the passage of modules out of the building for installation. Wideband Hall will be the location for:

1. Construction of the module mapper.
2. Receipt and storage of detector components provided by university groups.
3. The module assembly and mapping factory. All full-sized prototype modules (including the full module prototype and tracking prototype) and final detector modules will be assembled in Wideband Hall.
4. Installation and commissioning and testing of the tracking prototype.
5. Welding of the OD steel frames (done by WBS8).

Within the Hall, we will require several assembly stations, storage space for detector components, storage racks for completed modules and a mapping station. Because the module mapper will contain radioactive sources, the mapping station must be a fenced enclosure posted with appropriate signage. Figure 59 shows the proposed layout of Wideband Hall. This layout has been negotiated with WBS8 and reviewed by appropriate safety interests from Fermilab.

Most labor for these heavier tasks will be provided by the University of Rochester. The University employs several experienced technicians who will construct the module mapper, coordinate delivery and receipt of detector components, and assemble and map the modules. The technicians will be supervised by Robert Bradford and other UofR personnel. Bradford will relocate temporarily to Fermilab during times of major activity.

During module assembly and mapping, the FNAL Alignment Group will conduct surveys of several modules.

Finally, software for the module mapper will be developed by a number of parties. While the mapper DAQ and motion control software will be provided by Fermilab engineers through WBS7, there will also be input from two institutions located in Lima, Peru, the Pontificia Universidad Catolica del Peru and Universidad Nacional de Ingenieria. Graduate students from these institutions will develop simulations that will guide the design of the mapper, will help integrate the mapper data into the broader MINERvA software environment.

4.3.3 Interfaces with other WBS Tasks

WBS 9 interfaces most closely with WBS3, 8, and 11. WBS3 provides all scintillator assemblies, both the ID planes and the OD towers. These modules will be constructed at two institutions in Virginia, and then shipped to Fermilab. WBS 9 will take delivery of the scintillator units and store them in Wideband Hall. WBS8 will provide steel OD frames for module assembly. The frames will be built in Wideband Hall at the same time that the detector modules are being assembled. Each OD frame will be constructed on one of the three strongbacks in the Wideband Hall assembly area. Having three strongbacks (see Figure 59.) will allow frame welding, module assembly, and module mapping to occur in tandem. Frames will be delivered by WBS8 one-at-a-time as they are constructed. After a frame has been constructed, it will remain on the strongback and WBS 9 will begin using that frame to construct a detector module. After each production module has been assembled and mapped, it will be moved to a detector stand in Wideband Hall. These modules will be stored here until the detector is installed in the NuMI experimental hall by WBS11. We will also provide WBS11 with the cable routing layouts for the clear fiber cables and PMT racks.

WBS 9 has more minor interfaces with several of the other task groups. These interfaces include:

1. WBS4 - Clear Fiber Cables: WBS 9 used early prototype models to spec the clear fiber cable lengths for WBS4 and develop the connector-to-PMT mapping scheme. WBS4, in turn, will provide WBS 9 will clear fiber cables required for the module mapper and the tracking prototype.
2. WBS5 - PMT boxes: WBS5 will provide WBS 9 with six Hamamatsu M-64 PMT's for use with the module mapper and an additional 110 PMT's for the tracking prototype. These PMT's will have been acquired and tested by WBS6; electronic components of the PMT boxes will be supplied by WBS7.
3. WBS7 - Electronics: A prototype data acquisition system will be supplied by WBS7 for use with the module mapper. This will be used to read out the scintillator response as the scintillator

planes are scanned by the mapper. WBS7 will also be providing the DAQ and motion control software for the mapper.

4.3.4 Major Tasks

This section will give an overview of the tasks that we have scheduled for the next several years. The subsections will each refer to a specific task or group of tasks in the MINER ν A Project file.

- WBS 9.1.1 - Rochester Prototypes: During the summer of 2005, we constructed wooden models of various detector components. In particular, we built two half-scale detector modules and a full-scale PMT rack. The wooden modules were then used in a series of mock module assembly exercises during which we outlined the assembly protocol, tested materials, and conducted basic time-motion studies. The model PMT rack was used to design the routing scheme of the clear fiber cables.
- WBS 9.1.2 - Full Module Prototype Assembly Fixtures: After studies with the wooden prototypes, then we will prepare for construction of the full-scale module prototype to be built at Fermilab in the Fall of 2006. These preparations include design and fabrication of hardware to be used for the prototype assembly, selection of tools, and acquisition of materials and hardware.
- WBS 9.1.3 - Veto Wall Counters and Veto Wall Design: In the spring and summer of 2006, work will begin on the veto wall. An inventory of the scintillator counters at the University of Rochester will be taken to verify of sizes and quantities of the available counters. Work will then commence on refurbishment and testing of the counters; this will be done by high school teachers and their students as part of a summer outreach activity lead by Kevin McFarland. The counters will be tested during two summers, 2006 and 2007. At this time, initial engineering drawings will be made on the veto wall to verify that the available counters will be sufficient for the detector's needs.
- WBS 9.1.4 - Design and Construct Mapper: The module mapper will be designed and constructed during the summer and fall of 2006. The design work will be done by a mechanical engineer at the University of Rochester. The same engineer will spec the required parts and begin the procurement. The mapper will require a large number of custom parts. We will have these fabricated by local machine shops so that the engineer will be able to readily interact with the machinists.

The mapper will be constructed at Fermilab using space in Wideband Hall. Once the parts have been acquired at Rochester, then they will be delivered to Fermilab by truck. The University of Rochester employs several technicians that are resident at Fermilab who will be responsible for the physical assembly of the mapper.

At this time, work will also begin on the readout and motion control software for the mapper.

- WBS 9.1.5 - Full Module Prototype Assembly: At the end of 2006, the collaboration will construct one prototype detector module. The module will be full-sized and should be fully

functional, but it will be constructed from prototype components. WBS 9 will assemble this module. This will provide us with the opportunity to train the technicians using actual components and facilities, further refine our assembly procedures, and test the module mapper.

- WBS 9.1.6 - Module Assembly and Mapping Preparations: 2007 will be spent preparing for assembly of the tracking prototype. This will begin with a redesign of any hardware and facilities based on our experience with the full module prototype. Much of the procurement work for the tracking prototype and final detector will be done this year. We will build the PMT racks, further optimize the module mapper, and fabricate a lifting jig that will be used for PMT installation and maintenance.
- WBS 9.2.1 - Assemble, Map, and Install Tracking Prototype Modules: WBS 9 will assemble and map all 20 modules for the tracking prototype, and install all modules into a detector stand in Wideband Hall.
- WBS 9.2.2 - Install Modules at Wideband: Once the modules have been assembled, WBS 9 will complete the assembly and installation of the tracking prototype in Wideband Hall. These activities will include installation of PMT racks, PMT's, and all cables. Electronics will be installed by WBS7.
- WBS 9.2.3 - Test and Evaluate Tracking Prototype: We will then commission the tracking prototype. We will have it surveyed to verify that the detector dimensions are within spec and collect cosmic ray data to test tracking. WBS 9 will set up a shift schedule and ensure that the counting room is staffed. We will also ensure that all shift takers have been adequately trained.
- WBS 9.3.1 - Veto Wall Assembly: After the tracking prototype has been assembled, then we will complete work on the veto wall. By late 2007, all veto wall counters will have been tested. Based on this information, we will then select the best counters to use in the veto wall. At this point, the design of the veto wall will then be revisited to verify that the support structure will accommodate the actual dimensions of the selected counters. Fabrication of the support structure will be completed and all materials will be shipped to Fermilab. The steel wall will be constructed at Fermilab. All items will be stored until the detector is installed in the NuMI hall.
- WBS 9.3.3 - Assemble and Map Production Modules: In early 2009, we will begin to assemble and map the modules for the MINER ν A detector.

4.3.5 Future Work and Engineering

As we are still in the R&D phase of the MINER ν A schedule, much of our engineering and optimization work is underway.

While we have practiced and rehearsed our initial assembly procedures, we are attempting to verify that these procedure will be compatible with the actual detector components. The assembly protocols were developed and rehearsed with our half-scale wooden prototype modules. These procedures have been written up in a document which is available in the MINER ν A Docdb [168]. We are currently trying to verify our understanding of the OD frames with WBS8 and the scintillator

modules with WBS3. These components are crucial for module assembly, so even small changes in the frames or scintillator assemblies could greatly impact WBS 9. We are working to finalize a set of engineering drawings of the OD frame with WBS8. Since our initial prototyping efforts, more details of the scintillator assemblies have become available. We have acquired samples of the materials to be used by WBS3, and we are currently testing to verify that our assembly procedures will work well with the scintillator assemblies. These efforts include such tests as verifying that our adhesives will adhere well to the materials that WBS3 has selected. We are also awaiting delivery of a prototype scintillator plane from WBS3 which we will use to verify dimensional tolerances and use to further test compatibility of our procedures. The full module prototype will give us our first chance to test our assembly procedures on actual full-size and full-weight detector components. We anticipate that this exercise will reveal weaknesses in our procedures or materials, so we have scheduled adequate time after the prototype module assembly to revise our assembly procedures and design.

We are also attempting to optimize work flow in light of the module mapper. Currently, the module assembly schedule in the MINER ν A Project file is based on a assembly and mapping rate of one module per day. This rate is largely dominated by time required to map a module, which is predicted to be around 20 hours if we scale from the MINOS mapping rate. Based on initial mapper designs, we feel that we may be able to significantly increase the mapping rate by using two scanning heads in the MINER ν A module mapper (MINOS mappers each had one scanning head.). The final mapping rate is yet to be determined, but we feel it may be 10-12 hours. Mapping at this rate would lead to a savings in the assembly costs and would remove much of the schedule contingency associated with the module assembly and mapping. This 10-12 hours spec will be the design goal of the mapper. Much remains to be done before we will know if this rate is feasible. Final design of the mapper will take place during the summer of 2006 and the mapper will be first tested on the full module prototype early in the winter of 2006-2007. Based on the outcomes of this test, we have scheduled time to debug and optimize the mapper in early 2007.

4.4 Detector Installation

WBS 11 is responsible for the installation of the detector, as well as a series of physical improvements required to make the NuMINear Hall suitable for MINER ν A. This work is most closely related to WBS8, and much the work required for WBS 11 will be completed by the same individuals.

WBS 11 is not an official part of the MINER ν A project. There are two major reasons for this. First, all of the infrastructure improvements in this WBS element are tasks that need to be done for the installation of any experiment and are not unique to MINER ν A. These include extension of the hall's drip ceiling, moving the MINOS magnet power supply to make additional room, and installing the quiet power to service any experiment.

Second, the installation of the experiment is off project because with MINOS running the MINER ν A project has no control over the timing of the detector installation. The MINER ν A project has made various tests with the help of the MINOS experiment to determine how various installation tasks might affect data taking in MINOS. We have taken some test data with the MINOS detector while doing welding and also while using the overhead crane, either of which could generate electronic noise that would interfere with MINOS data taking. While tests so far show minimal effects on MINOS data, the testing has not been comprehensive. Therefore it is entirely possible that MINER ν A

may have to wait for a shutdown to carry out the installation of the detector. In order to define a clear set of CD4 deliverables, then, the detector installation has not officially been included in the MINER ν A project.

This section, then, will give an overview of WBS 11. Emphasis will be placed on the scope of WBS 11, which will be covered first. This will be followed by a discussion of required resources and interfaces with other WBS tasks. An overview of the WBS structure and schedule will not be included.

4.4.1 Task Objectives and Overview

WBS 11 has two main objectives. These include, first, preparation of the NuMINear Hall to house MINER ν A, and second, the actual installation of the detector. These two objectives will be discussed in more detail in the following two subsection.

Improvements to the Numi Near Hall The WBS 11 element provides for installing a drip ceiling over the detector. As the hall is located underground, leakage of groundwater (from above) is a major concern. With MINOS, this situation was remedied by the installation of a drip ceiling above the detector. The drip ceiling is attached to the ceiling of the experimental hall and channels ground water away from the detector. The current drip ceiling is sufficient for MINOS, but would not adequately cover the proposed location of MINER ν A.

While it would suffice to simply extend the current drip ceiling to cover the MINER ν A detector, we will also solicit quotes for extending the drip ceiling to cover the remainder of Numi near hall. The initial design has been for a simple extension of the same roof system that exists over the MINOS detector, but other kinds of roof systems are also being explored.

Quiet power services in the hall will be expanded with the addition of one more 75 KVA transformer and distribution panel. This addition would allow servicing of one experiments power system without having to shut down both experiments. In the recent shutdown the MINOS power supply and its water skid were moved upstream to the end of the hall. This move will provide extra room for experiments directly upstream of the MINOS detector where space is most valuable. With MINER ν A in place the power supply would not have been serviceable in the old location if, for example, a transformer needed replacing.

Prior to installation, WBS 11 must install the required detector stands into the NuMIHall. The detector stand consists of a large rail system that supports the MINER ν A detector. The detector modules will hang on the rails like a hanging file folder system. Figure 58 shows the side view of the detector on the stand. During the installation of the stand the Alignment Group will provide services to make sure the rails are at the proper elevation and that the rails are on the beamline axis. They will also measure the bookend to make sure that all of the frames are hanging plumb on the stand. The stand columns also supply the support for an additional set of rails that hold the phototube access platform over the top of the detector. This access platform allows servicing of the phototube and front end electronics of the detector. The access platform is not shown in Figure 58.



Figure 67: MINOS detector module being lowered into the cavern at the shaft.

4.4.2 Detector Installation

The design of MINER ν A is similar to MINOS because it is a series of frames that are assembled in a certain order to make up the detector. This allows us to use similar installation techniques that have already been worked out for the assembly of the MINOS detector. Pictures taken during the MINOS Near detector assembly can illustrate the procedure. Frames are brought over from the Wideband Lab to the MINOS Service building by tractor trailer truck one at a time in the order in which they are installed (from downstream to upstream). The strongbacks will be used as the transport fixture for this. They will maintain the frames flat during transport and will also be the lifting fixture during the lowering and raising crane operations. Figure 67 shows a MINOS detector module being lowered into the NuMINear Hall.

The MINOS surface building has two overhead cranes. The first will be used to load the detector modules off of the flatbed truck and stage them in the surface building. The second crane will then lift the modules and lower them down the access shaft into the NUMI Near Hall.

As modules are lowered into the NuMI hall, they will be secured to a cart. The MINOS cart, shown in Figures 67 and 68, will be re-used for the MINER ν A installation after some minor modifications. The strongback and frame will be landed on the cart and secured by bolts. Then an electric forklift will be used to push the cart roughly 100 m to the experimental hall.



Figure 68: Cart in the Numi Near Hall holding a MINOS detector module.



Figure 69: Mounting a MINOS module on the detector stand.

After the frame is re-secured to the cavern crane it can be unbolted from the cart, moved into position on the detector stand and set in place. The frame will be secured to the detector by axial bolts that keep a uniform distance between frames. A bookend on the downstream end of the stand provides a framework that ensures that the assembly of the detector starts from a straight reference plane. During assembly of the following frames frequent measurements will be taken and adjustments made to maintain the detector straight and plumb. Figure 69 illustrates the mounting of a MINOS detector module.

As each module is installed, some quality assurance and testing will be done. Modules will be visually inspected for damage during transport and handling. The light-tightness of each module will also be verified.

As every four modules are installed, a PMT rack will be installed on top. This rack will hold all of the PMT's required to read out the four modules. The PMT's and electronics will be installed, and each module will be tested further.

After the detector is assembled a phototube access platform will be installed on its own rails. This

platform will allow for routine maintenance of the phototubes without the need of special equipment.

4.4.3 Facilities and Resources

Most of heavy work associated with detector installation will be handled by Fermilab technicians. WBS 11 will employ the crew used by WBS8 for the OD frame assembly and welding; this is also the same crew who handled the installation of the MINOS near detector. This crew will install the detector stand, handle installation of the detector modules, and install the PMT access platform.

At the time of installation, some physicist involvement will be required. In particular, a group from the University of Rochester will help install the PMT's and clear fiber cables, and test the modules. This group is associated with WBS9. Having been heavily involved in module assembly, they will be familiar with module QA procedures. WBS9 is responsible for commissioning the tracking prototype, so Rochester technicians and physicists will help test and commission each module as they are installed. Representatives from other task groups will handle installation and testing of the electronics and data acquisition system.

As discussed in the previous section, WBS 11 will make use of Wideband Hall, the MINOS surface building and the NuMIhall. Before installation, the assembled modules will be stored in Wideband Hall. All three locations are equipped with adequate overhead cranes to handle any lifting operations required. A flatbed truck will be required to transport modules from Wideband Hall to the MINOS surface building, and an electronic fork lift will be used in the NuMIexperimental hall to push the cart which moves modules from the bottom of the access shaft to the staging area for the overhead crane.

4.4.4 Interfaces with other WBS Tasks

WBS 11 will interface most closely with WBS9. WBS9 will deliver the assembled modules to WBS 11. These modules will be hanging on a storage rack in Wideband Hall. In addition, WBS9 will provide the PMT racks and the veto wall.

PMTs in boxes will be provided by WBS6, and electronics will be provided by WBS7.

References

- [1] MINOS Collaboration, “MINOS Technical Design Report“, NuMI-NOTE-GEN-0337 (1998).
- [2] N. V. Mokhov, “The MARS Monte Carlo”, FERMILAB FN-628 (1995); N. V. Mokhov and O. E. Krivosheev, “MARS Code Status”, FERMILAB-Conf-00/181 (20 00); <http://www-ap.fnal.gov/MARS/>.
- [3] N. Mokhov and A. Van Ginneken, *J. Nucl. Sci. Tech.* **S1**, 172 (2000).
- [4] M. Messier (private communication)
- [5] Y. Hayato, To be published in *Proceedings of the Second Workshop on Neutrino-Nucleus Interactions in the Few-GeV Region (NUINT02)*, Irvine, California (2002).
- [6] G. Ambrosini *et al.* [NA56/SPY Collaboration], *Eur. Phys. J. C* **10**, 605 (1999).
- [7] P-907: Proposal to Measure Particle Production in the Meson Area Using Main Injector Primary and Secondary Beams, May 2000

(http://ppd.fnal.gov/experiments/e907/Proposal/E907_Proposal.html
)
- [8] NuMI Technical Design Handbook

(http://www-numi.fnal.gov/numiwork/tdh/tdh_index.html)
- [9] K. Kodama *et al.*, *Nucl. Phys. Proc. Suppl* **98**, 43-47 (2001)
- [10] M. Hasegawa *et al.* [K2K Collaboration], *Phys. Rev. Lett.* **95**, 252301 (2005) [arXiv:hep-ex/0506008].
- [11] S. Kopp, Z. Pavlovic, and D. Indurthy, “Systematic Uncertainties in the NuMI Beam Flux” MINOS-doc-1283, (2006)
- [12] C.H. Llewellyn Smith, *Phys. Rep.* 3C (1972).
- [13] J. Arrington, nucl-ex[0305009].
- [14] M. K. Jones *et al.*, *Phys. Rev. Lett.*, 84, (2000) 1398 ; O. Gayou *et al.*, *Phys. Rev. Lett.*, 88 (2002) 092301.
- [15] J.J. Kelly, *Phys. Rev. C*70 (2004) 068202.
- [16] R. Bradford, et al., hep[ex0602017].
- [17] H. Budd, A. Bodek and J. Arrington, hep-ex[0308005].

- [18] R. F. Wagenbrunn *et al.*, hep-ph[0212190].
- [19] R. C. Merenyi *et al.*, Phys. Rev. D 45, 743 (1992)
- [20] V. Bernard, L. Elouadrhiri, U.G. Meissner, J.Phys.G28 (2002), hep-ph[0107088].
- [21] G. Zeller, private communication.
- [22] K. Tsushima, Hungchong Kim, K. Saito, hep-ph[0307013].
- [23] T. Kitagaki *et al.*, Phys. Rev. D26 (1983) 436.
- [24] T. Kitagaki *et al.*, Phys. Rev. D42 (1990) 1331.
- [25] S.J. Barish *et al.*, Phys. Rev. D16 (1977) 3103.
BNL D2
- [26] N.J. Baker *et al.*, Phys. Rev. D23 (1981) 2499.
- [27] W.A. Mann *et al.*, Phys. Rev. Lett. 31 (1973) 844.
- [28] J. Brunner *et al.*, Z. Phys. C45 (1990) 551.
- [29] M. Pohl *et al.*, Lett. Nuovo Cimento 26 (1979) 332.
- [30] D. Allasia *et al.* Nucl. Phys. B **343** (1990) 285
- [31] S.V. Belikov *et al.*, Z. Phys. A320 (1985) 625.
- [32] S. Bonetti *et al.*, Nuovo Cimento 38 (1977) 260.
- [33] K.L. Miller *et al.*, Phys. Rev. D26 (1982) 537.
- [34] Glen Cowan, Statistical Data Analysis, Oxford Clarendon Press (1 998)
- [35] H. Budd, A. Bodek and J. Arrington, hep-ex[0410055].
- [36] D. Casper, Nucl. Phys. Proc. Suppl. 112 (2002) 161.
- [37] R.A. Smith and E.J. Moniz, Nucl. Phys. B43 (1972) 605.
- [38] Ghent Theory group in Belgium, Jan Ryckebusch (jan@inwpent5.UGent.be).
- [39] D. Rein and L. M. Sehgal, Annals Phys. **133**, 79 (1981).
- [40] M.H. Ahn, et al. (K2K), Submitted to PRD, hep-ex/0606032.
- [41] T. Sato, D. Uno, and T.-S.H. Lee, Phys. Rev. C**67** 065201 (2003).
- [42] E. Paschos, M. Sakuda, J.-Y. Yu, Phys. Rev. D**69** 014013 (2004).

- [43] E. Paschos, et al., Proc. NuInt04 (L'Aquila), hep-ph/0408185.
- [44] O. Lalakulich and E. Paschos, Phys. Rev. **D71** 074003 (2005).
- [45] O. Lalakulich, E. Paschos, G. Piranishvili, Phys. Rev. **D74** 014009 (2006).
- [46] T. Sato, et al., Proc. NuInt05 (Okayama),nucl-th/0601069.
- [47] T. Kitagaki, et al., Phys. Rev. **D34** 2554 (1986).
- [48] T. Kitagaki, et al., Phys. Rev. **D42** 1331 (1990).
- [49] M. Hasegawa, et al. (K2K), Phys. Rev. Lett. **95** 252301 (2005).
- [50] M. Wascko (MiniBoone), Proc. NuInt05 (Okayama), hep-ex/060 2050.
- [51] D. Rein and L. M. Sehgal, Nucl. Phys. **B223**, 29 (1983).
- [52] E. A. Paschos and A. V. Kartavtsev, (2003), hep-ph/0309148.
- [53] Super-Kamiokande and K2K, C. Mauger, Nucl. Phys. Proc. Suppl. **112**, 146 (2002).
- [54] BooNE, J. L. Raaf, Nucl. Phys. Proc. Suppl. **139**, 47 (2005), hep-ex/0408015.
- [55] B. Z. Kopeliovich, Nucl. Phys. Proc. Suppl. **139**, 219 (2005), hep-ph/0409079.
- [56] E. A. Paschos, A. Kartavtsev, and G. J. Gounaris, (2005), hep-ph/0512139.
- [57] D. Rein and L. M. Sehgal, (2006), hep-ph/0606185.
- [58] S. K. Singh, M. Sajjad Athar, and S. Ahmad, (2006), nucl-th/0601045.
- [59] MiniBooNE, J. Monroe, Nucl. Phys. Proc. Suppl. **139**, 59 (2005), hep-ex/0408019.
- [60] K2K, T. Ishida, Prepared for 1st Workshop on Neutrino - Nucleus Interactions in the Few GeV Region (NuInt01), Tsukuba, Japan, 13-16 Dec 2001.
- [61] N.J. Baker *et al.*, Phys. Rev. D **24**, 2779 (1981).
- [62] A. Alavi-Harati *et al.*, Phys. Rev. **87** 132001 (2001).
- [63] P.G. Ratcliffe, Phys. Rev. **D59**, 014038 (1999).
- [64] N. Cabibbo *et al.*, Semileptonic Hyperon Decay and CKM Unitarity, [arXiv:hep-ph/0307214] (July 2003).
- [65] T. Alexopoulos *et al.* (KTeV Collaboration), Phys. Rev. Lett. **93**, 181802 (2004).
- [66] T. Nakano *et al.*, [arXiv:hep-ex/0301020]; V.V. Barmin *em et al.*, [arXiv:hep-ex0304040]; S. Stepanyan [arXiv:hep-ex/0307018].

- [67] R. Jaffe and F. Wilczek, Di-quarks and Exotic Spectroscopy, [arXiv:hep-ph/0307341] (July 2003).
- [68] S. Kuhlmann *et al.*, Phys. Lett. B **476**, 291 (2000).
- [69] H. Deden and et al., [Gargamelle Neutrino Collaboration], “Experimental Study Of Structure Functions And Sum Rules In Charge Changing Interactions Of Neutrinos And Anti-Neutrinos On Nucleons,” Nucl. Phys. **B85**, 269 (1975).
- [70] K. Varvell *et al.* [BEBC WA59 Collaboration], Z. Phys. C **36**, 1 (1987)
- [71] M. Shifman, Handbook of QCD, Volume 3, 1451, World Scientific (2001)
- [72] F. E. Close and N. Isgur, Phys. Lett. B **509**, 81 (2001)
- [73] W. Melnitchouk, R. Ent and C. Keppel, Phys. Rept. **406**, 127 (2005) [arXiv:hep-ph/0501217].
- [74] I. Niculescu *et al.*, Phys. Rev. Lett. **85**, 1186 (2000)
- [75] C. E. Keppel, *Prepared for Exclusive Processes at High Momentum Transfer, Newport News, Virginia, 15-18 May 2002*
- [76] J. Arrington, R. Ent, C. E. Keppel, J. Mammei and I. Niculescu, arXiv:nucl-ex/0307012 (submitted to Phys. Rev. Lett.)
- [77] A. Fantoni [HERMES Collaboration], Eur. Phys. J. A **17**, 385 (2003).
- [78] I. Niculescu *et al.*, Phys. Rev. Lett. **85**, 1182 (2000).
- [79] A. Bodek and U. K. Yang, arXiv:hep-ex/0203009.
- [80] D. Dolgov *et al.* [LHPC collaboration], Phys. Rev. D **66**, 034506 (2002) [arXiv:hep-lat/0201021].
- [81] I. Niculescu, J. Arrington, R. Ent and C. E. Keppel, Phys. Rev. C **73**, 045206 (2006) [arXiv:hep-ph/0509241].
- [82] X. Ji, Phys. Rev. Lett. **78**, 610 (1997).
- [83] X. Ji, Phys. Rev. **D55**, 7114 (1997).
- [84] A. V. Radyushkin, Phys. Lett. **B380**, 417 (1996).
- [85] A. V. Radyushkin, Phys. Lett. **B385**, 333 (1996).
- [86] J.C. Collins, L. Frankfurt, and M. Strikman, Phys. Rev. **D56**, 2982 (1997).
- [87] A. V. Radyushkin, Nucl. Phys. **A711**, 99 (2002).
- [88] M. Vanderhaeghen, Nucl. Phys. **A711**, 109 (2002).

- [89] M. Diehl, hep-ph/0307382 (2003).
- [90] C. Munoz Camacho, et al. nucl-ex/0607029 (2006).
- [91] A. Psaker, W. Melnitchouk and A. Radyushkin, in preparation.
- [92] D. Drakoulakos *et al.* [Minerva Collaboration], fine-grained detector in the NuMI beam,” arXiv:hep-ex/0405002. Pgs. 99 - 108, 192 - 200.
- [93] B.Z. Kopeliovich, hep-ph/0409079.
- [94] M.K. Jones *et al.*, Phys. Rev. **C48**, 2800 (1993); R.D. Ransome *et al.*, Phys. Rev. **C46**, 273 (1992); R.D. Ransome *et al.*, Phys. Rev. **C45**, R509 (1992).
- [95] D. Rowntree *et al.*, Phys. Rev. **C60**, 054610 (1999); B. Kotlinksi *et al.*, Eur. Phys. J. **A9**, 537 (2000).
- [96] E. A. Paschos, M. Sakuda, I. Schienbein and J. Y. Yu, arXiv:hep-ph/0408185.
- [97] M. Arneodo, Phys. Rept. **240**, 301 (1994).
- [98] G. Piller and W. Weise, Phys. Rept. **330**, 1 (2000).
- [99] B. L. Ioffe, V. A. Khoze, and L. N. Lipatov, *Hard processes: Phenomenology, Quark-Parton Model* (Elsevier Science Publishers, North Holland, 1984).
- [100] G.B. West, Ann. Phys. **74** (1972) 464.
- [101] S. V. Akulinichev, S. A. Kulagin, and G. M. Vagradov, Phys. Lett. B **158**, 485 (1985); S. V. Akulinichev, S. Shlomo, S. A. Kulagin, and G. M. Vagradov, Phys. Rev. Lett. **55**, 2239 (1985).
- [102] S. A. Kulagin, Nucl. Phys. A **500**, 653 (1989).
- [103] C. Ciofi degli Atti and S. Liuti, Phys. Rev. C **41**, 1100 (1990).
- [104] F. Gross and S. Liuti, Phys. Rev. C **45**, 1374 (1992).
- [105] S. A. Kulagin, G. Piller and W. Weise, Phys. Rev. C **50**, 1154 (1994).
- [106] S. A. Kulagin, W. Melnitchouk, G. Piller, and W. Weise, Phys. Rev. C **52**, 932 (1995).
- [107] S. A. Kulagin, Nucl. Phys. A **640**, 435 (1998).
- [108] W. Melnitchouk, A. W. Schreiber and A. W. Thomas, Phys. Rev. D **49**, 1183 (1994).
- [109] J. Gomez, *et al.*, Phys. Rev. D **49**, 4348 (1994).
- [110] S. I. Alekhin, S. A. Kulagin and S. Liuti, Phys. Rev. D **69**, 114009 (2004).
- [111] S. A. Kulagin and R. Petti, paper in preparation.

- [112] T. H. Bauer, R. D. Spital, D. R. Yennie and F. M. Pipkin, *Rev. Mod. Phys.* **50**, 261 (1978) [Erratum-ibid. **51**, 407 (1979)].
- [113] C. A. Pickety, and L. Stodolsky, *Nucl. Phys. B* **15**, 571 (1970).
- [114] S. L. Adler, *Phys. Rev.* **135**, B963 (1964).
- [115] R. J. Glauber, *Phys. Rev.* **100**, 242 (1955).
- [116] V. N. Gribov, *Sov. Phys. JETP* **29**, 483 (1970) [*Zh. Eksp. Teor. Fiz.* **56**, 892 (1969)] ; *Sov. Phys. JETP* **30**, 709 (1970) [*Zh. Eksp. Teor. Fiz.* **57**, 1306 (1969)].
- [117] B. Z. Kopeliovich, and P. Marage, *Int. J. Mod. Phys. A* **8**, 1513 (1993).
- [118] S. A. Kulagin, arXiv:hep-ph/9812532.
- [119] E. A. Paschos and L. Wolfenstein, *Phys. Rev. D* **7**, 91 (1973).
- [120] G. P. Zeller *et al.* [NuTeV Collaboration], *Phys. Rev. Lett.* **88**, 091802 (2002) [Erratum-ibid. **90**, 239902 (2003)] [arXiv:hep-ex/0110059].
- [121] S. A. Kulagin, *Phys. Rev. D* **67**, 091301 (2003) [arXiv:hep-ph/0301045].
- [122] S. A. Kulagin, arXiv:hep-ph/0406220.
- [123] S. A. Kulagin, arXiv:hep-ph/0409057.
- [124] D. H. Lu, A.W. Thomas, and K. Tsushima, arXiv:nucl- th/0112001, K. Tsushima, H. Kim, and K. Saito, *Phys. Rev. C* **70**, 038501 (2004)
- [125] J.J. Aubert *et al.*, *Phys. Lett.* **123B**, 275 (1983); D.F. Geesaman, K. Saito, and A.W. Thomas, *Annu. Rev. Nucl. Part. Sci.* **45**, 337 (1995).
- [126] B. Buck and S.M. Perez, *Phys. Rev. Lett.* **50**, 1975 (1983).
- [127] S. Dieterich, *et al.*, *Phys. Lett. B* **500**, 47 (2001), S. Strauch *et al.*, *Phys. Rev. Lett.* **91**, 052301 (2003).
- [128] JLab experiment E3-104, co-spokespersons R. Ent, R. Ransome, S. Struach, P. Ulmer. http://www.jlab.org/exp_prog/proposals/03/PR03-104.ps
- [129] C.H.Q. Ingram, *Nucl. Phys. A* **684**, 122 (2001).
- [130] M. K. Jones *et al.*, *Phys. Rev. C* **48**, 2800 (1993).
- [131] M. Nakahata *et al*, *Nucl. Instrum. Meth.* **A421**, 113 (1 999); E. Blaufuss *et al*, *Nucl. Instrum. Meth.* **A458** 638 (2001).
- [132] M. Diwan and J. Nelson, NuMI-NOTE-STEEL-0639 (2000)

- [133] PhD Thesis of C. Smith, University College London, London, 2002 *Calibration of the MINOS Detectors and Extraction of Neutrino Oscillation Parameters*; PhD Thesis of R. Nichol, University College London, London, 2003 *Calibration of the MINOS Detectors*
- [134] PhD thesis of M. A. Kordosky, University of Texas at Austin, August 2004 *Hadronic Interactions in the MINOS Detectors*
- [135] PhD thesis of P. L. Vahle, University of Texas at Austin, August 2004 *Electromagnetic Interactions in the MINOS Detectors*
- [136] E. A. Paschos, L. Pasquali and J. Y. Yu, Nucl. Phys. B **588**, 263 (2000) and E. A. Paschos, J. Y. Yu and M. Sakuda [arXiv:hep-ph/0308130].
- [137] D. Ashery *et al.*, Phys. Rev. **C23**, 2173 (1981).
- [138] H. Gallagher, Nucl. Phys. Proc. Suppl. **112**, 188 (2002)
- [139] NuMI Fluxes courtesy of Mark Messier
- [140] The simulation assumed the active material was resistive plate chambers and the absorber was particle board (hydrocarbons).
- [141] G.P.Zeller, submitted to proceedings of 2nd International Workshop on Neutrino - Nucleus Interactions in the Few GeV Region (NUINT 02), Irvine, California, 12-15 Dec 2002 [hep-ex/0312061]
- [142] Kamiokande Collaboration, S. Hatakeyama *et al.*, Phys. Rev. Lett. **81** (1998) 2016; Soudan-2 Collaboration, W. W. Allison *et al.*, Phys. Lett. **B 449** (1999) 137; MACRO Collaboration, Ambrosio *et al.*, Phys. Lett. **B434**, 451 (1998)
- [143] Y. Fukuda *et al.*, Phys. Rev. Lett. **81** (1998) 1158; Erratum **81** (1998) 4279, B.T. Cleveland *et al.*, Astrophys. J. **496** (1998) 505. W. Hampel *et al.* (GALLEX Collaboration), Phys.Lett. **B 447** (1999) 127., J.N. Abdurashitov *et al.* (SAGE Collaboration), Phys. Rev. **C 60** (1999) 055801 [astro-ph/9907113]
- [144] Q.R. Ahmad *et al.* Phys.Rev.Lett.**89** (2002) 011302 nucl-ex/0204009
- [145] Y. Fukuda *et al.*, Phys.Rev.Lett.**81** (1998) 1562 [hep-ex/9807003]; M. Sanchez *et al.*, Phys. Rev. **D 68**, 113004 (2003)
- [146] KamLAND Collaboration (K. Eguchi *et al.*), Phys. Rev. Lett.**90** (2003) 021802 [hep-ex/0212021]
- [147] K2K Collaboration (M.H. Ahn *et al.*), Phys.Rev.Lett.**90** (2003) 41801 [hep-ex/0212007]
- [148] B. Pontecorvo and J. Exptl, Theoret. Phys. **34** 247 (1958); Z. Maki, M. Nakagawa and S. Sakata, Prog. Theor. Phys. **28**, 870 (1962).

- [149] M. Maltoni *et al*, submitted to New J. Phys, [hep-ph/0405172]
- [150] By CHOOZ Collaboration (M. Apollonio et al.), Phys.Lett.**B466** (1999) 415 [hep-ex/9907037]
- [151] W. Grimus and L. Lavoura, Phys. Lett. **B572**, 189 (2003); A. Aranda, C.D. Carone, R.F. Lebed, Phys. Rev. **D62**, 016009 (2000).
- [152] “A Long Baseline Neutrino Oscillation Experiment at Fermilab”, E.Ables *et al*, FERMILAB-PROPOSAL-0875, Feb. 1995, 241pp.
- [153] “NOVA: Proposal to build an Off-Axis Detector to Study $\nu_\mu \rightarrow \nu_e$ oscillations in the NuMI Beamline”, I. Ambats *et al.*, FERMILAB-PROPOSAL-0929, Mar 2004.
- [154] Y. Itow *et al*, “The JHF-Kamioka Neutrino Project”, KEK report 2001-4, June 2001. [hep-ex/0106019]
- [155] J. Nelson, “MINOS Oscillation Results”, Neutrino 2006, Santa Fe, NM, June, 2006.
bibitemingram C.H.Q. Ingram, Nucl. Phys. A **684**, 122 (2001).
- [156] E. Gallas & J. Li., “Polishing Optical Fibers for the D0 ICD in Run II”, FNAL-TM-2062, 1998.
- [157] The MINER ν A Collaboration,
Proposal to perform a high-statistics neutrino scattering experiment using a fine-grained detector in the NuMI beam, Fermilab Proposal P-938, e-print hep-ex/0405002; see Sect. 16.5.2.
- [158] M. Bonkowski, *Magnetic Field Measurement Results*,
MINER ν A note MINER ν A-doc-88-v1, (measurements of December 2004).
- [159] D. Cherdack and W.A. Mann, *Magnetic Shielding Capabilities of the MINER ν A PMT Box*, MINER ν A note MINER ν A-doc-164-v1.
- [160] P. Adamson, et al., Nucl. Inst. Meth. **A492**,
325 (2002).
- [161] P. Shanahan, priv. comm. (Nov., 2005).
- [162] A. Cabrera, et al., NuMI-934 internal report.
- [163] P. Harris (Sussex Univ.) provided excellent
guidance and some pieces necessary for prototyping.
- [164] “MCM II and the Trip Chip”, J. Estrada, C. Garcia, B. Hoeneisen and P. Rubinov, August 2002, FERMILAB-TM-2226.

- [165] MINOS Technical Design Report, Chapter 5: Scintillator detector fabrication, Fermilab Public
- [166] Specification 9216.000-ES-435360. Available through the Fermilab Particle Physics Division.
- [167] Specification 9216.000-ES-435361. Available through the Fermilab Particle Physics Division.
- [168] R. Bradford, *Assembly Roadmap from Prototype Studies*, posted to FNAL MINER ν A Docdb as document number 561.
- [169] R. Flight, *Detector Assembly Drawings, as of 11/15/05*, available in MINER ν A Docdb as document number 226.
- [170] R. Flight, *Mapper Drawings*, available in MINER ν A Docdb as document number 897.
- [171] R. Flight, *Fiber Routing Update*, available in MINER ν A Docdb as document number 741.
- [172] D. Casper, “The nuance Neutrino Physics Simulation, and the Future”,
http://nuint.ps.uci.edu/nuance/files/nuance_nuint01.pdf
- [173] O. Benhar, [arXiv:nucl-th/0307061].
- [174] K. Ruddick (private communication).
- [175] L. Mualem (private communication).
- [176] MINOS Collaboration, P. Adamson *et al.*, IEEE Trans. Nucl. Sci. **49**, 861 (2002).
- [177] R. Fruhwirth, Nucl. Inst. Meth. **A262**, 444 (1987).
- [178] “Studies of Extruded Plastic Scintillator for MINOS”, Karol Lang and Todd Soesby, NuMI-NOTE-L-250, Feb 1997.
- [179] M. Andrews, MINER ν A Hazard Assessment, MINER ν A Document 310 (2006)
- [180] MINER ν A Project Management Plan, MINER ν A Document 59 (2006)
- [181] L. Mualem, *The case for using Cesium-137 on the module mapper instead of Co-60*, NuMI-L-0653 (2000)
- [182] American Institute of Steel Construction, Inc., *Manual of Steel Construction, Allowable Stress Design*, Ninth Edition
- [183] American National Standard ANSI/ASME B30.20, *Below-the-hook lifting devices*
- [184] Gage-Babcock & Associates, Inc. *Fire Protection/Life Safety Recommendations for the Fermilab NuMI Project* (1998)
- [185] Fermilab ES&H Manual, Chapter 5032.2, Guidelines for the Design, Review and Approval of Liquid Cryogenic Targets (1995)

[186] J. Livengood, Letter to G. Brown, *National Environmental Policy Act (NEPA) Determination at Fermi National Accelerator Laboratory - "Main Injector Neutrino Experiment ν -A(MINER ν A)"* MINER ν A Document 311 (December 2, 2005)